# Thermal Stresses in Pipes

**By**

**Iyad Al-Zaharnah,** BSc. & MSc. In Mechanical Engineering

This thesis is submitted to Dublin City University as the fulfillment of the requirement for the award of degree of

**Doctor of Philosophy**

**Supervisors**

**Professor M.J. Hashmi**

**Professor B.S. Yilbas**

**School of Mechanical & Manufacturing Engineering**

**Dublin City University**

**April 2002**

# DECLARATION

I hereby certify that this material, which I now submit for assessment on the programe of study leading to the award of Doctor of Philosophy is my own work and has not been taken from the work of others save and to the extent that such work has been cited and acknowledged within the text of my work.

**Signed:** _____ **I.D No.:** 9897021

**Date:** 13-08-2002

I dedicate this thesis to my beloved parents, brother and sister

# ACKNOWLEDGMENT

First and foremost, all praise to Almighty, Allah Who gave me the courage and patience to carry out this work and I Ask to accept my little effort. May He, S*ubhanahu-ta-Aala*, guide the humanity and me to the right path.

My deep appreciation is to my Ph.D., thesis advisors Professor M.S.J. Hashmi (Dublin City University, Ireland) and Professor B.S. Yilbas (King Fahd University of Petroleum and Minerals, Saudi Arabia) for their continuous support and matchless patience throughout this work. Their suggestions were always valuable and working with them was always indeed a wonderful and learning experience. Continuously, they were supportive and kind to me.

I would also like to thank both Dublin City University in Ireland and King Fahd University of Petroleum and Minerals in Saudi Arabia for providing everything necessary to make this work possible.

Thanks are due to my parents, brother and sister for their prayers and support throughout my academic life. I dedicate this work to them.

Appreciations are due to Mr. Abdallah Al-Gahtani for his kind support before the viva.

**Title of thesis:** Thermal Stresses in Pipes

**Name of student:** Iyad Al-Zaharnah **Student No:** 9897021

# ABSTRACT

This study presents results about thermal stresses in externally heated pipes that are subjected to different flow types: laminar flow, turbulent flow, and pulsating flow. The effect of flow Reynolds number on thermal stresses in the pipe is studied. To investigate the influence of fluid and solid properties on the resulting thermal stresses in pipes, two solids namely; steel and cooper and three fluids namely; water, coolanol-25, and mercury are used in the study. Pipes with different diameters, length to diameter ratios, and thickness to diameter ratios are covered in the study to examine the effects on thermal stresses. Different parameters for pressure difference and oscillating frequency are used in the case of pulsating flow to find their influence on the resulting thermal stresses in the pipe. The amount of heat flux at the outer wall of the pipe is also included in the study.

In order to account for the turbulence, the k-ε model is introduced in the analysis. The numerical scheme employing control volume approach is introduced to discretize the governing equations of flow and heat transfer. The grid independent tests are carried out to ensure grid independent solutions. To validate the present predictions, data presented in the open literature are accommodated.

# Table of Contents

# CHAPTER 3

## Mathematical Modeling, Numerical Solution and Results Validation



# CHAPTER 4

## Results and Discussion

# LIST OF TABLES

# LIST OF FIGURES

# Nomenclature

| | | |
|---|---|---|
| A | velocity amplitude | (m/s) |
| $C_p$ | specific heat of fluid | (J/kg×k) |
| $C_{psolid}$ | specific heat of solid | (J/kg×k) |
| D | inside diameter of the pipe | (m) |
| E | modulus of elasticity of the pipe material | (Pa) |
| e | constant in law of wall | |
| h | heat transfer coefficient | ($W/m^2$×k) |
| J | total flux across a face of the finite control volume | ($J/m^3$) |
| k | turbulent kinetic energy generation variable | ($m^2/s^2$} |
| $k_f$ | thermal conductivity of the fluid | (W/m×k) |
| $k_s$ | thermal conductivity of the solid | (W/m×k) |
| $k_{fluid}$ | thermal conductivity of the fluid | (W/m×k) |
| $k_{solid}$ | thermal conductivity of the solid | (W/m×k) |
| L | length of the pipe | (m) |
| n | oscillating frequency of a pulsating flow | (Hz) |
| p | pressure | (Pa) |
| $P_r$ | laminar Prantle number | |
| $Pr_t$ | turbulent Prantl number | |
| q | heat flux | ($W/m^2$) |
| Re | laminar Reynolds number | |
| $Re_t$ | turbulent Reynolds number | |
| r | radial coordinate | (m) |
| $r^*$ | dimensionless radius of a grid point = $(r-r_i)/(r_o-r_i)$ | |
| $r_o$ | pipe outer radius | (m) |
| $r_i$ | pipe inner radius | (m) |
| $S_\phi$ | source or sink of variable $\phi$ | |
| t | thickness of the pipe | (m) |
| T | temperature at a grid point | (K) |

$T_{avs}$ average temperature in the solid (K)

$T^*$ dimensionless temperature at a grid point (K)

$T_{inlet}$ pipe inlet temperature (K)

$T_{mean}$ mean temperature of all grid points (K)

$T_{solid}$ solid-side temperature (K)

$T_{sw}$ temperature at the first radial grid point in solid at a certain axial plane (K)

$T_{fluid}$ fluid-side temperature (K)

$T_{fw}$ temperature at the last radial grid point in fluid at a certain axial plane (K)

$T_{inlet}$ pipe inlet temperature (K)

$T_{ow}$ outer-wall temperature (K)

$T_{iw}$ inner-wall temperature (K)

u fluid axial velocity (m/s)

$U_i$, $u_i$ cartesian velocity components (m/s)

v fluid radial velocity (m/s)

$V_o$ resultant radial velocity (m/s)

x axial coordinate (m)

## Greek Symbols

$\varepsilon$ turbulent dissipation variable ($m^2/s^3$)

$\varepsilon_\upsilon$ tangential strain

$\varepsilon_r$ radial strain

$\varepsilon_x$ axial strain

$\sigma_v$ effective stress (Pa)

$\sigma_\upsilon$ tangential stress (Pa)

$\sigma_r$ radial stress (Pa)

$\sigma_x$ axial stress (Pa)

$\nabla$ gradient/divergence operator

$\Gamma_\phi$ exchange coefficient for $\phi$

$\eta,\xi$ orthogonal coordinate directions

$\tau_{wall}$ wall shear stress (Pa)

$\nu$ Poisson's ratio

$\nu^*$ fluid kinematic viscosity $(m^2/s)$

$\kappa$ constant in law of wall

$\mu$ fluid dynamic viscosity $(N\times s/m^2)$

$\mu_t$ fluid dynamic turbulent viscosity $(N\times s/m^2)$

$\rho$ fluid density $(kg/m^3)$

$\rho_{solid}$ solid density $(kg/m^3)$

$\chi$ thermal diffusivity of the solid = $k_{solid}/(\rho_{solid}\, C_{psolid})$ $(m^2/s)$

$\Phi$ viscous dissipation $(1/s^4)$

$\upsilon_{ow}$ dimensionless temperature at outer wall = $(T_{ow}-T_{inlet})/(T_{avs}-T_{inlet})$

$\upsilon_{iw}$ dimensionless temperature at outer wall = $(T_{iw}-T_{inlet})/(T_{avs}-T_{inlet})$

**Subscripts**

E,N,S,W values at east, north, south and west grid points

e,n,s,w values at east, north, south and west edges of the cells

i,j tensor subscript notation

P values at grid point

**Superscripts**

* guessed value

′ correction in value

# CHAPTER 1

# INTRODUCTION AND SCOPE OF THE WORK

## 1.1 Introduction

One of the most important areas in the mechanics is the mechanical behavior of materials when subjected to thermal effects. Meeting the need for materials, which can function usefully at different temperature levels, is one of the most challenging problems facing our technology. Some examples are the dilation effects like the strengthening of bridges on a hot day or the bursting of water pipes in freezing weather and distortions set up in structures by thermal gradients. Sometimes-drastic changes in the properties of materials, such as tensile strength fatigue and ductility could also result by the change in material temperature. With rising temperature the elements of pipe body expand. Such an expansion generally cannot proceed freely in a continuous medium, and stresses due to the heating are set-up. The difficulty is that operating conditions not only at elevated temperature levels, but frequently also at severe temperature gradients. Such temperature differentials may produce thermal stresses significantly high enough to limit the material life. Fatigue failure could also occur due to temperature fluctuations.

Thick-walled pipes subjected to internal heat flow are used in many applications. When a thick-walled cylindrical body is subjected to a temperature gradient, non-uniform deformation is induced and thermal stresses are developed. The resulting thermal stresses add to the stresses resulting from internal and external pressures in the pipe material. One of the causes of thermal stresses in pipes is the non-uniform heating or cooling; such a situation that exists when for example pipes are welded, causing residual stresses. Nuclear engineering structures, military industries, chemical and oil industries, gun tubes, nozzle sections of rockets, composite tubes of automotive suspension components, launch tubes, landing gears, turbines, jet engines and dies of hot forming steels are typical examples.

The evaluation of thermal stresses in thick-walled pipes is important for principal design considerations. When an unrestrained material is heated or cooled, it dilates in accordance with its characteristic coefficient of thermal expansion. Many attempts were made using different techniques to avoid problems resulting from temperature differentials, such as compound cylinders with shrink fits and functionally gradient materials. Also, providing expansion joints for piping systems to accommodate length changes that take place with changes in temperature were used to achieve a better use of hollow higher working capacity. Without such provision, severe stresses could be setup and buckling or fracture of the part could occur. In the design and analysis of thermal piping systems, heat transfer in general plays an important role.

The transfer of heat in a solid occurs in virtue of heat conduction alone for time periods longer than phonon relaxation time. This does not have any macroscopic levels of movement in the solid body such as non-uniform electrons motion. At the surface of a body, heat transfer can occur in three ways: heat conduction, convection, or radiation. The heat exchange in the case of convection occurs by virtue of the motion of non-uniformly heated fluid or gas contiguous with the body. Convective heat transfer is the sum of the heat carried by the fluid. Heat exchange by means of electromagnetic waves takes place between bodies separated by a distance in the case of radiation. The pipe flow subjected to conjugate heating, where heat conduction in the solid interacts with convection heat transfer in the fluid, situations that result in large temperature gradients finds wide applications in engineering disciplines. This is due to the fact that the thermal loading can have a significant effect on the thermal resistance of the pipe. Examples of systems, in which the conjugate heat transfer exists, include heat exchangers, geothermal reservoirs, marine risers, sub-surface pipelines engineering structures, refrigeration ducts and nuclear reactors. Based on the conditions of flow and heat transfer, the temperature gradients resulting in pipes differ.

Two types of flow mainly exist in pipes namely, laminar and turbulent flows. The characteristic that distinguishes laminar from turbulent flow is the ratio of inertial force to viscous force, which can be presented in terms of the Reynolds number. Viscosity is a fluid property that causes shear stresses in a moving fluid, which in turn results in frictional losses. This is more pronounced in laminar type of flow; however, the viscous forces become less important for turbulent flows. The reason behind this is due to that in turbulent flows random fluid motions, superposed on the average, create apparent shear stresses that are more important than those produced by the viscous shear forces. The eddy diffusivities are much larger than the molecular ones in the region of a turbulent boundary layer removed from the surface (the core region). Associated with this condition, the enhanced mixing has the effect of making velocity, temperature and concentration profiles more uniform in the core. As a result, the velocity gradient in the surface region, and therefore, the shear stress, is much larger for the turbulent boundary layer than for the laminar boundary layer. In a similar manner, the surface temperature, and therefore, the heat transfer rate is much larger for turbulent flow than for laminar flow. Due to this enhancement of convection heat transfer rate, the existence of turbulent flow can be advantageous in the sense of providing improved heat transfer rates. However, the increase in wall shear stresses in the case of turbulent flow will have the adverse effect of increasing pump or fan power requirements. On the other hand, the conductive heat transfer becomes more important in laminar flow than the turbulent flow.

Unsteady flows, including pulsating flows, in pipelines are a common occurrence. Many reasons could cause the unsteadiness in pipe flow system such as; an adjustment of a valve in a piping system, or stopping a pump and the time-dependent wall heat flux; as in the case of solar collectors. Steady, laminar, incompressible flows can be tackled analytically; however, more complex flow situations require computational studies. The analysis of unsteady flow is much more complex than that of steady flow. Time as an independent variable enters the equations, and equations may be in partial differential form rather than ordinary differential equations (particularly in one-dimensional situation), which are solved using numerical methods. The unsteady internal flows importance has long been recognized. The situations in which pulsations are superimposed on a mean flow inside a pipe are of much practical importance. Industrial applications can be found in

ducts, manifolds and combustor pipes, and heat exchangers. In heat exchangers, the accurate prediction of the transient response of temperatures in equipment is highly important. This is not only to provide for an effective control system, but also important for understanding of undesirable effects such as reduced thermal performance and severe thermal stresses which can be produced, with eventual mechanical failure. The thermal response of unsteady temperature subjected to a periodic variation of inlet temperature in heat exchangers and other engineering applications is similarly of great interest for the effective control systems of thermal equipment. The determination of effects of thermal stress oscillations on induced fatigue damage has always been a research interest.

## 1.2 Scope of the Present Study:

The present study investigates the thermal stresses in external heated pipes when they are subjected to different flow conditions and it covers both the steady and the unsteady types of flow. The thermal stresses in pipes due to either fully developed laminar or fully developed turbulent flows are considered and the Reynolds number is taken into account in this regard.

Moreover, in many applications, the temperature gradient within the pipe may be time dependent, especially at the beginning of the operation. However, the temperature gradient may be oscillating during the operating time. Therefore, the design of such pipes needs to be combined with a more accurate thermal stress analysis taking into account the time-dependent variation. The unsteady thermal stresses in pipes subjected to pulsating flow are examined. The pulsation frequency and amplitude effects are covered.

Since the temperature of the solid-fluid boundary depends on the fluid properties, the effect of the fluid Prandtl number on thermal stresses is investigated. In actual practice, the temperature and heat flux distributions on the boundary depend strongly on the thermal properties and the flow characteristics of the fluid as well as on the properties of the wall. In order to account for this effect, different pipe wall materials are considered. Similarly, the temperature level and the temperature gradients within the solid are highly influenced by the amount of heat flux supplied at the outer wall of the pipe, therefore, different heat flux levels are used in the study to examine the effect of heat flux on thermal stresses in pipes.

The study parameters also include the change of thermal stresses with the pipe dimensions. Different pipe diameters, thickness to diameter ratios and length to diameter ratios are also employed in the study.

# CHAPTER 2

## LITERATURE REVIEW

Thick-walled pipes experiencing internal flow through pipes with heat interaction finds wide applications in industry. The solution of the conjugate heat problem includes the modeling of three types of flow namely; laminar flow, turbulent flow and pulsating flow. Considerable research studies were carried out in the past to explore the modeling such flows in pipes. The temperature gradient in the pipe material results in thermal stresses that are important when assessing the size and material properties of the pipes. Intensive research has been conducted in this regard in the past. The previous studies pertinent to the conjugate heat transfer in pipes and modeling of laminar, turbulent and pulsating types of flow and thermal stresses in pipes are given as follows.

### Laminar Flow

Davis and Gill [1] investigated the effects of axial conduction in the wall on heat transfer with laminar Poiseuille - Couette flow between parallel plates. They showed that the parameters determining the relative importance of axial conduction were the Peclet number and the wall thickness to length ratio. Their results agreed well with the experimental findings.

Faghri and Sparrow [2] studied the simultaneous wall and fluid axial conduction in laminar pipe-flow heat transfer. They considered the case where the upstream portion of the wall was externally insulated while the downstream portion of the wall was uniformly heated. They indicated that the wall axial conduction could readily overwhelm fluid axial conduction, which resulted in a preheating of both the wall and the fluid in the upstream region, with the zone of preheating extending back as far as twenty radii. The local Nusselt number exhibited fully developed values in the upper stream and downstream regions of the pipe.

Krishan [3] studied the unsteady heat transfer to fully developed flow in a heat conducting pipe of finite thickness when the outer periphery of a pipe that underwent a step change in heat flux or surface temperature. He used the method of Laplace transformation to solve for the temperature distribution in the composite regions of the fluid and solid coupled through matching boundary conditions at the interface yielding series solutions, which were valid for small time periods after the transition has occurred. He showed that the interfacial temperature decreased with the increase of the diffusive and conductive properties of both the fluid and solid.

Analytical solutions for the convective heat transfer due to steady laminar flow between concentric circular pipes with wall heated and/or cooled independently and subjected to uniform heat generation were presented by Arnas and Ebadian [4]. They showed that the Nusselt number might be affected positively or negatively by the heat generation depending on the flow situations.

A method to solve the conjugate heat transfer problems for the case of fully developed laminar flow in a pipe was introduced by Barozzi and Pagliarini [5]. The superposition principle with finite element method was employed. They considered the wall conduction effect on heat transfer to fully developed laminar pipe flow with the exterior boundary was uniformly heated along a finite length. They showed that axial conduction in the wall lowered the Nusselt number with respect to the case in which the axial conduction was largest.

Parakash and Liu [6] analyzed the laminar flow and heat transfer in the entrance region of an internally finned circular duct by numerically integrating the governing partial differential equations. They considered two types of boundary conditions, the uniform heat input per unit axial length with peripherally uniform temperature at any cross section and the uniform temperature both axially and peripherally. Their results exhibited the expected high-pressure gradients and heat transfer coefficients in the entrance region, approaching asymptotically the fully developed values at large axial distance.

The transient convective heat transfer to a fluid flow within a pipe due to sudden change in the temperature of the ambient medium outside the pipe was considered by Sucec [7]. He developed a solution by the Laplace transformation for the pipe wall temperature, surface heat flux, and fluid bulk mean temperature. He developed a criterion for the zero thermal capacity wall solution, which could be used with adequate accuracy.

Unsteady conjugate heat transfer in laminar pipe flow, where the flow was both hydrodynamically and thermally fully developed was investigated by Olek et al [8]. They considered two cases: a prescribed constant wall temperature and a constant heat flux at the wall and they applied a non-standard method of separation of variables, which treated the fluid and the solid as single region with certain discontinuities. They indicated that the degree of conjugation and viscous dissipation might have a great impact on the temperature distribution in the fluid.

The conjugate heat transfer in the entrance region of a circular pipe was analyzed by Yen and Lee [9]. They solved the Navier-Stokes and energy equations by the Galerkin finite element method for the pipe heated externally by a uniform heat flux. They found that the influence of solid wall heat conduction on the flow was significant.

Numerical simulation of transitional flow and heat transfer in a smooth pipe was considered by Huiren and Songling [10]. A low-Reynolds number k-ε turbulence model was used to simulate the laminar, transitional and turbulent flow zones. They indicated that the flow and heat transfer were not affected by the inlet turbulence intensities in the fully developed region. The predicted relation between average Nusselt number and Reynolds number, which was in good agreement with the experimental data.

A numerical study of fully developed laminar flow and heat transfer in a curved pipe with arbitrary curvature ratios was carried out by Yang and Chang [11]. They correlated the friction and Nusselt number ratios with the parameters of the curvature ratios, the Dean, and the Prandtl numbers.

The transient conjugate heat transfer in developing laminar pipe flow was investigated by Al-Nimr and Hader [12]. They applied the finite difference equations to solve the governing equations. They found that increasing the thermal conductivity ratio increased the wall heat flux, while increasing the diffusivity ratio increased the thermal entrance length of the pipe. However, increasing the radius ratio reduced the thermal entrance length.

Laminar flow heat transfer in pipes including two-dimensional wall and fluid axial conduction was studied numerically by Bilir [13]. He considered the thick-wall and two regional pipe, which had constant outside surface temperature. His method exhibited a simple and fast tool to solve the complicated heating problem. He indicated that the Peclet number, thickness ratio and wall to fluid conductivity ratio were the important parameters on the resulting temperature profiles.

The transient conjugate heat transfer in a thick-walled pipe with developing laminar flow was studied by Schutte et al [14]. By simultaneously solving for conduction in the pipe wall and for convection in the fluid stream, they analyzed the transient behavior of the flow and temperature fields. They considered two transient situations namely; the transient heat transfer in developing pipe flow, and heat transfer in simultaneous development flow in a pipe. They found that the ratio of wall thickness to inner diameter, Peclet number, ratio of wall to fluid thermal conductivities, significantly influenced the duration of the transient as well distribution of Nusselt number, interfacial temperature, bulk temperature, and interfacial heat flux during the transient processes. The ratio of wall to fluid thermal diffusivities had also an important effect.

Shome and Jensen carried a numerical analysis on thermally developing mixed flow and heat transfer with variable viscosity in an isothermally heated horizontal tube [15]. They performed parametric computations on the effects of inlet Prandtl temperature, inlet Rayleih number, wall-to-inlet temperature difference and inlet axial velocity profile on the Nusselt numbers and apparent friction factors for both heating and cooling conditions. Their results indicated that the effect of variable velocity is more pronounced on the friction factor than on Nusselt numbers. The effect of inlet Rayleih number and inlet velocity profile on the Nussselt number and friction factors is significant only in the near-inlet region. They noted that the correlation developed between the Nusselt number and the friction data had wider applicability than those available in the literature.

Min et al [16] analyzed the thermally fully developed and thermally developing laminar flows of a Bingham plastic in a circular pipe. He has obtained the solution to the Graetz problem by using the method of separation of variables and discussed the effects of the Peclet number and Brinkman numbers on the Nusselt number.

Lin and Faghri [17] investigated the flow behavior and the related heta transfer characteristics of stratified flow in axially rotating heat pipes with cylindrical and stepped wall configurations. They developed theoretical and semi-empirical models for calculation of the condensation and evaporation heat transfer coefficients. They found a good agreement between the predicted results and the experimental data.

**Turbulent Flow**

Chien [18] introduced a low-Reynolds-number turbulence model to study the behavior of the turbulent channel stress, the kinetic energy and its rate of dissipation near a solid wall. He applied his model to the problem of a fully developed turbulent channel flow and the results compared well with the experimental data.

The vertical tube air flows in the turbulent mixed convection region was investigated by Cotton and Jackson [19]. They indicated that the prediction agreed with the experimental results provided that the major discrepancies were due to strongly buoyancy-influenced descending flow. They introduced an unsteady version of the k-ε scheme when modeling the turbulence. They indicated that the accuracy of the model deteriorated with an increasing level of unsteadiness. One important observation in their study was the occurrence of very long thermal-hydraulic development lengths arising in the ascending flow configuration.

A low Reynolds number k-ε model was introduced to predict rough-wall boundary layers by Tarada [20]. He formulated and calibrated a complemetary roughness drag coefficient model that took into account the isolated, wake interference and skimming roughness flow regimes.

The quasi-steady turbulence modeling of unsteady flows were studied by Mankbadi and Mobarak [21]. They introduced an unsteady version of the k-ε scheme when modeling the turbulence. They indicated that the accuracy of the model deteriorated with an increasing level of unsteadiness.

Velusamy et al [22] investigated the fully developed flow and heat transfer in semi-elliptical ducts using a control volume-based numerical scheme. They considered both an isothermal and a uniform axial heat flux condition on the duct walls and presented their numerical results for velocity and temperature profiles, friction factor, pressure defect, and Nusselt number for a wide range of duct aspect ratios. They found that the ratio of Nusselt number to friction factor was higher for semi-elliptical ducts in comparison to that for other ducts, such as sinusoidal, circular segmental, and triangular ducts.

The pressure drop and heat transfer in turbulent flow and heat transfer in duct flows were investigated by Ghariban et al [23]. A two-parameter variational method, which used the Prandtl mixing length theory to describe turbulent shear stress, was introduced to determine pressure distribution and heat transfer. Their analysis leaded to the development of a Green's function, which was used for solving a variety of conjugate heat transfer problems.

The friction and heat transfer characteristics of turbulent flow in long circular pipe was investigated by Choi and Cho [24]. They introduced a new turbulent heat transfer correlation for the prediction of local Nusselt number. They found that when a large heat flux was applied at the wall, the viscosity of water significantly decreased along the axial direction due to increasing temperature of fluid. They also introduced the concept of a "redeveloping region", where the local heat transfer coefficient increased, while the local friction coefficient decreased due to the decrease of the viscosity in the axial direction.

An experimental study of turbulent flow in pipe contractions was carried out by Bullen et al [25]. The effect of variations in contraction sharpness was established. The inlet sharpness was found to have a significant effect on the flow. The paper provided a summary of the pressure loss data and details of the contraction flow fields in terms of vena contracta size and position as well as detailed velocity profiles, derived enhancement factors and turbulence data for an incompressible flow.

Wosnik et al [26] proposed a theory for fully developed turbulent pipe flow. The theory extended from the classical analysis to include the effects of finite Reynolds number. Using the Reynolds-averaged Navier-Stokes equations, the proper scaling for flow at finite Reynolds number was developed from dimensional and physical considerations. An excellent description of the mean velocity and skin friction data for wide ranges of Reynolds numbers were.

A comparison was made for twelve versions of low Reynolds number k-ε and two low Reynolds number stress models for heat transfer by Thaker and Joshi [27]. The comparison included the predictions of the mean axial temperature, the radial and axial turbulent heat fluxes, and the effect of the Pradtl number on Nusselt number with experimental data. They showed that the k-ε models performed relatively better than the Reynolds stress models for predicting the mean axial temperature and the Nusslet number. In another study [28], they showed that the accurate predictions of turbulent energy dissipation rate in the thin layer near wall not only gave good energy balance, but also improved the predictions of the turbulence quantities.

**Pulsating Flow**

Siegel and Perlmutter [29] obtained heat-transfer solutions for pulsating laminar flow in ducts. The conditions of constant wall temperature ducts and a specified uniform heat flux transferred to the walls of the duct were considered. They showed that for high frequency oscillations, the effect of the velocity oscillations was not of practical significance and that the total heat transfer for laminar flow was not appreciably changed by the oscillations in the case of a constant wall temperature.

The flow due to an oscillating piston in a circular tube was studied by Gerard and Hughes [30]. They measured the velocity of flow on the axis of the circular tube over a range of distances from a reciprocating piston in simple harmonic motion. They calculated the developing flow based on a comparison with steady laminar flow, which, in the entry region of a circular tube, approached the fully developed state exponentially with the distance from the entry. A comparison was made between the experimental and the simple entrance flow theory results.

Calmen and Minton experimentally investigated the flow in an oscillating pipe [31]. They have measured the velocities of the pulsating water flow in a rigid circular pipe using the hydrogen-bubble technique. It was found that the velocities in the oscillating boundary layers on the pipe wall to be close to those predicted by laminar flow theory, while at the higher Reynolds numbers the velocities near the center of the pipe were lower than those predicted and more uniformly distributed.

Faghri et al [32] studied the problem of heat transfer from a cylindrical pipe for a case where the flow inside the pipe consisted of a periodic motion imposed on a fully developed steady laminar flow. They showed that the interaction between the velocity and temperature oscillation introduced an extra term in the energy equations, which reflected the effect of pulsations in producing high heat transfer rates.

The dynamic and thermal results for developing laminar pulsed flows in a duct were presented by Creff et al [33]. They used a finite difference model to carry on their investigations. The flow was described by imposing an unsteady pulsed flow on a steady incompressible one assuming a sinusoidal modulation for the pulsation and a uniform wall temperature. The study shows the existence of four developing regions beyond the entry of the duct.

The enhanced heat transfer via sinusoidal oscillating flow through circular tubes was investigated by Kurzweg [34]. A calculation for the effective thermal diffusivity was made and used to determine the enhanced conduction heat transfer. He indicated that the enhanced heat transfer produced by the oscillations was proportional to the square of the oscillation amplitude and a function of the Prandtl number, frequency and tube radius.

The laminar forced convection inside ducts with periodic variation of inlet temperature was examined by Cotta and Ozisik [35]. They used the generalized integral transform technique to reduce the original problem to a system of linear first order differential equations. They determined the amplitude and phase lag of temperature oscillation with respect to the inlet condition in terms of fluid bulk temperature and wall heat flux.

Siegel [36] studied the influence of oscillation-induced diffusion on heat transfer in a uniformly heated channel. He assumed that the channel was so long enough so that the thermal entrance effects could be neglected. He showed that for forced convection in slow laminar flow in a channel with uniform heat addition, the effect of flow oscillations was to reduce the channel heat transfer coefficient.

The case of ducts with periodically varying inlet temperature was investigated by Cotta et al [37]. The transient forced convection for slug flow inside circular ducts including conjugation to the walls was solved analytically. They solved the complex eigenvalue problem by using the advanced Count method and presented the amplitude of the phase lag oscillations with respect to the conditions at the inlet determined for the wall temperature, fluid bulk temperature and heat flux.

The heat transfer in laminar oscillating flow in cylindrical and conical tubes was examined by Peattie and Budwig [38]. They showed that the convective transport increased with frequency at constant amplitude.

Numerical solutions for flow and heat transfer characteristics were presented for pulsating flow in pipes in [39]. Complete time-dependent laminar boundary layers were solved for a wide range of parameter spaces, frequency of pulsation and amplitude of oscillation. It was also demonstrated that the Nusselt number increased with increasing amplitude and frequency of oscillation and that the skin friction was generally greater than that of a steady flow. The heat transfer characteristics were qualitatively consistent with previous theoretical predictions.

A study investigating the case of a duct with a periodically varying inlet temperature was carried out by Li and Kakac [40]. A uniform heat flux and/or external convection with or without wall thermal capacitance effects were considered in the study. They extended the generalized integral transform technique to obtain analytical expressions for these problems. They discussed the effects of the Biot number, fluid-to-wall thermal capacitance ratio and dimensionless inlet frequency of inlet heat input oscillations. It was shown that the effect of external convection, Biot number on the temperature responses along the duct was only important in the case of certain fluid-to-wall thermal capacitance ratio.

Laminar and turbulent oscillating flow in circular pipes was investigated by Ahn and Ibrahim [41]. A high Reynolds number k-ε turbulence model was used to account for the turbulence in the pipe. They indicated that the standard k-ε turbulence model could not adequately predict the oscillating flow properties in a transition flow regime.

The heat transfer in the thermally developing region of a pulsating channel flow was discussed by Kim et al [42]. They solved the Navier-Stokes equations numerically to simulate a flow with certain Prandtl and Reynolds numbers. Using Fourier-series representations for the numerical results, detailed analyses on local behavior of the heat transfer were made. Their results indicated that, due to pulsation, both heat transfer enhancement and reduction could be expected in various axial locations of the channel.

Valueva, E.P et al [43] solved numerically the problem of heat transfer under hydrodynamically stabilized laminar pulsating flow of a liquid in a round tube assuming constant wall temperature and fluid properties for a wide range of operating conditions. They found that the heat flow rate oscillated relative to the steady state with amplitude that decreased downstream.

A moving mesh to compute hydrodynamic forces and coefficients of damping acting on oscillating bodies was described by Brunet and Lise [44]. The flows were computed by the integration of the Navier-Stokes equations obtained from a k-ε turbulence model. Their model results proved credible when compared with experimental results.

Numerical and experimental analysis of unsteady heat transfer with periodic variation of inlet temperature in circular ducts was carried out by Brown et al [45]. They indicated that the variations in the periods and amplitudes of the thermal oscillations were observed to be a function of system variables only, and the predictions agreed well with the experimental results.

Inaba [46] investigated the effect of a thermally permeable wall on the enhanced logitudinal heat transfer by fluid pulsation in a pipe. He presented an analytical solution for the case when heat loss through the wall over a cycle of fluid pulsation was uniform along the pipe. He concluded that the rate of longitudinal heat transfer decreased linearly toward the lower temperature end of the temperature.

Bauwens, L [47] considered the case of oscillating flow of a heat-conducting fluid in a narrow tube. He assumed that the temperature differences between the two ends were assumed to have arbitrary magnitude and heat transfer in the transverse direction within the fluid to be very effective and the thermal effect of the wall was large. He showed from the results obtained for tubes open at both ends that when velocities at both ends are in opposite phases, internal singularities in the temperature profiles might occur and in the case, where of one end closed, a singularity occurred at the closed end.

A numerical study on the interaction of a steady approach flow and the forced transverse oscillation of a circular cylinder was presented by Zhang, et al [48]. A semi-implicit finite difference scheme was used to solve the Navier-Stokes equations based on a two-dimensional stream-function/vorticity formulation. The finite difference calculations agreed well with the experimental results.

The Nusselt number in pulsating pipe flow, for an unsteady, laminar as well as fully developed flow was investigated by Guo and Sung [49]. They tested many versions of the Nusselt numbers to clarify the conflicting results in the heat transfer characteristics for a pipe flow.

The pulsating flow and heat transfer characteristics in a circular pipe partially filled with a porous medium were studied numerically by Guo et al [50]. They examined the enhanced longitudinal heat conduction due to pulsating flow and the enhanced convective heat transfer from high conducting porous material. The maximum effective thermal diffusivity was found at a critical thickness of porous layer.

Heat transfer in a tube with pulsating flow and constant heat flux was investigated analytically by Moschandreou and Zamir [51]. They indicated that in a range of moderate values of the frequency, there was a periodic peak in the effect of pulsations whereby the bulk temperature of the fluid and the Nusselt number were increased. However, the effect was reversed when the frequency was outside of this range.

The Richardson's "annual effect" in oscillating laminar duct flows was investigated by Yakhot et al [52]. They concluded that the Richardon's annual effect, which was found in high frequency oscillating flows in pipes, also took place for oscillating flows in ducts of arbitrary cross sectional shapes.

Habib et al [53] investigated experimentally the heat transfer characteristics of a pulsating turbulent pipe flow under different conditions of pulsation frequency, amplitude and Reynolds number. A uniform heat flux was applied to the pipe wall. They showed that a reduction of heat transfer coefficient was observed at higher frequencies and the effect of pulsation was found to be significant at high Reynolds number.

**Thermal stresses in Pipes**

A study about the stress distribution in a metal tube, which was subject to a very high radial temperature variation and pressure, was presented by [54]. From experimental data, the radial temperature distribution across the tube wall and the variations of the modulus of elasticity, and the coefficient of thermal expansion were obtained and taken into account in calculations. The corresponding solutions were obtained by the method of variation of parameters and in terms of Kummer series. Examples for the stress solutions were given.

Sinha [55] applied the finite element method to analyze the thermal stresses and temperature distributions in a hollow thick cylinder subjected to a steady-state heat load in the radial direction. He studied three test models of a cylinder with different geometric configurations, elastic properties, and temperature gradients assuming a logarithmic temperature field over the thickness of the cylinder. The finite element method results and the analytical results were agreed well.

Stresses in hollow orthotropic elastic cylinders due to steady-state plane temperature distribution were analyzed by Kalam and Tauchert [56] for traction free boundary conditions. They obtained analytical solution for the stress field using a Fourier-series form.

A thermal-stress analysis of hollow cylinder with temperature-dependent thermal conductivity was investigated by Stasyuk et al [57]. Assuming a heat flux on the outside wall of the cylinder, the temperature distribution was obtained. Formulas for the radial and tangential stresses were derived.

The effect of induction heating stress remedies on existing flaws in pipes was investigated by Shadley et al [58]. They indicated that the smaller diameter pipes were subjected to higher thermal stresses.

Naga [59] presented a stress analysis and optimization of both thick walled impermeable and permeable cylinders under the combined effect of temperature and pressure gradients. He concluded that in thick walled solid and porous cylinder operating under high pressure and applications, the stress distribution could be optimized by just introducing a heat source in the cylinder in such away to satisfy certain optimization criteria.

Tamma and Railkar [60] introduced a new unified computational approach for applicability to nonlinear/linear thermal-structural problems. The approach was demonstrated for thermal stress and thermal-structural dynamic applications. By combining the modeling versatility of contemporary finite element schemes in conjunction with transform techniques and the classical Bubnov-Galerkin schemes, their proposed transfinite element approach provided a viable hybrid computational methodology.

The relationship between material properties and structural ratcheting for thin cylindrical shells subjected to severe thermal loading was discussed by Kardeniz et al [61]. The finite element technique was used to find the solution. They showed that for tubes subjected to moving temperature fields, ratcheting could occur even when no mechanical loads were applied and that stationary thermal cycling was less likely to produce ratcheting.

Kardomateas [62] studied the initial phase of transient thermal stresses due to general boundary thermal loads on orthotropic hollow cylinders. He used the Hankel asymptotic expansions for the Bessel functions of the first and second kinds and illustrated the variation of stresses with time and through the thickness in the initial transient phase under the condition of constant applied temperature at outer surface.

The dynamic thermal stresses in composite hollow cylinders and spheres caused by sudden heating were investigated by Sumi and Ito [63]. They introduced a numerical method to determine transient uncoupled dynamic thermal stresses. They demonstrated the existing discontinuities in stress and velocity fields due to the sudden heating on the inner boundary of the cylinders.

Kurashige [64] studied the thermal stresses in a fluid-saturated Poroelastic hollow cylinder. He used the thermoporoelastic theory developed by him to analyze the thermal stresses, which were induced in a fluid-saturated porous hollow cylinder, subjected to a sudden increase in temperature and pressure on its inner surface. The coupled diffusion equations for heat and fluid flows were solved by the Crank-Nicolson implicit method. The influence of heat transportation, by fluid flow through pores on the temperature and thermal stress distributions was found to be significant in the case where the fluid diffusivity was much larger than the thermal diffusivity, which in turn suggested the possible control of thermal stresses by active fluid injection.

The steady thermal stresses in a hollow circular cylinder and a hollow sphere made of functionally gradient material were investigated by Obata and Noda [65]. They discussed the influence of inside radius size on stresses and the temperature regions. They also investigated the effect of the composition on stresses as well as the design of optimum fuctionally gradient material hollow circular cylinder and hollow sphere.

The thermal stresses produced by a thermal gradient in the wall of a partially filled horizontal cylindrical vessel were investigated by Russo et al [66]. They considered three types of thermal gradients, namely the discontinuous temperature change, the hyperbolic temperature change and the linear temperature change at the liquid level.

Kaizu et al [67] used the finite difference method to analyze the two-dimensional dynamic thermal stresses in semi-infinite circular cylinder. The method employed the integration of differential equations along the bi-characteristics. By this, they investigated the propagation, reflection, and interaction of the stress waves in a body.

Transient thermal stresses in hollow cylinders were studied by Russo et al [68]. They nine types of boundary conditions were introduced. They have showed that the transient stresses might be momentary and rapidly decay as the temperature spreaded inward and contraction or expansion of the outer layer of the cylinder was permitted. They showed that the transient stresses could be sufficient to produce a permanent set in the material, which in turn caused residual stresses to be present.

Zhdanov et al [69] studied the thermoelastic stresses in ribbons and tubes grown from the melt using the Stepanov method. They calculated the dependence of thermoelastic stresses in ribbons and tubes on different parameters, such as the wall thickness and the tube diameter. They concluded that the normal stress in the ribbons was maximum at the center on the interface boundary and that an increase in the heat transfer from the tube surface caused an increase in the maximum circular and tangential stresses.

The transient thermal stress analysis of thick-walled cylinders was studied by Kandil et al [70]. They concluded that the maximum effective stress occurred at the inside surface of the cylinder, and its peak value took place at the start of the operating temperature. Furthermore, they suggested that the inner surface should be heated gradually up to the operating temperature, which in turn resulted in reduced effective stress on the cylinder.

Thermal stresses in a cylinder with longitudinal circular cylinder cutouts were studied by Naghdi [71]. He used a special class of basis functions of Laplace and biharmonic equations when solving a steady-state thermal stress distribution in a long cylinder with N equally spaced longitudinal circular cylindrical cavities. He considered the case where the inner and outer walls of the cylinder were kept at constant temperatures and the case of a constant temperature applied at the inner wall and convection applied at the outer wall.

The analysis of thick-walled cylindrical pressure vessels under the effect of cyclic internal pressure and cyclic temperature was carried out by Kandil [72]. Using the finite difference technique, he obtained the time-dependent stress distribution in the wall of cylinder. The influence of the mean pressure, mean temperature, pressure and temperature amplitudes, diameter ratio on the effective stresses were included in the study. An approximate expression for the relation between the working parameters was introduced. He demonstrated that the result of the approximate solution was found to fit well with the numerical findings.

Tanaka et al [73] formulated a method of macroscopic material tailoring in order to reduce the thermal stresses induced in the functionally gradient materials. This was done with the help of the direct sensitivity analysis and the multiobjective optimization technique associated with the heat conduction/thermal stress analysis by means of incremental finite element method. They tailored successfully a hollow cylinder in a ceramic-metal functionally gradient material when was subjected to asymmetric thermal boundary/initial conditions.

Two methods for solving the transient inverse heat conduction problems in complex shaped elements were presented by Taler et al [74]. They used the finite element method for finding the thermal stresses. When applied to practical problems, their methods showed high accuracy.

Random thermal boundary conditions applied to steam generator tubes and general applications were simulated by Klevtsov and Crane [75]. The transient heat transfer rates and the wall stresses were determined due to pressure and temperature oscillations. They analyzed statistically the resultant wall temperature and stress oscillation data to provide the effective parameters used to estimate the metal fatigue.

Praveen et al [76] studied the pseudodynamic thermoelastic response of functionally graded ceramic-metal cylinder. They used a finite element formulation of a 1-dimensional axisymmetric heat transfer equation and the thermoelastic radial boundary value problem. The nonlinearity due to temperature dependence of the material properties of the constituent ceramic and metal was considered. Their analysis provided information about the thermoelastic response of cylinders for different proportions of the ceramic and metal.

An analytical method of calculating thermal stress distributions in cylindrical vessels, which were nonuniformly heated on their circumference, was presented by Taler et al [77]. The finite element method was used to compute the thermal stresses based on the temperature measurements. Comparison of the thermal distributions from the analytical method and the finite element method demonstrated the accuracy of the new analytical method.

Beraun et al [78] studied the thermally induced elastic fracture around a localized energy source on a pressurized cylindrical vessel. Analytical solutions for the identification of the dominating parameters in thermal cracking were obtained. The transition between the thermally and the mechanically driven fracture patterns were determined in the study.

The nonlinear conduction-convection-radiation heat transfer equation was solved by the hyprid method, which combined the Taylor transformation and the finite difference approximation, to find the transient temperature distribution in isotropic annular fins by Yu and Chen [79]. The thermal stresses were integrated to find the temperature field. The model predicted quite accurately the dynamic performance of an annular fin in a transient state.

Reinhardt et al [80] modeled the perforated region of a tubesheet undergoing rapid transient thermal loading using a solid with equivalent elastic-plastic properties. They used an anisotropic Hill-type plasticity model. The result of a transient thermal and elastic-plastic structural analysis of a heat was presented.

Closed-form integrals for creep deflection of pipe spans were derived by Becht IV and Chen [81]. The integrals were based on steady-state creep law. The solutions provided insight into the problem of establishing span limits for elevated temperature pipes.

The thermal ratcheting due to traveling temperature distribution in a hollow cylinder was presented by Igari et al [82]. An evaluation for a proposed mechanism for ratcheting was evaluated. The model based on the hoop-membrane stress due to the axial temperature distribution, and considered the influence of axial bending stress and traveling distance of temperature distribution. The results were obtained numerically by using the finite element method.

# CHAPTER 3

# MATHEMAYICAL MODELLING, NUMERICAL SOLUTION AND RESULTS VALIDATION

## 3.1 Introduction

In this chapter, the mathematical models for the three types of flow employed in the study and the governing thermal stress formulae are introduced. The numerical solutions used to solve the three models are also presented. In addition, the result validations with previous studies are included.

## 3.2 Mathematical Modeling

In this section, the mathematical models of the three types of flow employed in the study and the thermal stress formulae will be presented. The pipe flow and conjugate heating is shown schematically in figure (3.1.1). The flow field is assumed to be axisymmetric and uniform heat source is applied externally along the pipe length. It is also assumed that the flow has constant properties, i.e. independent of temperature and pressure.

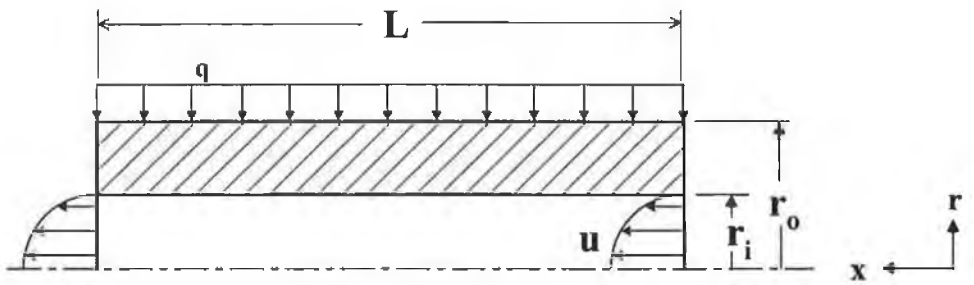


Figure 3.1.1 Schematic diagram of the pipe and coordinates

### 3.2.1 Boundary Conditions

The relevant boundary conditions for the conservative equations of flow and solid are:

1. At pipe axis:

Radial gradient of axial velocity and temperature are set to zero, while the radial velocity is taken as zero, i.e.:

$$\frac{\partial u}{\partial r}(x,0) = 0 \quad , \quad \frac{\partial T}{\partial r}(x,0) = 0 \quad \text{and} \quad v(x,0) = 0 \tag{3.2.1}$$

2. At inner solid wall ($r = r_i$, where $r_i$ is pipe inner radius):

No-slip conditions are considered, i.e.:

$$u(x,r_i) = 0 \qquad \text{and} \qquad v(x,r_i) = 0 \tag{3.2.2}$$

3. At pipe outlet:

All the gradients of the variables were set to zero, i.e.:

$$\frac{\partial \phi}{\partial \eta} = 0 \tag{3.2.3}$$

, where $\phi$ is the fluid property and $\eta$ is the arbitrary direction.

4. At outer surface of the pipe ($r = r_o$, where $r_o$ is pipe outer radius):
Uniform heat flux is assumed, i.e.:

$$r = r_o \qquad and \quad 0 \le x \le L \tag{3.2.4}$$

**5.** At solid-fluid interface, i.e.:

$$r = r_i \qquad \text{and} \quad 0 \le x \le L$$

$$\dot{q}_{specified} = k_{solid} \frac{\partial T_{solid}}{\partial r} = k_{fluid} \frac{\partial T_{fluid}}{\partial r} \tag{3.2.5}$$

and

$$T_{solid} = T_{fluid} \tag{3.2.6}$$

**6.** At pipe inlet:

The flow is assumed to be at uniform temperature, i.e.:

$$\frac{\partial T}{\partial r}(0, r, t) = 0 \tag{3.2.7}$$

The type of flow is specified based on the considerations made:

a. Fully developed laminar flow:

A unidirectional fully developed laminar flow is assumed. The local velocity is described by the formula:

$$u = 2u_{mean}\left(1 - \frac{r^2}{r_o^2}\right) \tag{3.2.8}$$

b. Turbulent flow:

A unidirectional flow with uniform inlet speed is assumed.

c. Pulsating flow:

The flow inlet to the to the pipe is considered as pulsating at a constant frequency and amplitude. A unidirectional flow with pressure pulsation is assumed, i.e.:

$$p(0,r,t) = A\sin(nt) \tag{3.2.9}$$

, where n is the pulsating frequency.

### 3.2.2 Governing Thermal Stresses Formulae

In the solid, the governing heat conduction equation for the steady-state cases (applicable for fully developed laminar and turbulent flow situations) is:

$$\frac{1}{r}\frac{\partial}{\partial r}\left(r\frac{\partial T}{\partial r}\right)+\frac{\partial^2 T}{\partial x^2}=0 \tag{3.2.10}$$

and for the transient case (pulsating flow):

$$\frac{\partial T}{\partial t}=\chi\left[\frac{1}{r}\frac{\partial}{\partial r}\left(r\frac{\partial T}{\partial r}\right)+\frac{\partial^2 T}{\partial x^2}\right] \tag{3.2.11}$$

The relation between thermal stress and strain follows the thermoelasticity formulae [72], i.e.:

$$\varepsilon_\theta=\frac{1}{E}\left[\sigma_r-\nu\left(\sigma_\theta+\sigma_x\right)\right]+\alpha T \tag{3.2.12}$$

$$\varepsilon_x=\frac{1}{E}\left[\sigma_x-\nu\left(\sigma_\theta+\sigma_r\right)\right]+\alpha T \tag{3.2.13}$$

$$\varepsilon_x=\frac{1}{E}\left[\sigma_x-\nu\left(\sigma_\theta+\sigma_r\right)\right]+\alpha T \tag{3.2.14}$$

Solving the above equations for a hollow cylinder results in [83]:

$$\sigma_\theta = \frac{E\alpha}{(1-\nu)r^2}\left[\frac{r^2+r_i^2}{r_o^2-r_i^2}\int_{r_i}^{r_o} T.r\,dr + \int_{r_i}^{r} T.r\,dr - T.r^2\right] \qquad (3.2.15)$$

$$\sigma_r = \frac{E\alpha}{(1-\nu)r^2}\left[\frac{r^2-r_i^2}{r_o^2-r_i^2}\int_{r_i}^{r_o} T.r\,dr - \int_{r_i}^{r} T.r\,dr\right] \qquad (3.2.16)$$

$$\sigma_x = \frac{E\alpha}{1-\nu}\left[\frac{2}{r_o^2-r_i^2}\int_{r_i}^{r_o} T.r\,dr - T\right] \qquad (3.2.17)$$

The effective stress according to Von-Mises theory [84] is:

$$\sigma_v = \left[\sigma_\theta^2 + \sigma_r^2 + \sigma_x^2 - (\sigma_\theta\sigma_r + \sigma_\theta\sigma_x + \sigma_r\sigma_x)\right]^{1/2} \qquad (3.2.18)$$

### 3.2.3 Fully Developed Laminar Flow

The governing flow equations can be written as follows:

1) The continuity equation:

$$\frac{\partial u}{\partial x} + \frac{1}{r}\frac{\partial (rv)}{\partial r} = 0 \qquad (3.2.19)$$

2) The axial momentum equation in the x-direction

$$u\frac{\partial u}{\partial x} + v\frac{\partial u}{\partial r} = -\frac{\partial p}{\partial x} + \frac{1}{r}\frac{\partial}{\partial r}\left(r\mu\frac{\partial u}{\partial r}\right) \qquad (3.2.20)$$

3) The energy equation

$$\frac{1}{r}\frac{\partial}{\partial r}(\rho rvT)+\frac{\partial}{\partial x}(\rho uT)=\frac{1}{r}\frac{\partial}{\partial r}\left[r\left(\frac{\mu}{P_r}\right)\frac{\partial T}{\partial r}\right] \tag{3.2.21}$$

### 3.2.4 Turbulent Flow

The mean flow equations are simplified after the consideration of Boussinesq approximations [85]. In cylindrical polar coordinates the conservation equations are written.

Continuity:

$$\frac{\partial u}{\partial x}+\frac{1}{r}\frac{\partial}{\partial r}(vr)=0 \tag{3.2.22}$$

Momentum:

$$\frac{1}{r}\frac{\partial}{\partial r}(rvu\rho)+\frac{\partial}{\partial x}(\rho u^2)=-\frac{dp}{dx}+\frac{1}{r}\frac{\partial}{\partial r}\left[r(\mu+\mu_t)\frac{\partial u}{\partial r}\right] \tag{3.2.23}$$

Energy:

$$\frac{1}{r}\frac{\partial}{\partial r}(rvT\rho)+\frac{\partial}{\partial x}(\rho uT)=\frac{1}{r}\frac{\partial}{\partial r}\left[r(\frac{\mu}{Pr}+\frac{\mu_t}{Pr_t})\frac{\partial T}{\partial r}\right] \tag{3.2.24}$$

, where Pr and $Pr_t$ are bulk and turbulent Prandtl numbers respectively. In order to determine the turbulent viscosity and the Prandtl number, the k-ε model is used. The constitutive equations for the turbulent viscosity are as follows:

$$\mu_t=c_\mu c_d\frac{\rho k^2}{\varepsilon} \tag{3.2.25}$$

, where k and ε are the turbulent kinetic energy generation and the dissipation variable respectively. The transport equation for k is:

$$\frac{1}{r}\frac{\partial}{\partial r}(rvk\rho)+\frac{\partial}{\partial x}(\rho uk)=\mu_t(\frac{\partial u}{\partial r})^2+\frac{1}{r}\frac{\partial}{\partial r}\left[r(\mu+\frac{\mu_t}{Pr_t})\frac{\partial k}{\partial r}\right]-\rho(\varepsilon+D_\varepsilon) \qquad (3.2.26)$$

, where

$$D_\varepsilon=2(\mu/\rho)(\frac{\partial k}{\partial y})^2 \qquad (3.2.27)$$

ε attains zero at y = 0.

The transport equation for ε is:

$$\frac{1}{r}\frac{\partial}{\partial r}(rv\varepsilon\rho)+\frac{\partial}{\partial x}(\rho u\varepsilon)=c_{\varepsilon 1}\frac{\varepsilon}{k}\mu_t(\frac{\partial u}{\partial r})^2+\frac{1}{r}\frac{\partial}{\partial r}\left[r(\mu+\frac{\mu_t}{Pr_t})\frac{\partial \varepsilon}{\partial r}\right]-$$
$$c_{\varepsilon 2}\frac{\rho\varepsilon^2}{k}+\frac{2\mu\mu_t}{\rho}(\frac{\partial^2 w}{\partial r^2})^2 \qquad (3.2.28)$$

In order to minimize computer storage and run times, the dependent variables at the walls were linked to those at the first grid from the wall by equations, which are consistent with the logarithmic law of the wall. Consequently, the resultant velocity parallel to the wall in question and at a distance $y_1$ (where $y^+ \leq 2$) from it corresponding to the first grid node was assumed to be represented by the law of the wall equations [85], i.e.:

$$\frac{V_o c_d c_\mu k^{1/2}}{\tau_{wall}/\rho}=\frac{1}{\kappa}\ln[e(c_d c_\mu)^{1/2}k^{1/2}y_1\frac{\rho}{\mu}] \qquad (3.2.29)$$

, where

$\kappa = 0.417$ and $e = 9.37$

, from which the wall shear stresses were obtained by solving the momentum equations.

The constants used in the transport equations are:

$$c_\mu = 0.5478 \quad ; c_d = 0.1643 \quad ; c_{\varepsilon 1} = 1.44 \quad ; c_{\varepsilon 2} = 1.92$$

$$\mathrm{Re}_t = \frac{k^2}{(\mu/\rho)\varepsilon} \quad ; \mathrm{Pr}_k = 1.0 \quad ; \mathrm{Pr}_\varepsilon = 1.314 \qquad (3.2.30)$$

In order to be consistent with the conditions for the previous findings, turbulent Prandtl number ($Pr_t$) was changed as indicated in figure (3.2.1).

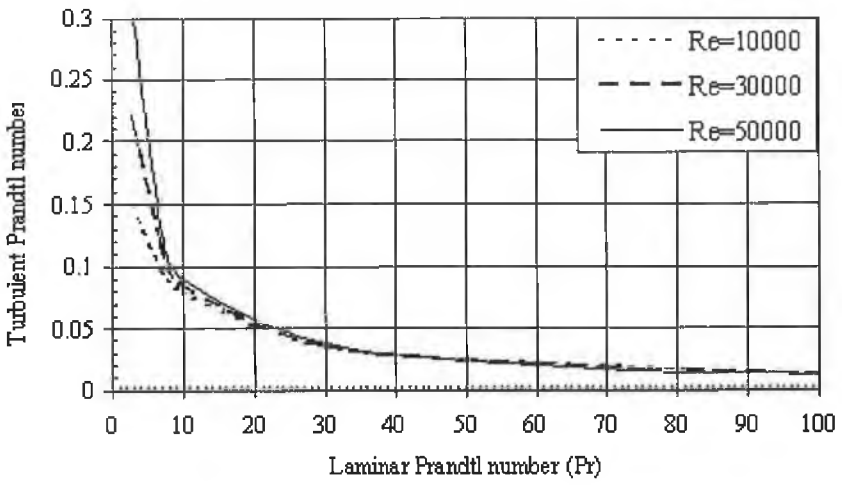


Figure 3.2.1 The turbulent Prandtl numbers for various Reynolds numbers at different Laminar Prandtl numbers [86].

### 3.2.5 Pulsating Flow

The equations governing the flow and heat transfer can be written as follows.

**The continuity equation:**

$$\frac{\partial u}{\partial x}+\frac{1}{r}\frac{\partial(rv)}{\partial r}=0 \tag{3.2.31}$$

**The momentum equation:**

$$\frac{\partial u}{\partial t}+u\frac{\partial u}{\partial x}+v\frac{\partial u}{\partial r}=-\frac{1}{\rho}\frac{\partial p}{\partial x}+\frac{1}{r}\frac{\partial}{\partial r}\left(r\nu\frac{\partial u}{\partial r}\right) \tag{3.2.32}$$

**The energy equation:**

$$\rho c_p\frac{\partial T}{\partial t}+\frac{1}{r}\frac{\partial}{\partial r}(\rho c_p vT)+\frac{\partial}{\partial x}(\rho c_p uT)=k_f\left[\frac{\partial^2 T}{\partial x^2}+\frac{1}{r}\frac{\partial}{\partial r}\left(r\frac{\partial T}{\partial r}\right)\right]+\mu\Phi \tag{3.2.33}$$

, where

$$\Phi=2\left[\left(\frac{\partial v}{\partial r}\right)^2+\frac{1}{r^2}v^2+\left(\frac{\partial u}{\partial z}\right)^2\right]+\left[\frac{\partial u}{\partial r}+\frac{\partial v}{\partial z}\right]^2 \tag{3.2.34}$$

## 3.3 Numerical Solution and Results Validation

The thermal stresses (equations (3.2.15)-(3.2.18)) due to the pipe heating are computed numerically after obtaining the temperature distribution in the pipe wall.

Generally, the numerical method used to determine a numerical solution to a set of differential equations has the following steps:

1. Discretization of the differential equations into algebric equations using approximations for the differential operators.

2. Solution of the algebric equations by direct or iterative methods.

Numerical methods differ from each other in the method of approximation introduced for the discretization of the differential equations. The second step i.e. solution to the resulting algebraic equations is general for all the numerical methods. In this study, the Finite Volume Method is employed to discretize the calculation domain by dividing it into a number of non-overlapping control volumes such that there is one control volume surrounding each grid point. The differential equation is integrated over the control volume. Piecewise profiles expressing the variation of variable $\phi$ for a group of grid points. The discretization equation obtained in this manner expresses the conservation principle for the finite control volume such as the differential equation expresses it for the infinitesimal control volume.

In vector notation, the general transport equation for steady state situation is given by

$$\nabla.(\rho U\phi) = \nabla.(\Gamma_\phi \nabla\phi) + S \qquad (3.3.1)$$

This equation is integrated over the finite control volume around the node P, shown in figure 3.3.1.

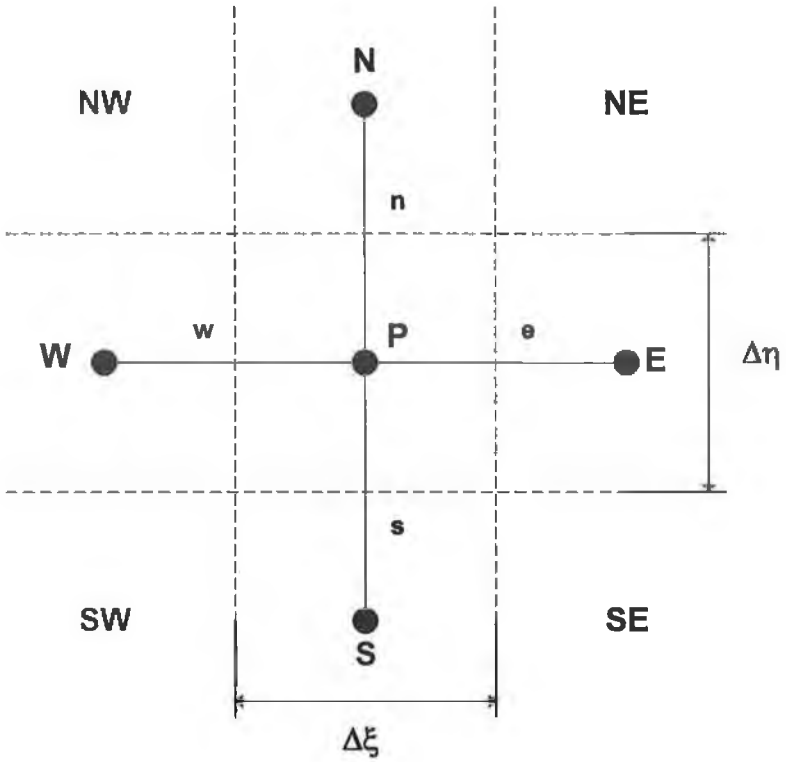


Figure 3.3.1 A finite control volume

We have

$$\int_s^n \int_w^e [\nabla.(\rho U\phi)]d\eta d\xi = \int_s^n \int_w^e \nabla.(\Gamma_\phi \nabla\phi)d\eta d\xi + \int_s^n \int_w^e S d\eta d\xi \qquad (3.3.2)$$

or

$$\left[\left(\rho u_\eta \phi - \Gamma_\phi \frac{\partial\phi}{\partial\eta}\right)\Delta\xi\right]_s^n + \left[\left(\rho u_\xi \phi - \Gamma_\phi \frac{\partial\phi}{\partial\xi}\right)\Delta\eta\right]_w^e = \overline{S}_\phi \Delta\xi\Delta\eta \qquad (3.3.3)$$

, where $u_\xi$ and $u_\eta$ are the compnents of the velocity vector U in the orthogonal coordinate directions $\xi$ and $\eta$ respectively and $\overline{S}_\phi$ is the average value of S over the finite control volume.

The total flux across the face of the finite control volume is represented by J for convenience. For the east face

$$J_e = \left[ \rho u_\xi \phi_e - \left( \Gamma_\phi \frac{\partial \phi}{\partial \xi} \right)_e \right] \Delta\eta \tag{3.3.4}$$

It is clear that total flux is composed of a convective flux and a diffusive flux. We represent them by $C_e$ and $D_e$ respectively.

$$C_e = \rho u_\xi \phi_e \Delta\eta \tag{3.3.5}$$

and

$$D_e = \left( \Gamma_{\phi e} \frac{\partial \phi}{\partial \xi} \right)_e \tag{3.3.6}$$

To get the linear algebric equations, the source term is appropriately linearized.

$$S_\phi = S_o + S_p \phi_p \tag{3.3.7}$$

Hence we have

$$J_e - J_w + J_w - Js = (S_o + S_p \phi_p) \Delta\eta \Delta\xi \tag{3.3.8}$$

To make further progress we need to make profile assumptions about the variation of $\phi$ within the finite control volume. For the diffusion flux a linear profile can be assumed. This results in the central discretization

$$D_e = \left( \Gamma_{\phi e} \frac{\partial \phi}{\partial \xi} \right)_e = \Gamma_{\phi e} \frac{(\phi_E - \phi_p)}{\Delta\xi_{PE}} \tag{3.3.9}$$

Central discretization is usually not appropriate for the convective flux and may be in non-physical oscillations in the solution. To make the discretization compatible with physical reality a hyprid scheme is used. Depending on the Cell Peclet number it uses either an upwind or central discretization for the convective flux $C_e$, Cell Peclet number is defined as

$$P_e = \frac{(\rho u_\xi \Delta\xi_{PE})}{\Gamma_{\phi e}} \tag{3.3.10}$$

Using Hybrid Scheme

$$C_e = \rho u_\xi \frac{(\phi_E + \phi_P)}{2} \Delta\xi \qquad \text{if } -2 \le P_e \le 2 \tag{3.3.11}$$

$$C_e = \rho u_\xi \phi_E \Delta\xi \qquad \text{if } P_e > 2 \tag{3.3.12}$$

$$C_e = \rho u_\xi \phi_P \Delta\xi \qquad \text{if } P_e < 2 \tag{3.3.13}$$

Similar expressions are obtained at other faces of the finite control volume. Substituting these expressions in equation 3.3.8, we get

$$(A_p - S_p)\phi_P = A_n\phi_n + A_s\phi_s + A_e\phi_e + A_w\phi_w + S_o \tag{3.3.14}$$

where

$$A_e = \frac{\Gamma_{\phi e}}{\Delta\xi_{PE}} - \rho u_\xi)_e \tag{3.3.15}$$

$$A_w = \frac{\Gamma_{\phi w}}{\Delta\xi_{WP}} - \rho u_\xi)_w \tag{3.3.16}$$

$$A_n = \frac{\Gamma_{\phi n}}{\Delta\eta_{PN}} - \rho u_\eta)_n \tag{3.3.17}$$

$$A_s = \frac{\Gamma_{\phi s}}{\Delta\eta_{SP}} - \rho u_\eta)_s \qquad (3.3.18)$$

$$A_P = A_e + A_w + A_n + A_s \qquad (3.3.19)$$

Here $u_\xi)_e$ represents $u_\xi$ velocity at east cell face. In this connection it should be clear that this velocity is not as interpolated one, but it is indeed calculated at cell faces in contrast to other variables whose values are calculated at the center of the cells, therefore, at faces the values can be obtained through interpolation. This arrangement is highly beneficial to avoid non-physical oscillatory solution for the pressure field and to increase the accuracy.

For an imcompressible flow, no explicit equation is given for the pressure. Also, the resulting velocity field obtained from the solution of the momentum equations will not satisfy the continuity equation. PHOENICS uses the SIMPLE (Semi-Implicit Method for Pressure Linked Equations) algorithm to handle the pressure linkage through the continuity equation .The details of the algorithm, which is basically an iterative process are given in [87].

Let a tentatively calculated velocity field based on a guessed pressure files $p^*$ is denoted by $u_\xi^*$ , $u_\eta^*$ and let the correct pressure p be obtained from

$$p = p^* + p' \qquad (3.3.20)$$

The corresponding correction in velocities $u_\xi'$ , $u_\eta'$ can be introduced in a similar manner

$$u_\xi = u_\xi^* + u_\xi' \qquad (3.3.21)$$

$$u_\eta = u_\eta^* + u_\eta' \qquad (3.3.22)$$

Making certain assumptions, the velocity correction formula for east face of the grid element, for example is given by

$$u_\xi = u_\xi^* + \frac{\Delta\eta}{A_e}\left(p_P' + p_E'\right) \qquad (3.3.23)$$

Now, discretizing the continuity equation and using the velocity correction formulas, one can obtain the equation for pressure correction

$$\left(A_p - S_p\right)p_P = A_n p_n' + A_s p_s' + A_e p_e' + A_w p_w' + S_o \qquad (3.3.24)$$

Thus we have obtained an equation for pressure correction or in turn for pressure. The important steps to compute the flow properties are as follows:

1. Guess the pressure field $p^*$.
2. Solve the momentum equations to obtain $u_\xi^*$ and $u_\xi'$.
3. Solve the pressure correction equation.
4. Calculate p by solving $p'$ and $p^*$.
5. Solve equations for other variables $\phi$ (e.g. turbulence kinetic energy), if they have a coupling with momentum equations.
6. Treat the correct pressure as a new guessed pressure $p^*$. Return to step 2 and repeat the whole procedure until a converged solution is obtained.

The discretization procedure to the heat conduction equation leads to algebraic equations of the form similar to flow equations with temperature T replacing the general variable. No special calculation procedure is required to solve this equation since the energy equation is a stand alone independent equation.

The computer package called PHEONICS is employed to determine the flow and temperature fields in the pipe while a computer code is developed in FORTRAN language for stress calculations. The temperature field obtained from the pre-processor (PHEONICS code) is feed into the stress code for post-processing. The flow chart associated with the calculations is flow chart below.


The fluid and solid fields are meshed with rectangular grids generated as shown in figure (3.3.2) provided that the grid independent tests are carried out to ensure grid independent solutions.

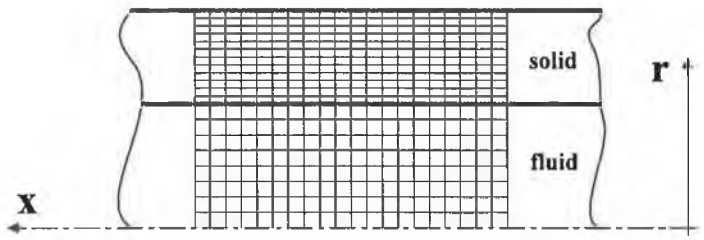


Figure 3.3.2 Meshes used in the study

In this study, the interior wall temperature at a given axial plane is calculated using the following formula:

$$T_w = \frac{2 \times T_{fw} \times T_{sw}}{T_{fw} + T_{sw}} \qquad (3.3.1)$$

The details of results validation for the three flow types in the study are provided in the following sub-headings.

### 3.3.1 Fully Developed Laminar Flow

To validate the fully developed laminar flow predictions, the study carried out previously [5] is considered. The conditions for the previous study are employed at present and these are as follows: A Peclet number equal to 500, dimensionless thickness equal to 0.1, a solid to fluid thermal conductivity ratio equal to 500 and a dimensionless length equal to $2\times10^{-2}$ are considered due to the previous study for comparison. The definitions of the parameters and the dimensionless temperature and distance can be found in the previous study. Figure (3.3.3) shows the dimensionless wall temperature ($\theta_w$) predicted from the present study and obtained from the previous study [5] with the dimensionless axial distance (x*). It can be observed that both results appear to be very close to each other. The small discrepancies in the results may be due the fact that in the reference study a finite element method was used to predict the temperature field while in the present study a control volume approach is used. Nevertheless, the discrepancies appear to negligibly small.

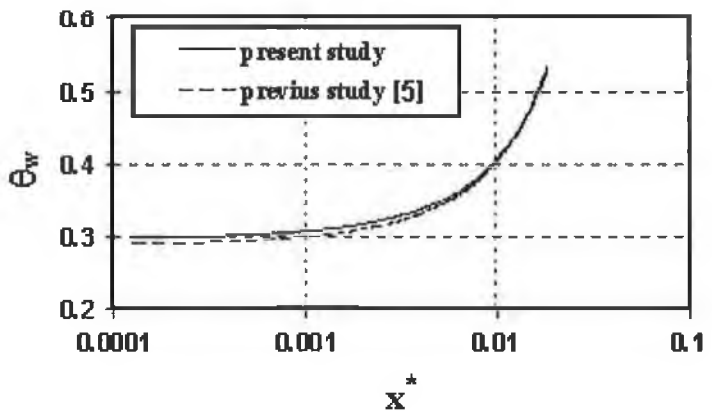


Figure 3.3.3 Axial distribution of the dimensionless temperature distribution

### 3.3.2 Turbulent Flow

A radial step length of approximately two viscous sub-layer thickness ($y^+ = 5$), where $y^+ = y[(\tau_w/\rho)^{1/2}/(\mu/\rho)]$ is employed. In the axial and radial directions, the grid contains 64×300 nodes in the fluid region and 64×100 nodes in the solid region, employed to obtain the grid independent solution. The grid nodes are distributed to give a high concentration lines near the wall provided that the wall adjacent nodes are positioned at $y^+ \approx 5$. The grid independency tests were carried out by using the different grid nodes and the grid distribution tests were also conducted and based on the findings, the grids giving optimum solution is ensured as consistent with the early work [23,86].

The K-ε model was used to account for the turbulence. The predictions of the Nusselt number variation with Reynolds number are compared with their counterparts obtained from the literarture [86]. The Nusselt number (Nu) predicted from the present study and the results of the previous study [86] are shown with Reynolds number in table (3.3.1) and plotted in figure (3.3.4). It can be observed from the table and curves in the figure that the present predictions for Nu agree well with the previous results. However, small discrepancies are observed between both results at high Reynolds numbers. This may be due to slightly over predicting the turbulent kinetic energy generation at high Reynolds number by the turbulent model (k-ε model) introduced in the present study. However, this difference is small.

| | Laminar Reynolds Number (Re) | Laminar Prandtl Number (Pr) | Turbulent Prandtl Numbers | | Nusselt Number (Nu) | | Abs. % Diff. |
|---|---|---|---|---|---|---|---|
| | | | $Pr_t(k)$ | $Pr_t(\varepsilon)$ | Reference No. ( 86) | Present Study | |
| a. Validation cases | 10000 | 3 | 0.15 | 0.15 | 53.82 | 51 | 5.3 |
| | 10000 | 10 | 0.08 | 0.08 | 86.45 | 88 | 1.8 |
| | 10000 | 30 | 0.035 | 0.035 | 128.74 | 130 | 1 |
| | 10000 | 100 | 0.013 | 0.013 | 195.53 | 191 | 2.3 |
| | 30000 | 3 | 0.22 | 0.22 | 146.1 | 144 | 1.4 |
| | 30000 | 10 | 0.085 | 0.085 | 242.16 | 237 | 2.1 |
| | 30000 | 30 | 0.036 | 0.036 | 366.12 | 388 | 5.6 |
| | 30000 | 100 | 0.0126 | 0.0126 | 560.62 | 543 | 3.1 |
| | 50000 | 3 | 0.30 | 0.30 | 238.4 | 239.6 | 0.5 |
| | 50000 | 10 | 0.09 | 0.09 | 397.8 | 401 | 0.8 |
| | 50000 | 30 | 0.0375 | 0.0375 | 603.5 | 644 | 6.7 |
| | 50000 | 100 | 0.012 | 0.012 | 925.7 | 946.5 | 2.2 |
| b. Present study | 10000 | 7.0 (Water) | 0.097 | 0.097 | 80 | 77.5 | 3.1 |
| | 10000 | 64.4 (Coolanol-25) | 0.02 | 0.02 | 175 | 175 | 0 |
| | 30000 | 7.0 (Water) | 0.117 | 0.117 | 215 | 206 | 4.3 |
| | 30000 | 64.4 (Coolanol-25) | 0.019 | 0.019 | 470 | 485 | 3.2 |
| | 50000 | 7.0 (Water) | 0.128 | 0.128 | 338 | 341 | 0.9 |
| | 50000 | 64.4 (Coolanol-25) | 0.018 | 0.018 | 770 | 754 | 2 |

Table 3.3.1. The turbulent Prandtl numbers and the resulting Nusselt numbers for the validation and the present study cases.

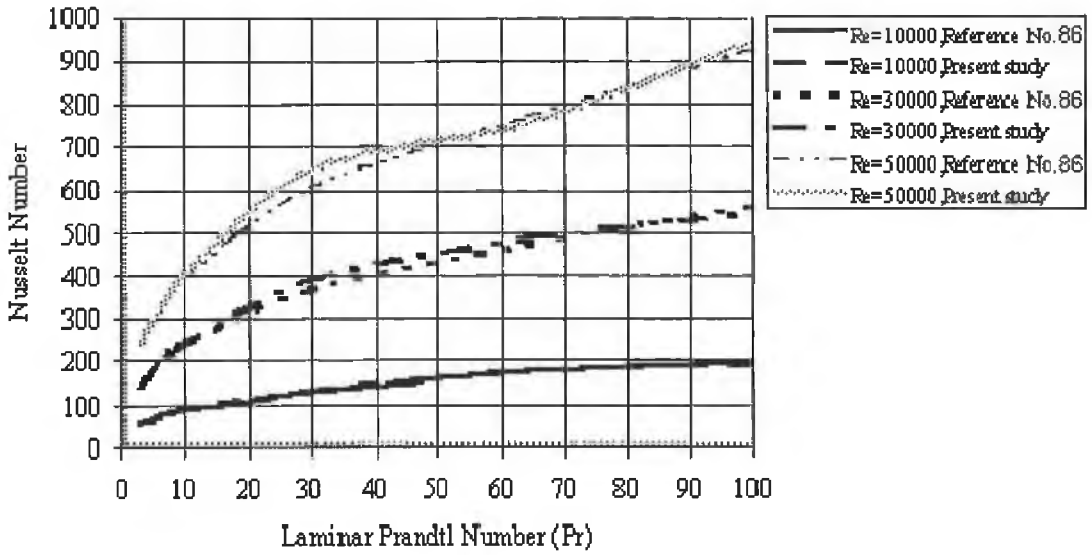


Figure 3.3.4 The Nusselt numbers for various Reynolds and Prandtl numbers from the present and previous studies

### 3.3.3 Pulsating Flow

To validate the present predictions, a case study introduced in the previous study [88] is simulated. Figure (3.3.5) shows the amplitude of the axial velocity oscillation with time predicted from the present study and obtained in the previous study [88]. The equation for the axial velocity and the simulation conditions are:

$$u(r,t) = \frac{K}{n}\left[\sin(nt) - \sqrt{\frac{r_i}{r}}\exp\left(-\sqrt{\frac{n}{2\nu^*}}(r_i - r)\right)\sin\left[nt - \sqrt{\frac{n}{2\nu^*}}(r_i - r)\right]\right] \qquad (3.3.2)$$

and

$$\frac{\Delta p}{\Delta L} = \frac{\partial p}{\partial x} = -\rho K\cos(nt) \qquad (3.3.3)$$

, where K = 0.08015, $\Delta p/\Delta L$=80 Pa/m and n=1.256 Hz. It can be observed that both results are in good agreement. Small discrepancies in extreme points of the velocity profiles are observed. However, these discrepancies are on the order of 2 % of the maximum velocity, i.e. they are negligibly small.

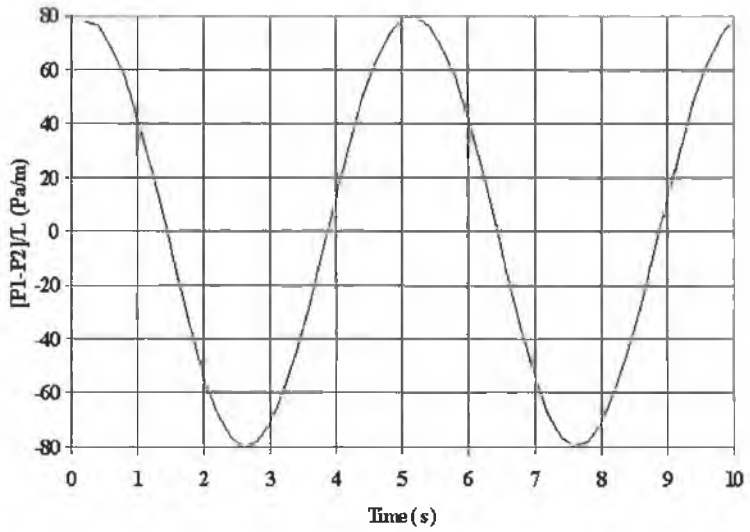


3.3.5.a Oscillating pressure difference per unit length between the inlet and outlet of the pipe

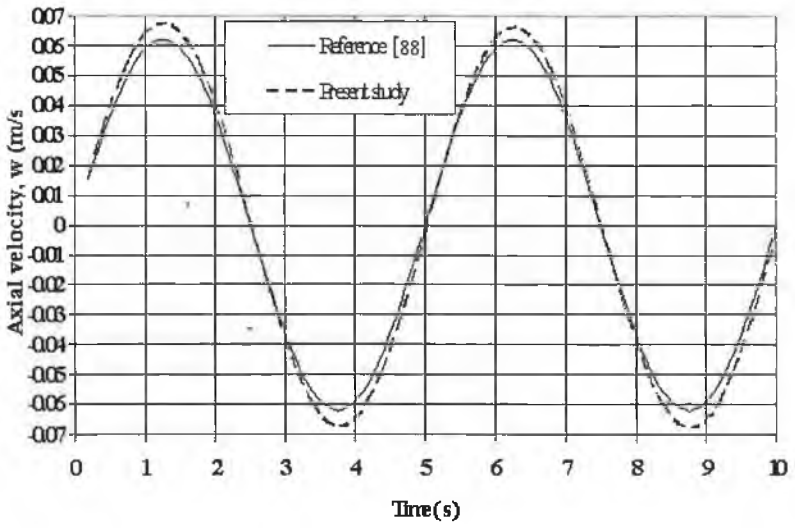


3.3.5.b Resulting axial velocity in the pipe due to the oscillating pressure difference input

Figure 3.3.5 The oscillating pressure difference input and the resulting output axial velocity.

# CHAPTER 4

## RESULTS AND DISCUSSIONS

### 4.1 Introduction

The results of this study about thermal stresses in thick-walled pipes subjected to fully developed laminar, turbulent and pulsating flows are given and analyzed in this chapter. The properties of the solids and fluid used in this study are presented in table 4.1.1. The properties of the fluids are selected to demonstrate the influence of fluid thermal properties on the results of the simulations, i.e. coolanol-25 has the lowest thermal conductivity while mercury has the highest. The simulation conditions are given in table 4.2.1 for laminar flow and in tables 4.4.1, 4.4.2 and 4.4.3 for pulsating flow.

| SOLIDS | | | | |
|---|---|---|---|---|
| | Copper | | Steel | Units |
| Thermal conductivity ($k_s$) | 381 | | 43 | W/m.K |
| Thermal expansion coefficient ($\alpha$) | $1.62\ 310^{-5}$ | | $0.37310^{-5}$ | 1/K |
| Modulus of elasticity (E) | 1.075 | | 2.1 | GPa |
| Poisson's ratio ($\nu$) | 0.335 | | 0.3 | Unitless |
| FLUIDS | | | | |
| | Coolanol-25 | Water | Mercury | Units |
| Thermal conductivity ($k_f$) | 0.13135 | 0.597 | 8.54 | W/mK |
| Density ($\rho$) | 900.00 | 998.23 | 13530 | $Kg/m^3$ |
| Specific heat($C_p$) | 1882.35 | 4181.8 | 139.3 | J/kgK |
| Kinemetic viscosity ($\mu/\rho$) | $5\times10^{-6}$ | $1.006\times10^{-6}$ | $1.125\times10^{-7}$ | $m^2/s$ |

Table 4.1.1 Properties of the pipe materials and fluids used in the study.

### 4.2 Fully Developed Laminar Pipe Flow

Two main studies about thermal stresses in pipes due to fully developed flow are presented in this section. The first study is parametric and investigates the effects

of pipe diameter, thickness and length on thermal stresses in pipes. The second one investigates the flow properties and the thermal solid to fluid conductivity ratio on the resulting thermal stresses.

### 4.2.1 The Effects of Diameter, Thickness and Length Sizees on Thermal Stresses:

The cases considered in the present study are given in table 4.2.1. The combination of three pipe wall thicknesses, three diameters and three lengths are taken into account. Both fluid and solid properties are kept constant. Steel and water are considered. The amount of heat flux employed for all cases is 1300 $W/m^2.K$. The pipe inlet temperature is taken as 293 K. The velocity at pipe inlet is kept constant at $1.25 \times 10^{-3}$ m/s to ensure the laminar flow in the pipe. The grid independent studies were carried on and the grid sizes used are given in table 4.2.1.

Figures (4.2.1), (4.2.2), (4.2.3) and (4.2.4) show the dimensionless temperature ($T^*$) distribution in the fluid and in the solid sides for cases 1,3,7 and 9 (Table 4.2.1), respectively. For thinner pipes (cases 1 and 3), as L/D ratio increases the temperature attains considerably high values in the solid wall vicinity. In this case, the temperature gradient at the fluid-solid interface increases considerably. However, the temperature gradient becomes larger in the vicinity of the solid pipe interior surface for case 1. Therefore, the location of the maximum temperature gradient changes as the L/D ratio increases; it moves inside the pipe. On the other hand, as the pipe thickness increases, the temperature in the fluid side close to the wall increases further. Similarly to the thinner pipe, the maximum temperature gradient occurs at fluid-solid interface. This is also true for low L/D ratio pipes (case 7). Consequently, as the pipe thickness increases the maximum temperature gradient remains at the fluid-solid interface. It should also be noted that for low L/D ratio pipes high temperature gradient attains in the solid side. The attainment of the high temperature gradient in the solid occurs due to the fact that the fluid temperature at the fluid-solid interface is relatively lower; the heat flux from solid wall to the fluid is high.

| Diameter of the pipe ( m ), D | Thickness of the pipe ( m ), t and Number of grid points | | Length of the pipe ( m ), L | | |
|---|---|---|---|---|---|
| | | | 5 × D | 15 × D | 25 × D |
| | | | **0.4** | **1.2** | **2.0** |
| D = **0.08** | t = 0.1×D = **0.008** | | Case 1 | Case 2 | Case 3 |
| | No. grid points in | in solid | 20 | 20 | 20 |
| | | In fluid | 100 | 100 | 100 |
| | | in axial direction | 20 | 120 | 200 |
| | t = 0.3×D = **0.024** | | Case 4 | Case 5 | Case 6 |
| | No. grid points in | in solid | 60 | 60 | 60 |
| | | in fluid | 100 | 100 | 100 |
| | | in axial direction | 40 | 120 | 200 |
| | t = 0.5×D = **0.04** | | Case 7 | Case 8 | Case 9 |
| | No. grid points | in solid | 100 | 100 | 100 |
| | | in fluid | 100 | 100 | 100 |
| | | in axial direction | 40 | 120 | 200 |
| D = **0.12** | t = 0.1×D = **0.012** | | Case 10 | Case 11 | Case 12 |
| | No. grid points | in solid | 40 | 40 | 40 |
| | | in fluid | 100 | 100 | 100 |
| | | in axial direction | 40 | 120 | 200 |
| | t = 0.3×D = **0.030** | | Case 13 | Case 14 | Case 15 |
| | No. grid points | in solid | 60 | 60 | 60 |
| | | in fluid | 100 | 100 | 100 |
| | | in axial direction | 40 | 120 | 200 |
| | t = 0.5×D = **0.06** | | Case 16 | Case 17 | Case 18 |
| | No. grid points | in solid | 100 | 100 | 100 |
| | | in fluid | 100 | 100 | 100 |
| | | in axial direction | 40 | 120 | 200 |
| D = **0.16** | t = 0.1×D = **0.016** | | Case 19 | Case 20 | Case 21 |
| | No. grid points | in solid | 60 | 60 | 60 |
| | | in fluid | 100 | 100 | 100 |
| | | in axial direction | 40 | 120 | 200 |
| | t = 0.3×D = **0.048** | | Case 22 | Case 23 | Case 24 |
| | No. grid points | in solid | 60 | 60 | 60 |
| | | in fluid | 100 | 100 | 100 |
| | | in axial direction | 40 | 120 | 200 |
| | t = 0.5×D = **0.08** | | Case 25 | Case 26 | Case 27 |
| | No. grid points | in solid | 100 | 100 | 100 |
| | | in fluid | 100 | 100 | 100 |
| | | in axial direction | 40 | 120 | 200 |

Table 4.2.1.Diameters, thicknesses, lengths and grid sizes of the pipes used in the parametric study.

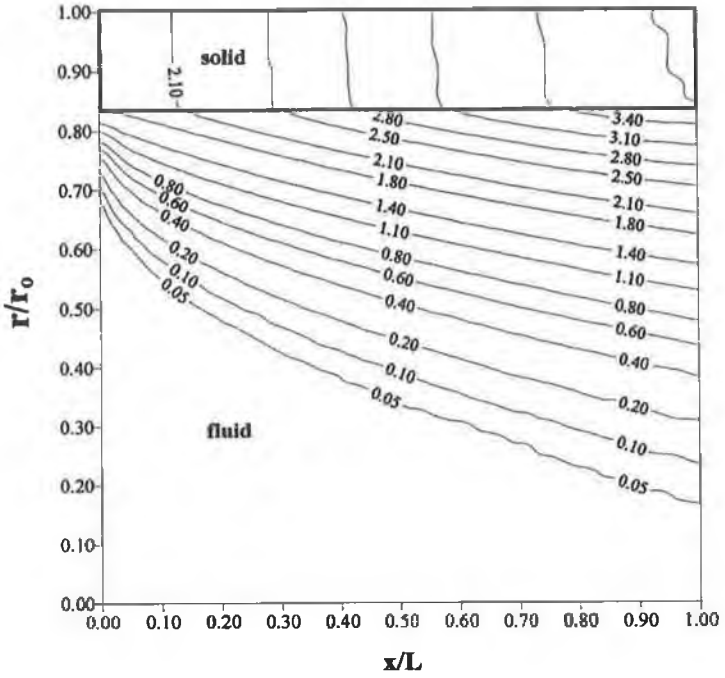


Figure 4.2.1 Dimensionless temperature contours for the conditions: D=0.08 m, t=0.1×D, L=5×D (case 1, Table 4.2.1), where D is the inside diameter of the pipe

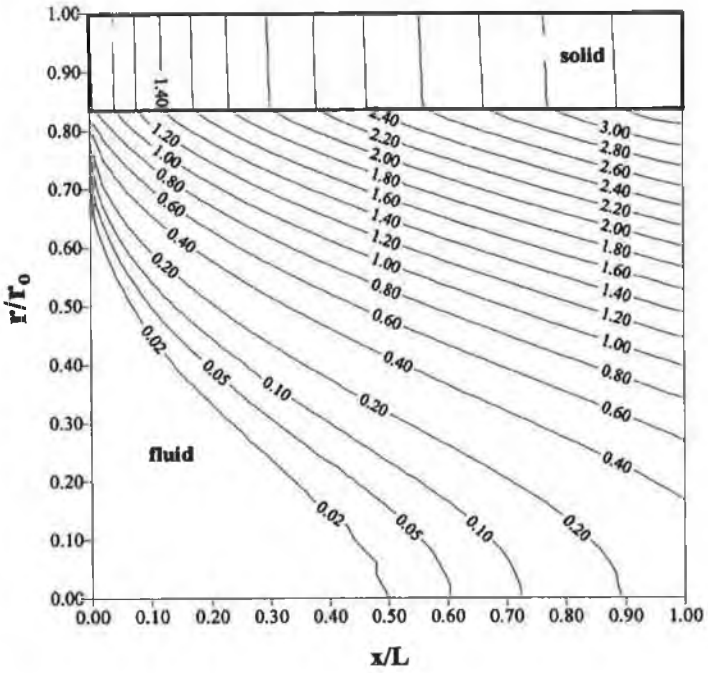


Figure 4.2.2 Dimensionless temperature contours for the conditions: D=0.08 m, t=0.1×D, L=25×D (case 3 in Table 4.2.1), where D is the inside diameter of the pipe

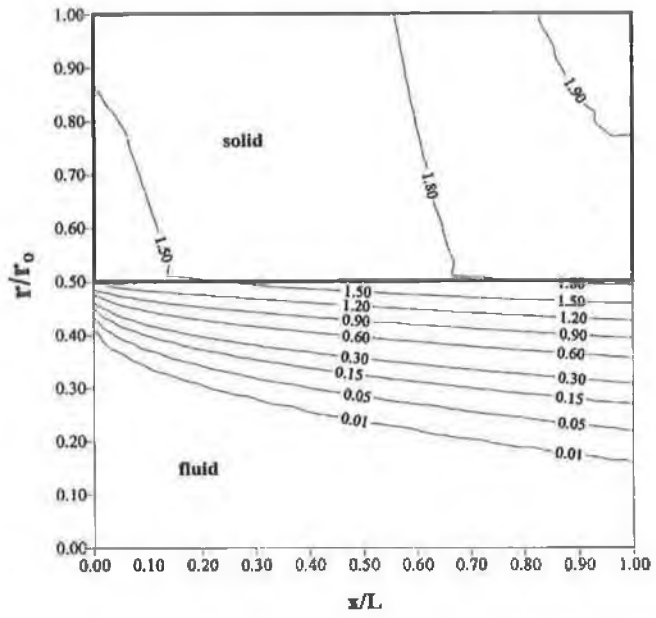


Figure 4.2.3 Dimensionless temperature contours for the conditions: D=0.08 m, t=0.5×D, L=5×D (case 7 in Table 4.2.1), where D is the inside diameter of the pipe

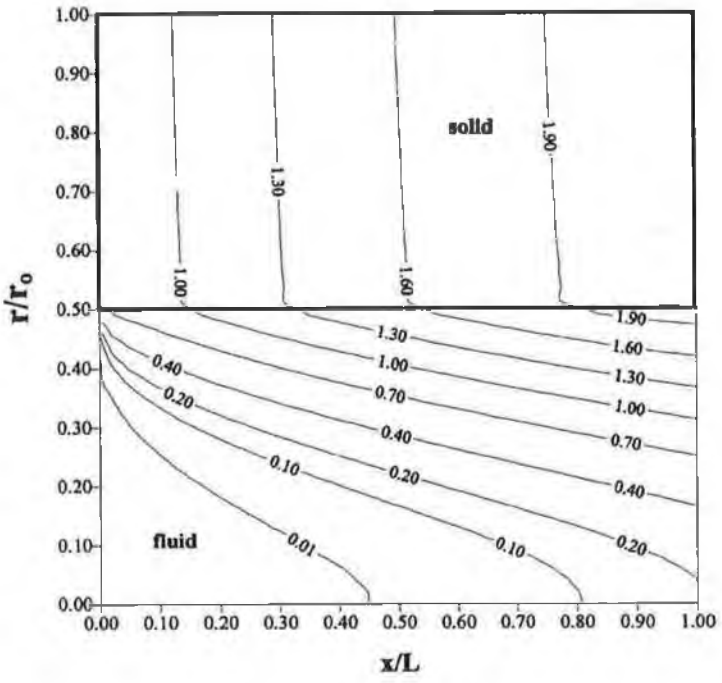


Figure 4.2.4 Dimensionless temperature contours for the conditions: D=0.08 m, t=0.5×D, L=25×D (case 9 in Table 4.2.1), where D is the inside diameter of the pipe

Figures (4.2.5) through (4.2.13) show the effective stress to yield stress ratio (stress-ratio) with the dimensionless radius ($r^*$) for the cases 1 through 27 respectively, as indicated in Table 4.2.1. The stress ratio at the inner radius ($r^*=0$) reaches to maximum for all axial planes (inlet, mid and outlet planes). The stress ratio reduces to minimum then increases as the $r^*$ increases. This occurs because of the temperature gradient variation in the pipe wall. Moreover, as the axial plane moves forward to the tube outlet, the location of the minimum stress ratio moves towards the pipe end; $r^*$ corresponding to the minimum stress ratio increases. On the other hand, as the pipe thickness increases, the decay of the stress ratio reduces along $r^*$, which is evident from the figures (4.2.7),(4.2.10) and (4.2.13). This is due to the temperature distribution in the pipe wall; the temperature gradient changes smoothly across the pipe wall as indicated earlier. The location of the minimum stress ratio moves closer to the pipe inlet as compared to that occurring for thinner pipe case. However, the value of stress ratio increases almost three times more than that corresponding to thinner pipe. Consequently, the values of stress ratio and its distribution in the pipe are highly dependent on the pipe wall thickness. As the pipe diameter increases, the location of minimum stress ratio moves closer to the pipe inlet. Moreover, its location becomes independent of the axial planes, i.e. the locations of the minimum stress ratio corresponding to inlet, mid and outlet planes almost coincide at the same location. This is more pronounced when the pipe wall thickness increases as shown in figure (4.2.13). Moreover, the stress ratio profile corresponding to inlet plane varies slightly as compared to that corresponding to mid and outlet planes; the gradient of the stress ratio changes as the location in the axial direction changes. In addition, as $r^*$ increases, the gradient of the stress ratio after the location of minimum stress increases. This becomes more visible at larger pipe diameters.

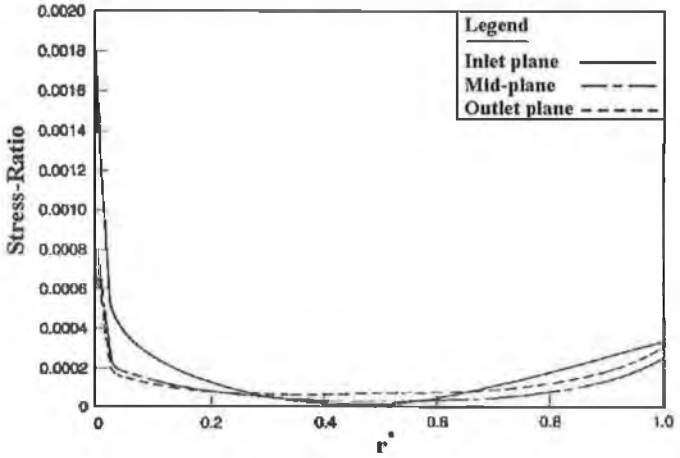


a. Case 1.

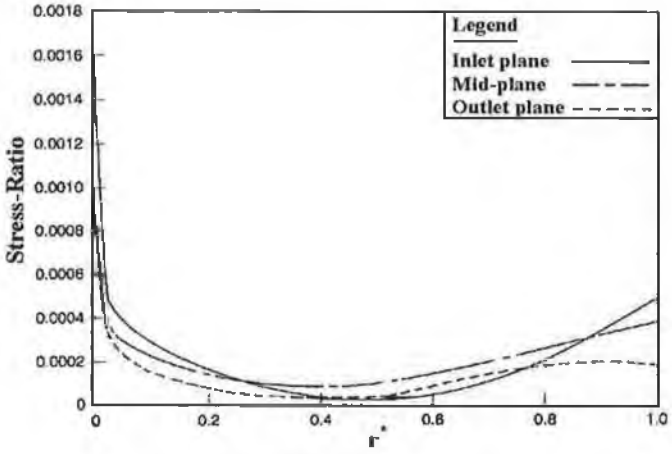


b. Case 2.

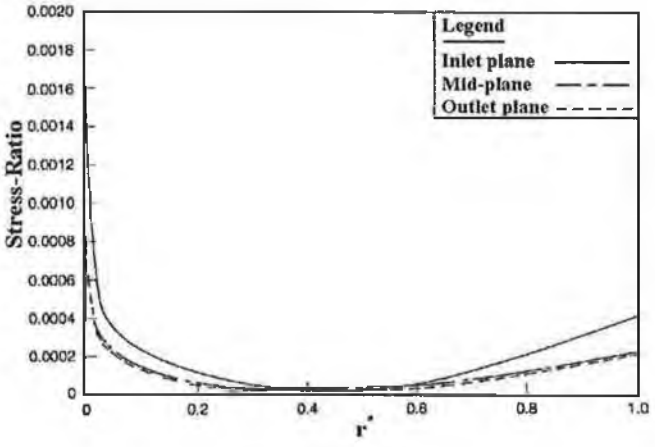


c. Case 3.

Figure 4.2.5 Thermal stresses for cases 1,2 and 3 in Table 4.2.1.

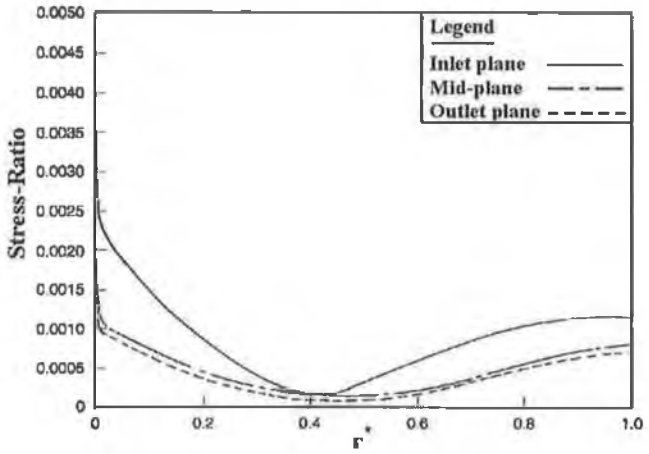


a. Case 4

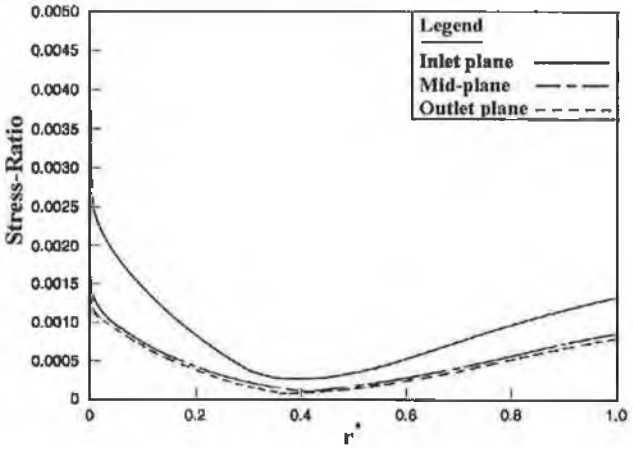


b. Case 5

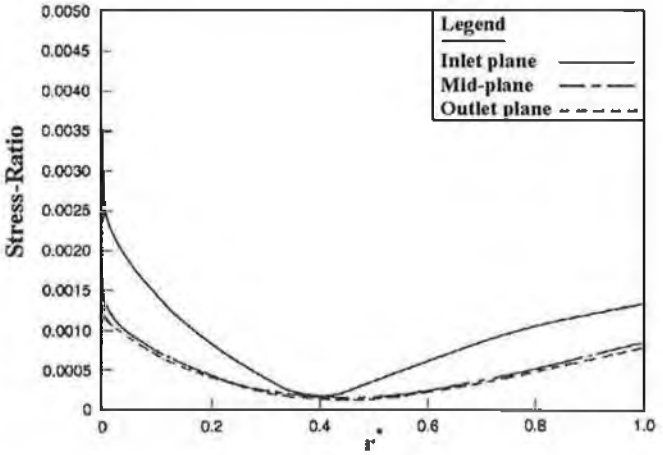


c. Case 6

Figure 4.2.6. Thermal stresses for cases 4,5 and 6 in table 4.2.1.

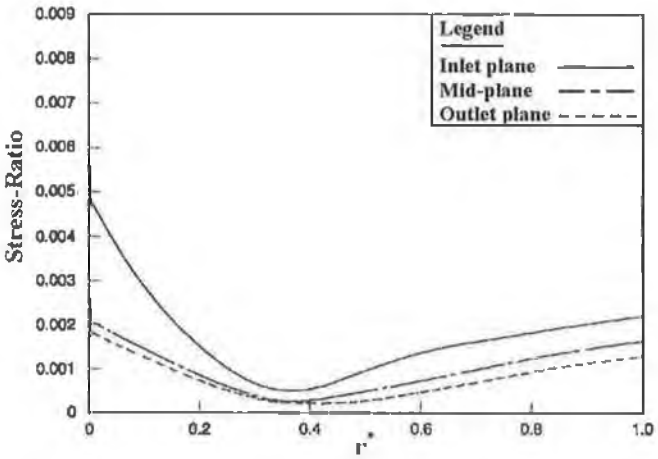


a. Case 7

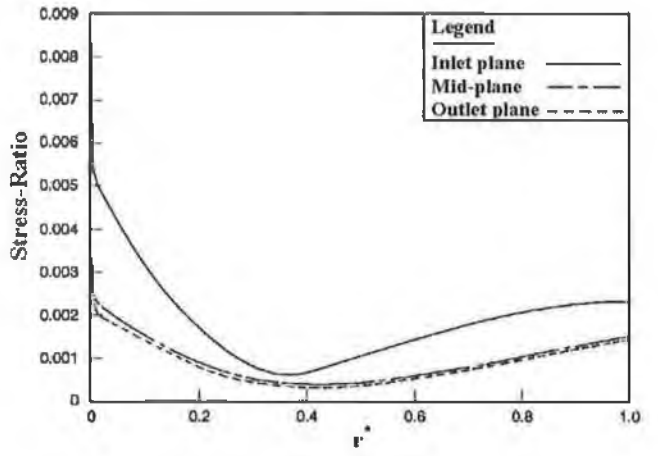


b. Case 8

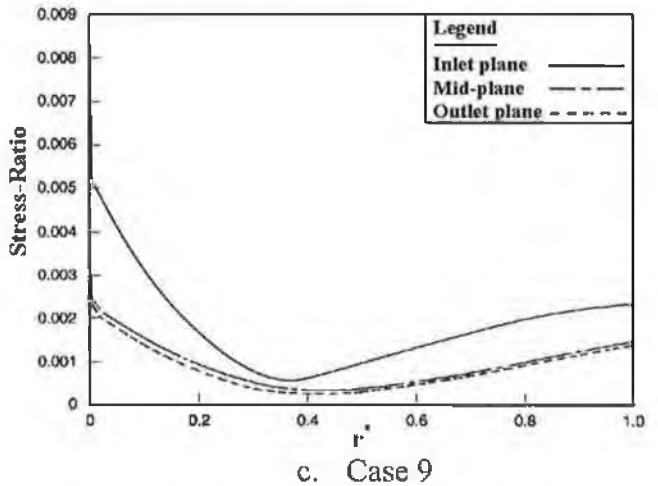


c. Case 9

Figure 4.2.7. Thermal stresses for the cases 7,8 and 9 in Table 4.2.1.

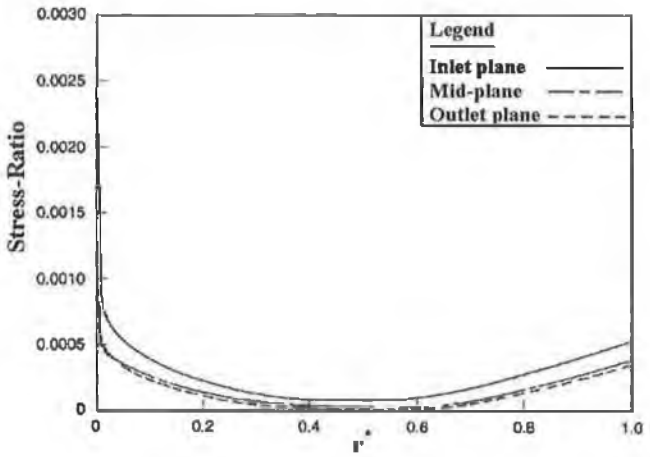


a. Case 10.

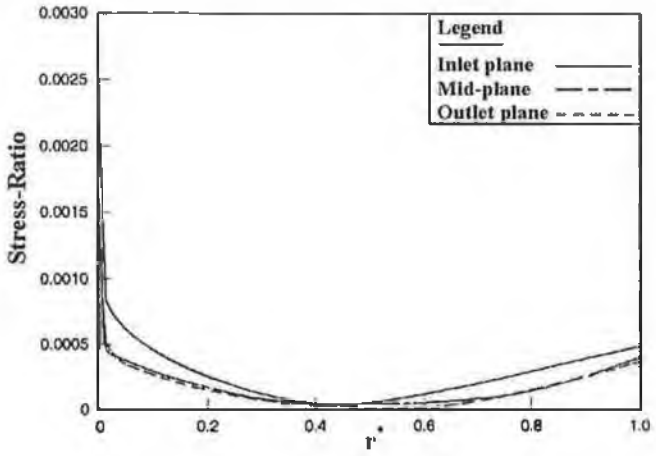


b. Case 11.

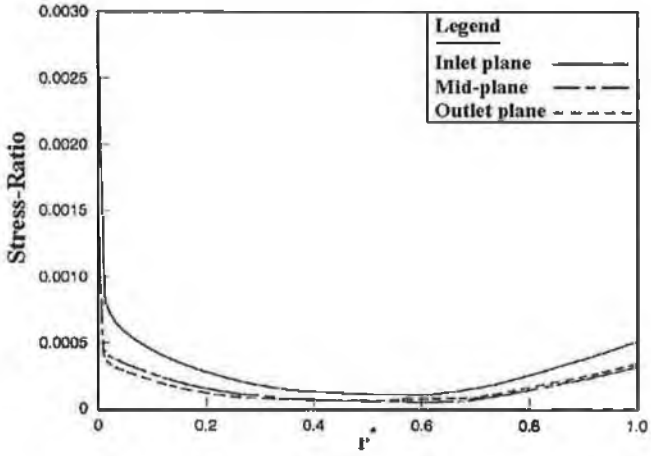


c. Case 12.

Figure 4.2.8. Thermal stresses for the cases 10,11 and 12 in Table 4.2.1.

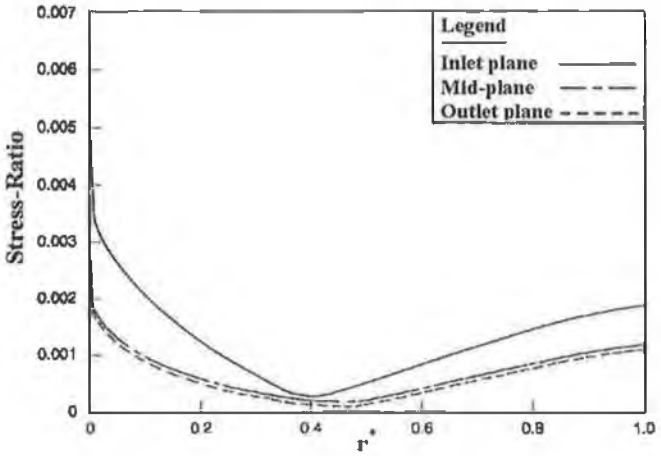


a. Case 13

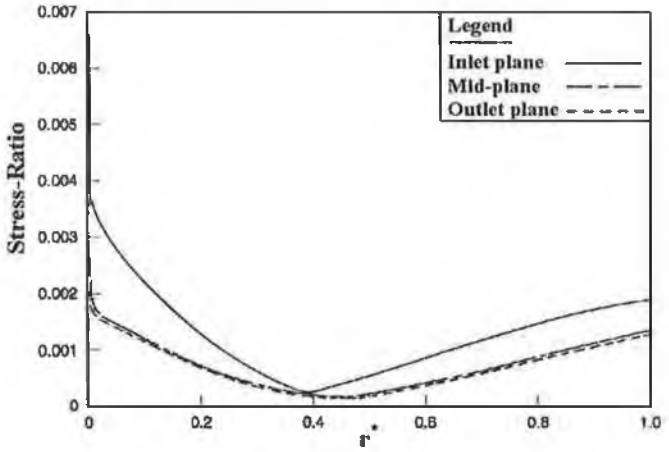


b. Case 14

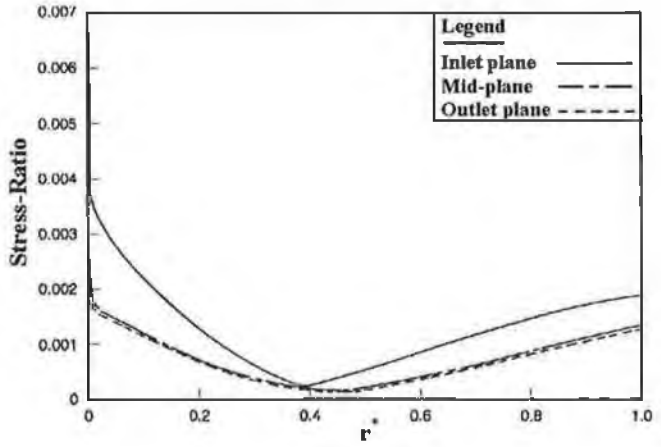


c. Case 15

Figure 4.2.9. Thermal stresses for the cases 13,14 and 15 in Table 4.2.1.

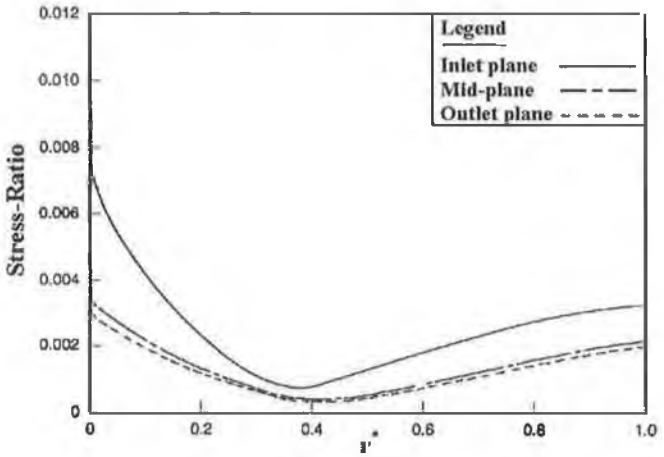


a. Case 16

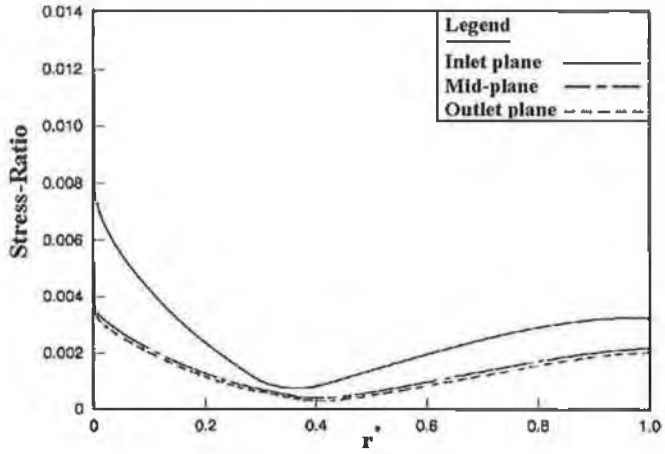


b. Case 17

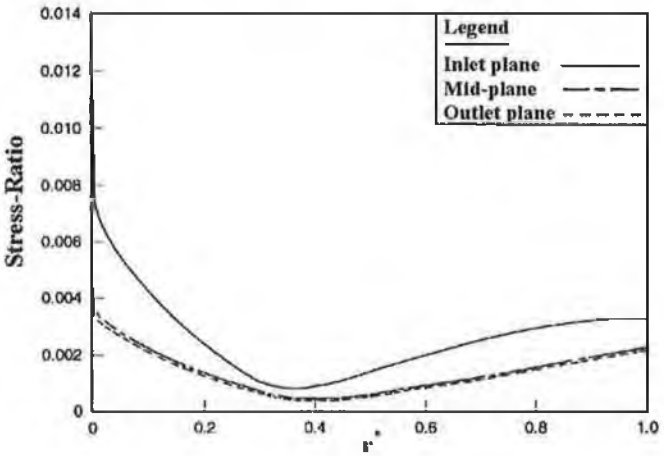


c. Case 18

Figure 4.2.10. Thermal stresses for the cases 16,17 and 18 in Table 4.2.1.

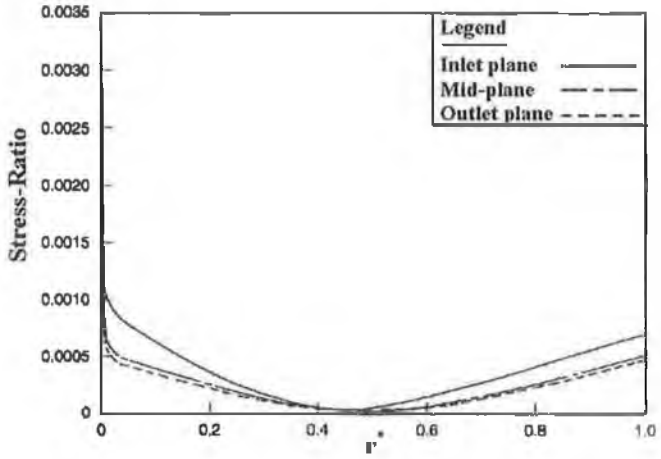


a. Case 19

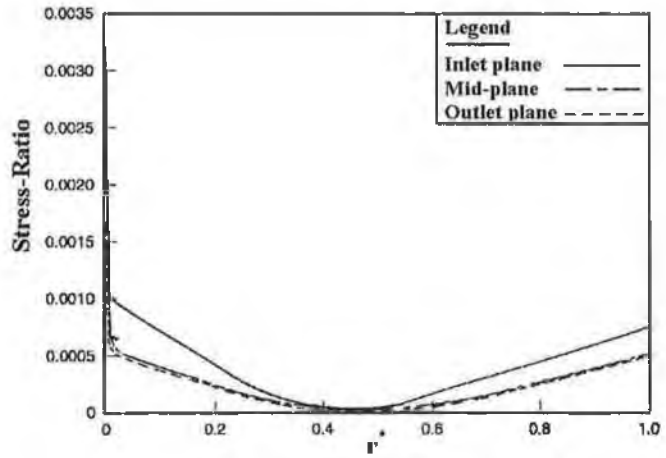


b. Case 20

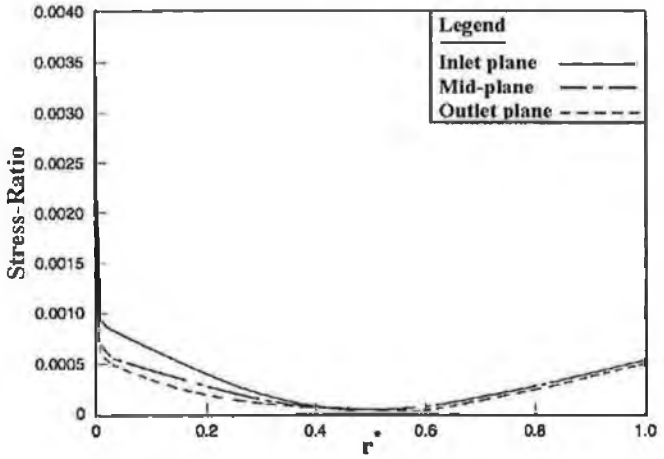


c. Case 21

Figure 4.2.11. Thermal stresses for the cases 19,20 and 21 in Table 4.2.1.

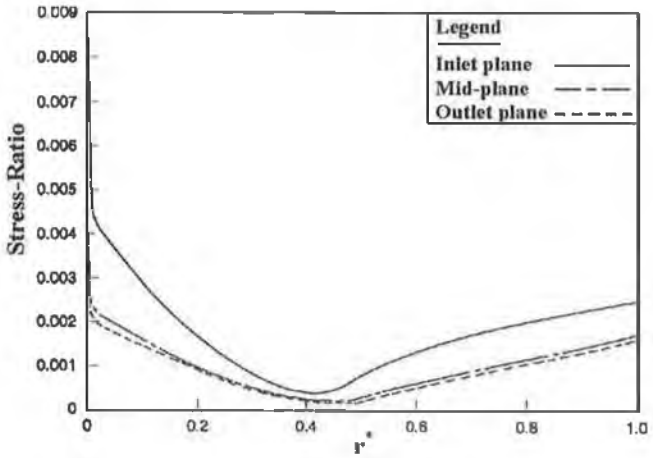


a. Case 22

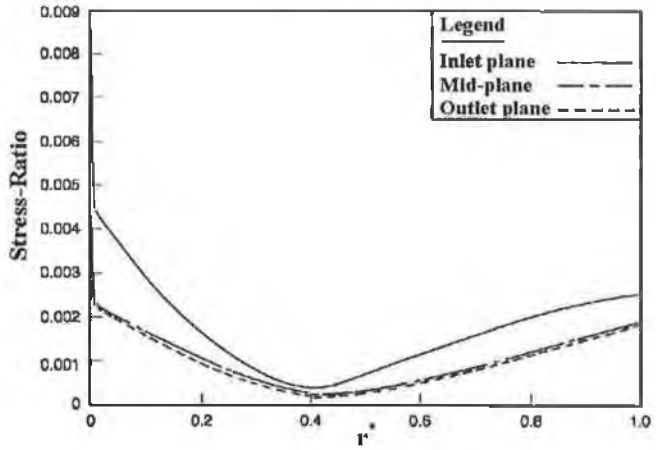


b. Case 23

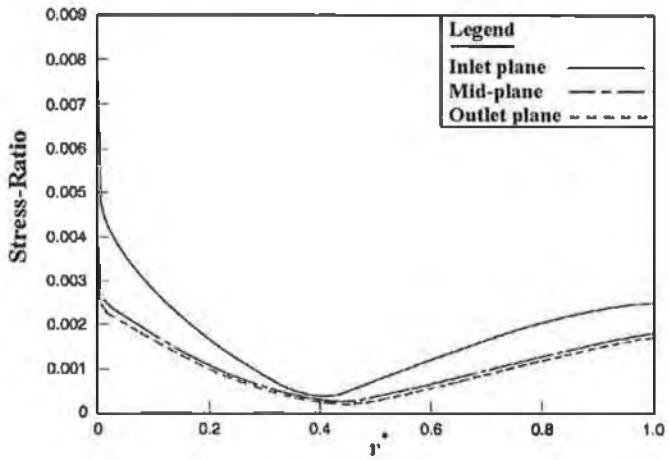


c. Case 24

Figure 4.2.12. Thermal stresses for the cases 22,23 and 24 in Table 4.2.1.

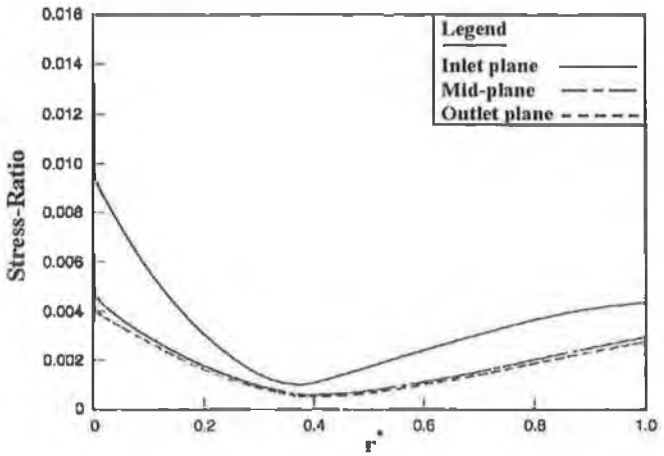


a. Case 25

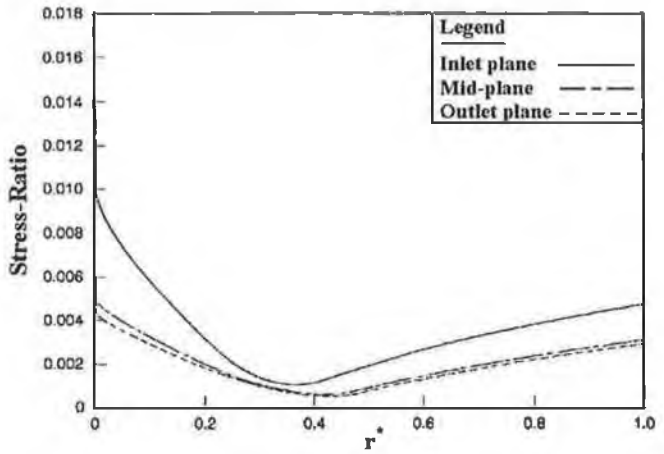


b. Case 26

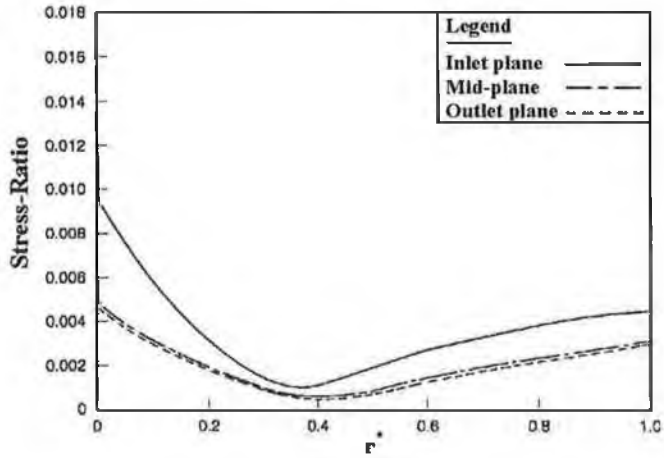


c. Case 27

Figure 4.2.13. Thermal stresses for the cases 25,26 and 27 in Table 4.2.1.

### 4.2.2 The Material Properties and the Thermal Conductivity Effects on Thermal Stresses:

To examine the effects of thermal properties of fluid and solid to fluid conductivity ratio on the resulting thermal stresses in pipes, a combination of three different fluids, namely water ($P_r$ = 7), coolanol-25 ($P_r$ = 64.4) and mercury ($P_r$ = 0.02), and two solids, namely, steel and copper are used.

Figures (4.2.14a) and (4.2.14b) show the dimensionless temperature distribution in the solid and fluid along the length for $P_r$ = 0.02. Almost uniform dimensionless temperature is observed in the radial direction; the temperature gradient in the radial direction in solid side remains almost constant. This argument is also valid for the fluid side. As the distance from the inlet along the pipe length increases, the dimensionless temperature increases because of the uniform heat supplied from the pipe external surface. Since the Prandtl number is low, the convection heat transfer is expected to be low in the axial direction; therefore, the temperature difference appears to be large in this direction. When comparing figures (4.2.14a) and (4.2.14b), it can be seen that temperature contours attain high values as the thermal conductivity ratio ($k_s/k_f$) increases. The temperature gradient at solid-fluid interface changes as the pipe length increases. This change is not influenced by the thermal conductivity ratio. This may occur because of the imposed heat conduction in the solid side, i.e. as the solid conductivity increases, the temperature in the solid side becomes almost uniform along the axial direction.

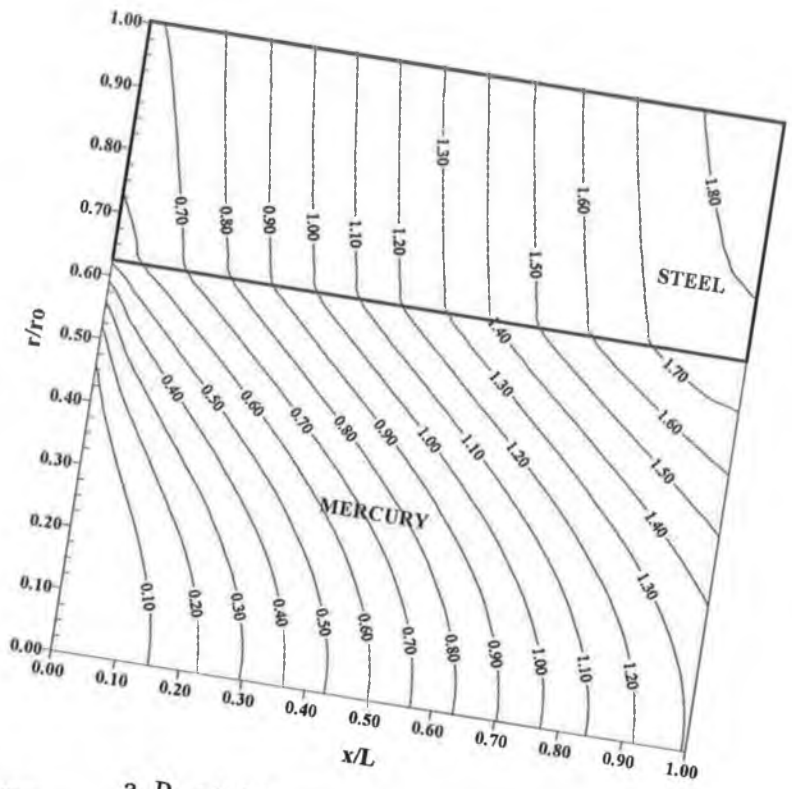


a. $P_r = 0.02$ and $k_s / k_f = 5.04$.

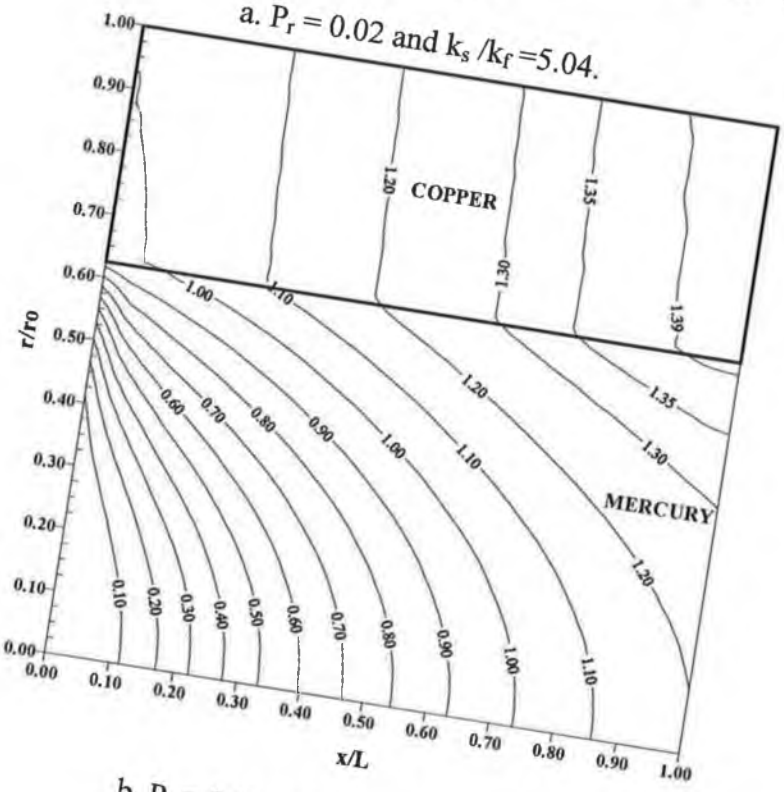


b. $P_r = 0.02$ and $k_s / k_f = 44.6$.

Figure 4.2.14 Dimensionless temperature ($T^*$) contours for the cases: a) steel and mercury and b) copper and mercury.

Figures (4.2.15a) and (4.2.15b) show the dimensionless temperature contours in the solid and fluid sides for two thermal conductivity ratios. The temperature contours attain considerably high values close to the solid wall and extends further inside the fluid. Moreover, no-radial uniformity is observed in the temperature contours. This is because of the high Prandtl number, which is 7, i.e. the convection heat transfer improves considerably resulting in extension of temperature contours inside the fluid. The rapid change in temperature gradient occurs in the solid close to the inner surface vicinity. This is more pronounced as the dimensionless axial distance (x/L) increases. In addition, the effect of thermal conductivity ratio on the temperature contours is considerable. In this case, as $k_s/k_f$ decreases, the temperature distribution in the radial direction becomes straight as well it attains high values. This is again due to the heat conduction in the solid, i.e. heat conduction in the solid slows as the thermal conductivity reduces, which in turn in results low temperature gradients in the radial as well as in axial direction.

Figures (4.2.16a) and (4.2.16b) show the dimensionless temperatures in the solid and fluid sides for two thermal conductivity ratios. The temperature profiles do not extend further inside the fluid in the radial direction, i.e. temperature profiles do not become straight in the radial direction. This is again due to the convection heat transfer effect, since the Prandtl number is 64.4, i.e. higher the Prandtl number results in enhanced convection heat transfer. The temperature gradient rapidly changes in the solid side. The location of this change moves further away from the inner surface of the pipe as the Prandtl number increases. The change of temperature gradient is more pronounced as the thermal conductivity ratio increases. This may indicate that the convection cooling of the inner wall of the pipe at solid-fluid interface is considerable, which in turn leads to low interface temperature.

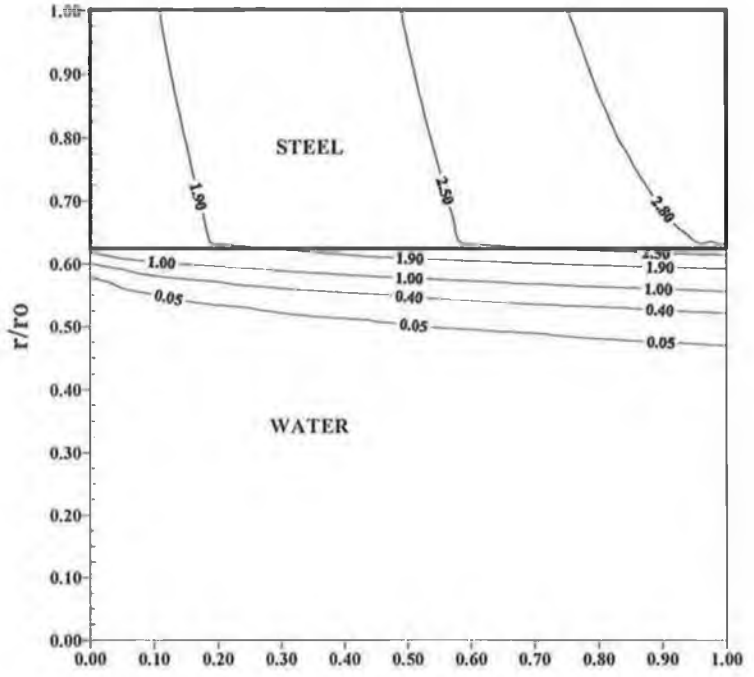


a. $P_r = 7$ and $k_s/k_f = 72$

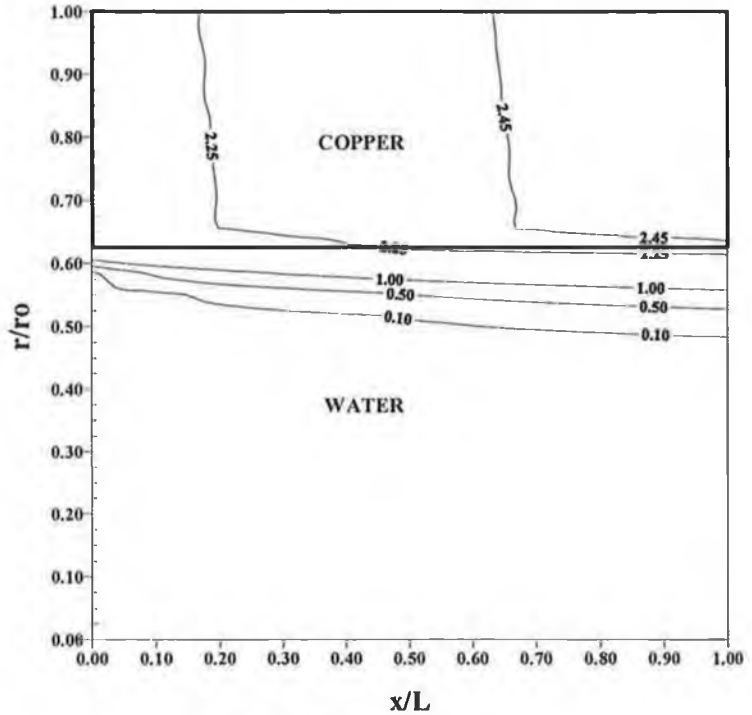


b. $P_r = 7$ and $k_s/k_f = 638.2$

Figure 4.2.15 Dimensionless temperature ($T^*$) contours for the cases: a) steel and water and b) copper and water.

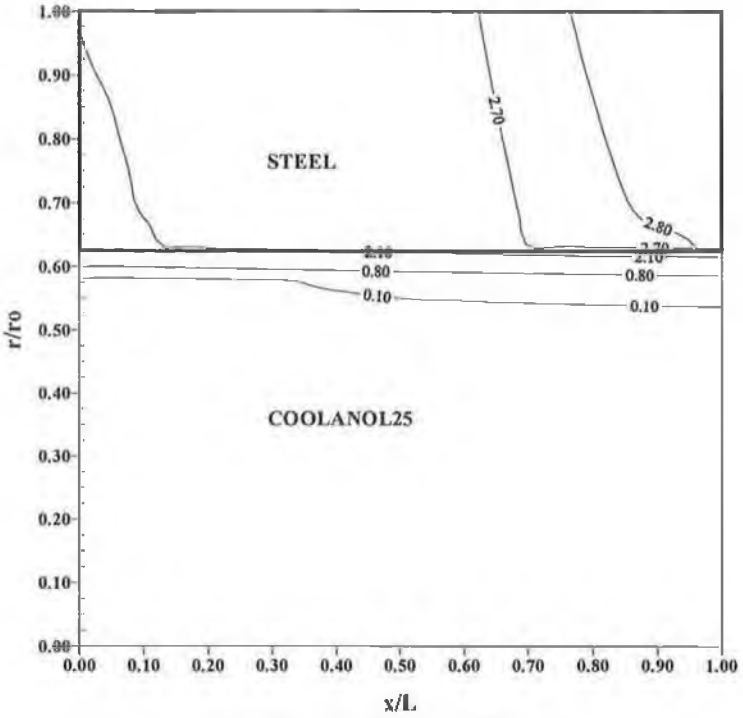


a. $P_r = 64.4$ and $k_s/k_f = 327$

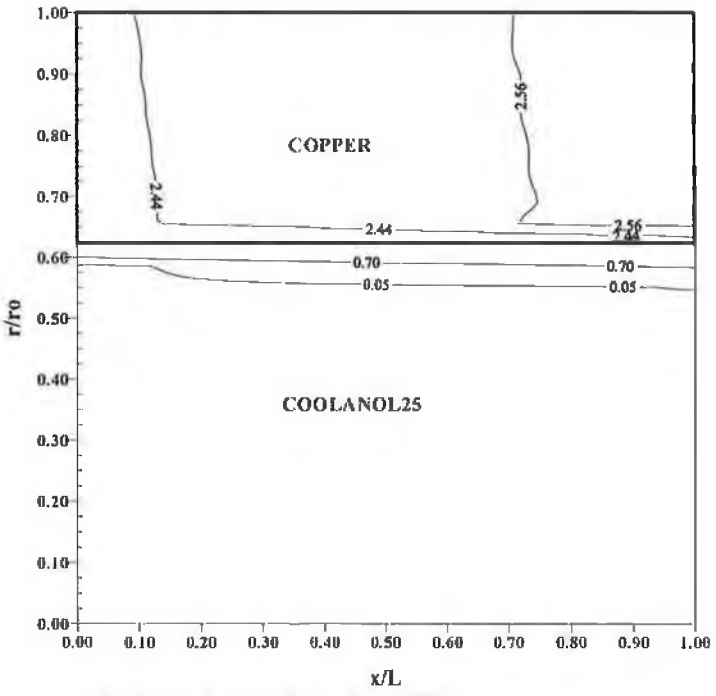


b. $P_r = 64.4$ and $k_s/k_f = 2901$

Figure 4.2.16 Dimensionless temperature contours ($T^*$) contours for the cases: a) steel and coolanol-25 and b) copper and coolanol-25.

Figure (4.2.17) shows the dimensionless temperature $\upsilon_{ow}$ along the pipe length, as thermal conductivity is variable. The dimensionless temperature attains almost the same value at the center of the pipe where $x/L \cong 0.5$. As the thermal conductivity ratio and Prandtl number increase, the dimensionless temperature along the pipe reduces. This indicates that the conduction has almost equally important effect on the temperature profiles as compared to convection cooling.

Figure (4.2.18) shows the effective stress distribution with $r^*$ at the inlet plane, as thermal conductivity ratio is variable. The effective stress attains considerable high values close to the solid-fluid interface ($r^* \cong 0$). This is because of the temperature gradient in this region, i.e. the temperature gradient changes at the interface. In the case of high Prandtl number and thermal conductivity ratio, the effective stress further increases in the region close to the solid-fluid interface. As the radial distance increases, effective stress remains constant except at $r^* \cong 0.5$. In this case, the effective stress reduces to minimum. This is again because of the temperature gradient which becomes almost constant at $r^* \cong 0.5$. Moreover, as $r^*$ increases further, effective stress increases slightly towards the outer surface of the pipe. In this case, the temperature gradient is expected to reduce in this region.

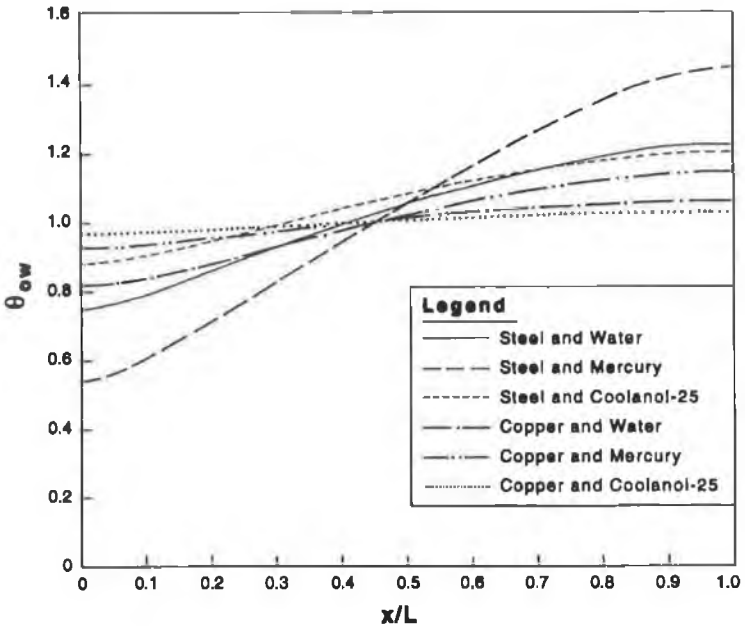


Figure 4.2.17 The dimensionless outer wall temperature vs. the dimensionless pipe length for various Prandtl numbers and thermal conductivity ratios.

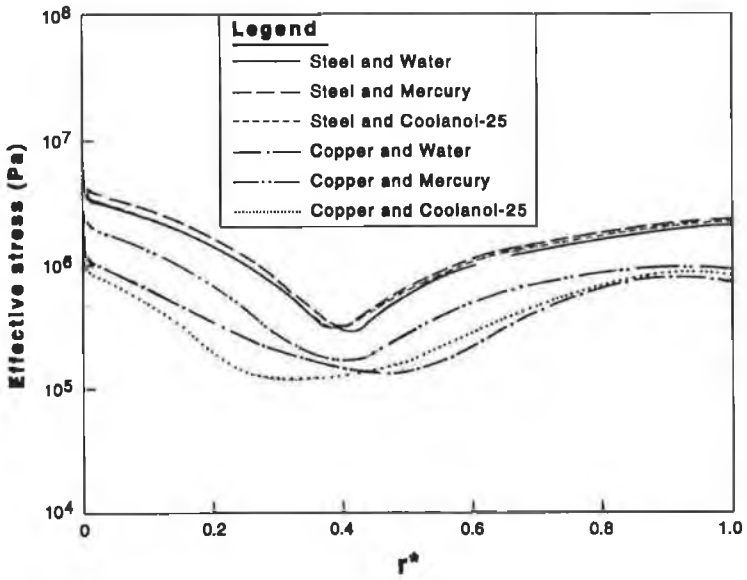


Figure 4.2.18 The effective stress distribution vs. the dimensionless pipe radius at the inlet- plane of the pipe for various Prandtl numbers and thermal conductivity ratios.

Figure (4.2.19) shows the effective stresses distribution with $r^*$ at the mid-plane of the pipe, as thermal conductivity ratio is variable. The effective stress attains the highest value at the solid-fluid interface and it reduces as the radial distance increases. At low Prandtl number and low thermal conductivity ratio, effective stress reduces considerably. Moreover, the effective stress reduces to minimum at $r^* \cong 0.5$. This is again due to the temperature gradient at this location in the solid. Moreover, the effective stress variation with $r^*$ is shown in figure (4.2.20) at outlet plane of the pipe. The stress behavior with $r^*$ is almost similar to that occurs for the inlet plane provided that the stress corresponding to low Prandtl number and low thermal conductivity ratio is less in the radial direction. When comparing the effective stress at pipe inlet plane, mid-plane and outlet plane, it can be observed that the effective stress reduces at mid and outlet planes. Therefore, the radial stresses reduce as the length in the axial direction increases. This may occur because of the convection and conduction effect of the heat transfer mechanism, i.e. convection heat transfer reduces the solid-fluid interface temperature at the pipe inlet, and as a consequence the conduction in the solid accelerates resulting in high temperature gradient in the radial direction at pipe inlet plane.

Figure (4.2.21) shows the dimensionless temperature ratio $\theta_{ow}/\theta_{iw}$ along the pipe length (x/L) pipe and fluid properties are variable. In general, the dimensionless temperature reduces as the distance along the pipe length increases. Steel pipe results in the highest dimensionless temperature at the pipe inlet plane irrespective of the fluid properties. This may occur because the thermal properties of the steel, i.e. it has relatively low thermal conductivity as compared to copper which in turn results in high outside pipe temperature. In the case of copper, the dimensionless temperature attains low values at pipe inlet plane and it reduces further as x/L increases. The decay rate of dimensionless temperature along x/L is considerably high in the case of steel. This may indicate that the axial heat conduction is smaller than copper resulting in relatively low temperature attainment at the solid-fluid interface. In addition, the effect of fluid properties on the dimensionless temperature is considerable. This is more pronounced for coolanol-25. In this case, the dimensionless temperature along the pipe reduces considerably.

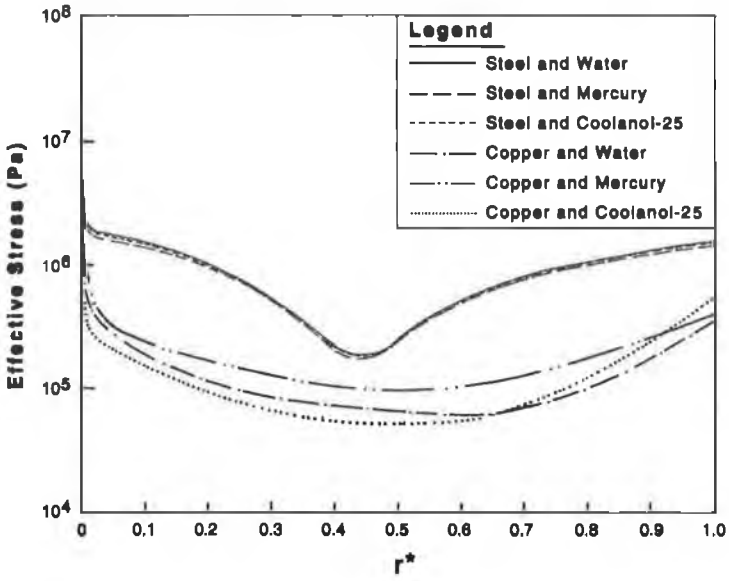


Figure 4.2.19 The effective stress distribution vs. the dimensionless pipe radius at the mid-plane of the pipe for various Prandtl numbers and thermal conductivity ratios.

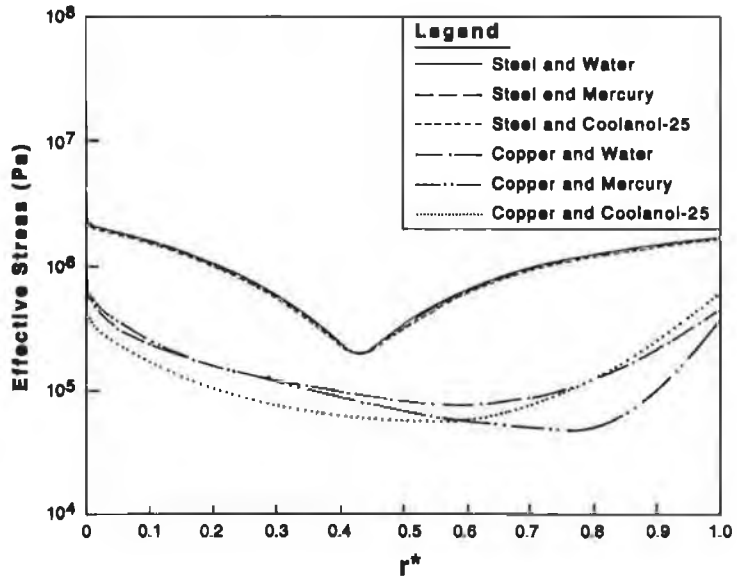


Figure 4.2.20 The effective stress distribution vs. the dimensionless pipe radius at the pipe outlet-plane for various Prandtl numbers and thermal conductivity ratios.

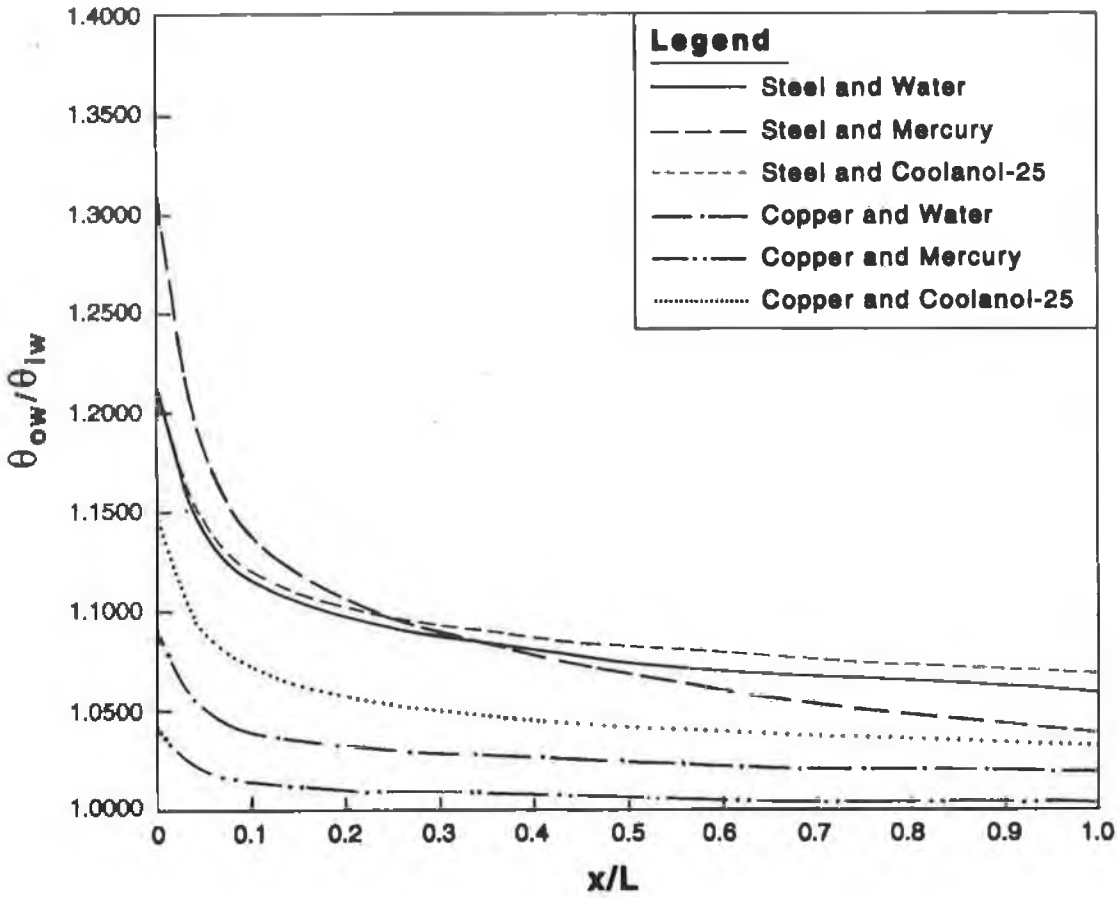


Figure 4.2.21 The dimensionless temperature ratio vs. the dimensionless distance along the pipe for various Prandtl numbers and thermal conductivity ratios.

Figure (4.2.22) shows the location of minimum effective stresses in the radial direction at inlet, mid and outlet planes of the pipe. The minimum effective stress occurs almost at $r^* \cong 0.5$ for all the pipes and fluids employed at present. However, the value of minimum stress increases considerably for steel. Similar results are obtained for the mid-plane provided that the effect of fluid properties is more pronounced. In this case, coolanol-25 results in less value of minimum stresses. At the outlet plane, the minimum effective stress scatters in the radial direction such away that it expands in a range $0.4 \leq r^* \leq 0.8$. This is again because of the temperature gradient developed in the pipe. When comparing the minimum stresses at inlet, mid and outlet planes, the minimum stress attains considerable high vales at the inlet planes. This occurs because of the considerably high temperature gradient development in this region.

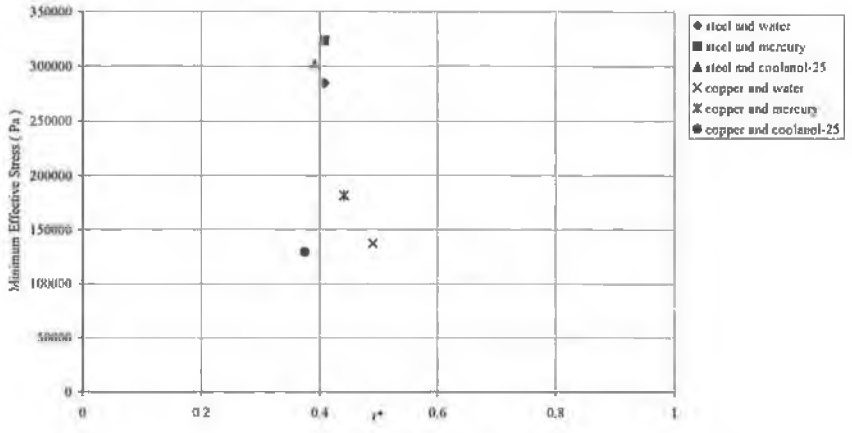


a. Inlet-plane

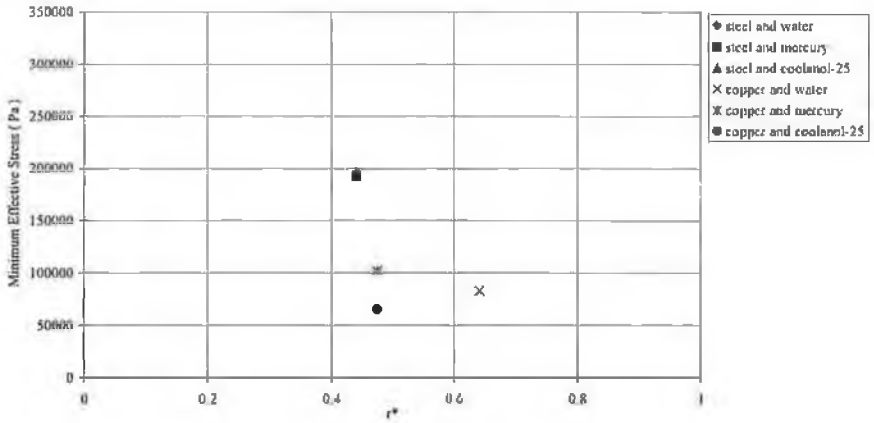


b. Mid-plane

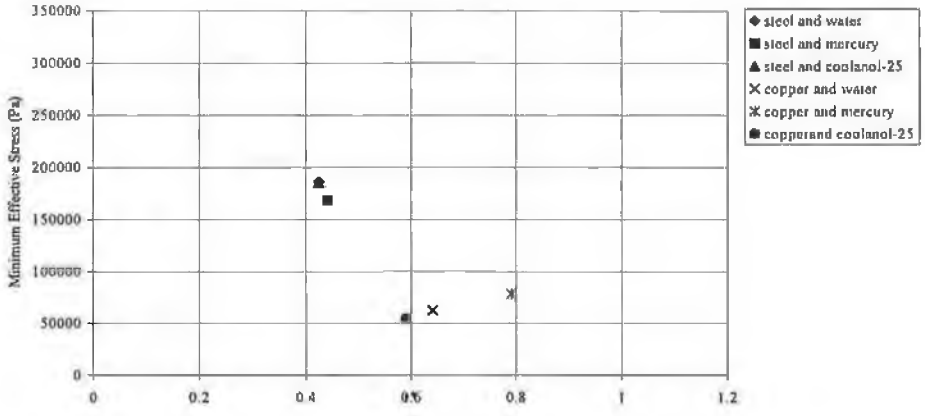


c. Outlet-plane

Figure 4.2.22 Location of the minimum effective stress at the inlet, mid and outlet planes of the pipe for various Prandtl numbers and thermal conductivity ratios.

## 4.3 Turbulent flow

This section presents the thermal stresses developed in pipes due to turbulent flow at different Reynolds numbers (10000, 30000 and 50000). Simulations are made for two fluids (water and coolanol-25) to investigate the effects of Prnadtl number on the resulting thermal stresses. Two solids (steel and copper) are also employed in the study to investigate the effect of solid to fluid conductivity ratio.

Figure (4.3.1) shows the local Nusselt number variation with dimensionless distance (x/L) for two different fluids, three Reynolds numbers and two pipe materials. The Nusselt number attains higher values in the region close to the pipe inlet where x/L is low. This is because of the relatively cold fluid entering the pipe. As the fluid passes through the pipe, its temperature increases because of heat transfer. This suppresses the heat transfer rate from solid wall to fluid. Consequently, the Nusselt number attains relatively lower values as compared to that corresponding to pipe inlet. As the Reynolds number increases, the Nusselt number increases as expected, since the Nusselt number is a function of the Reynolds number. Moreover, the Nusselt number attains higher values for coolanol-25 as compared to the case corresponding to water. This is because of the fluid properties, i.e. coolanol-25 has lower specific heat and density as compared to water [Table 4.1.1]. The effect of the pipe material properties on the Nusselt number is not significant. This may occur because of the steady state heating of the fluid, in which case heat supplied to pipe wall takes place at a constant rate. Consequently, the interface temperature between the wall and the fluid differs for different materials, but amount of heat transfer to the fluid remains constant.

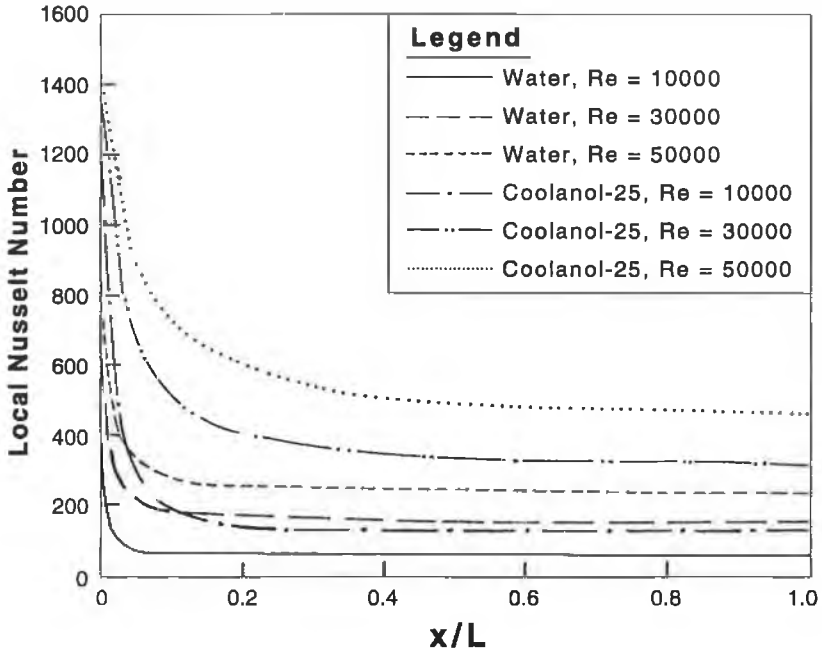


a. steel pipe

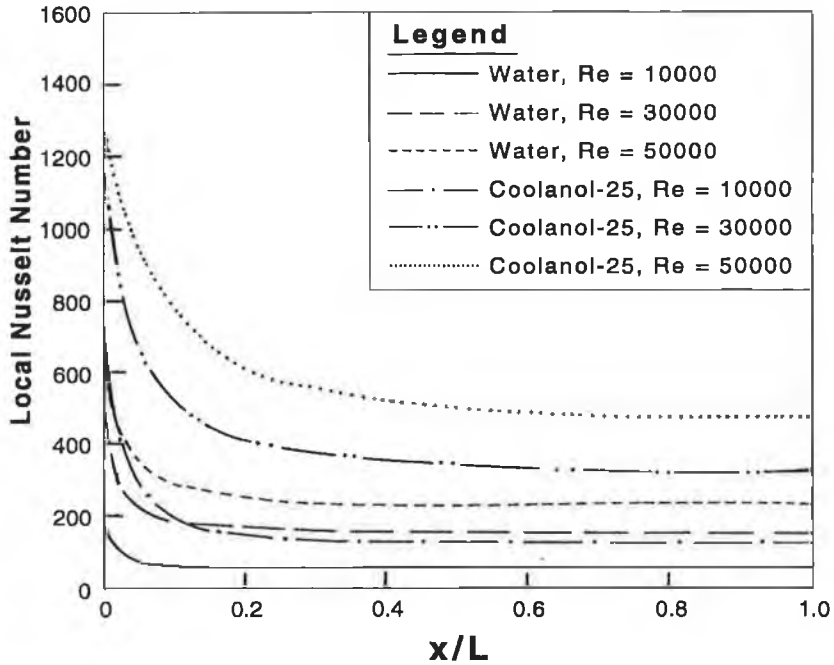


b. copper pipe

Figure 4.3.1 Variation of the local Nusselt number ($N_u$) with the dimensionless length of the pipe for two fluids at different Reynolds numbers for the cases of a) steel pipe and b) copper pipe.

Figure (4.3.2a) shows the dimensionless temperature ($T^*$) profiles in the solid and fluid for a copper pipe and water at Re=10000. The temperature profile in the copper changes its slope sharply at the pipe entrance. As the distance along the pipe increases, the temperature profiles gradual decay before the sharp change in slope. This is because of the heat transfer characteristics. The uniform heat supplied externally enhances the temperature rise along the x-axis in the pipe. Consequently, in the copper, the temperature contours attain higher values as the distance from the pipe inlet increases in the x-direction. The location of sharp temperature gradient change occurs in the solid and close to the fluid-solid interface. This is because close to the solid-fluid interface temperature decays rapidly due to high heat transfer coefficient at solid-fluid interface. In the case of fluid, the temperature attains high values close to the solid-fluid interface and reduces as the radial distance from the solid wall increases. Moreover, the temperature gradient along the pipe length changes as the radial location changes. In this case, the region of heated fluid expands in the radial direction towards the pipe end. The similar behavior is observed from figure (4.3.2b), in which the temperature contours in the solid and fluid are shown for copper pipe and coolanol-25 at Re=10000. When comparing figures (4.3.2a) and (4.3.2b), the temperature contours expand further inside the fluid. This is because of the fluid properties such that water has relatively higher heat capacity and thermal diffusivity as compared to coolanol-25 as evident from Table 4.1.

Figures (4.3.3a) and (4.3.3b) show the dimensionless temperature contours in the solid and fluid sides for steel pipe at Re=10000. The temperature gradient changes rapidly in the solid side close to the solid-fluid interface. As the axial distance along the pipe length increases, the temperature gradient changes rather smoothly due to the heat transfer characteristics. In the case of fluid side, the temperature contours expand into the liquid as the axial distance from the pipe entrance increases. This is more pronounced for water, since it has higher thermal diffusivity as compared to coolanol-25. The effect of fluid properties on the temperature is also visible in the solid side. In this case, water results in lower values of temperature contours in the solid as compared to its counterpart that resulted from coolanol-25.

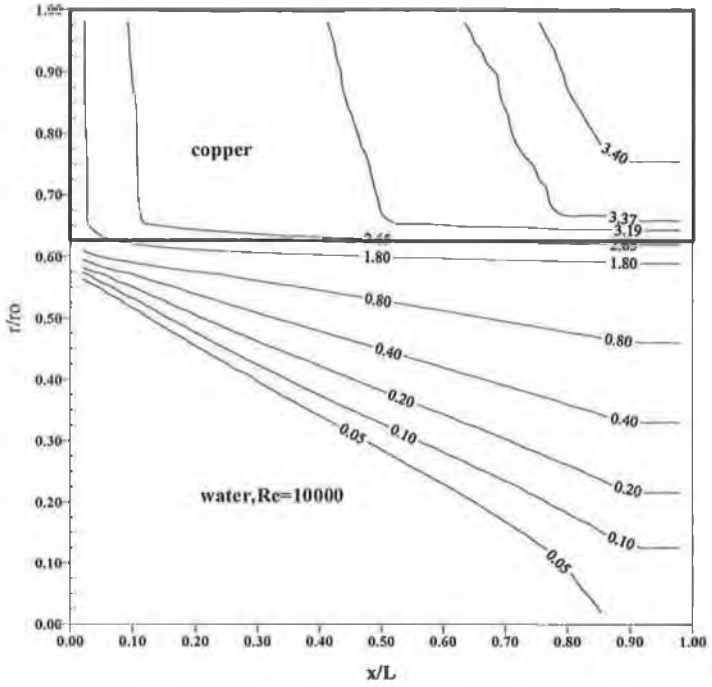


a. copper and water.

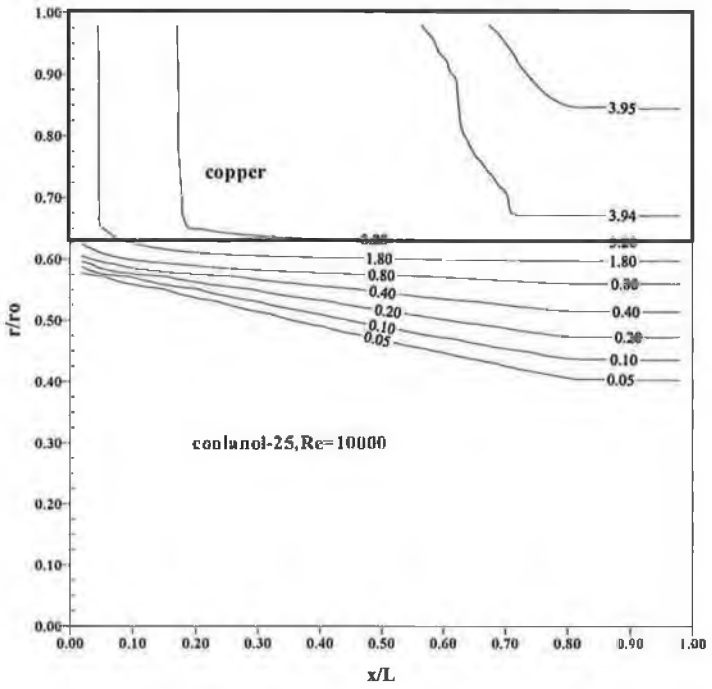


b. copper and coolanol-25.

Figure 4.3.2 Dimensionless temperature ($T^*$) contours for the case of copper pipe with water and coolanol-25 at Re = 10000.

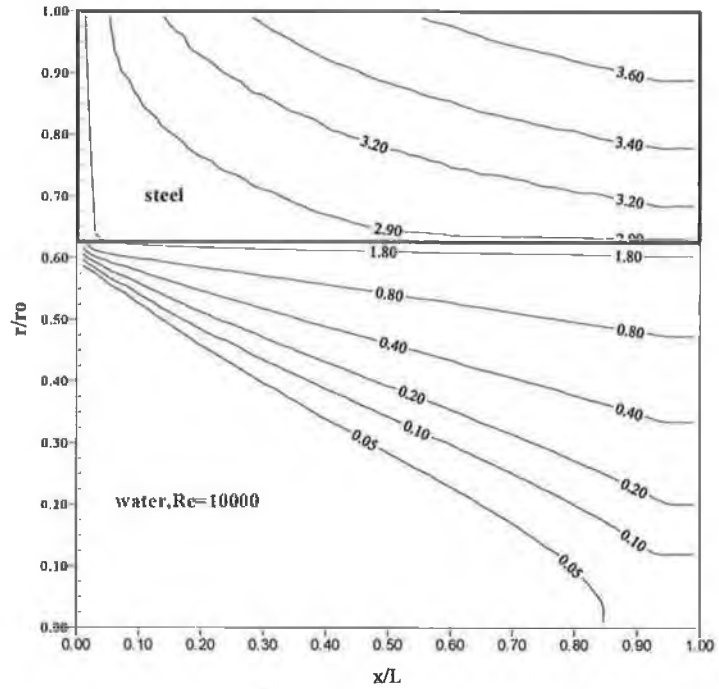


a. steel and water.

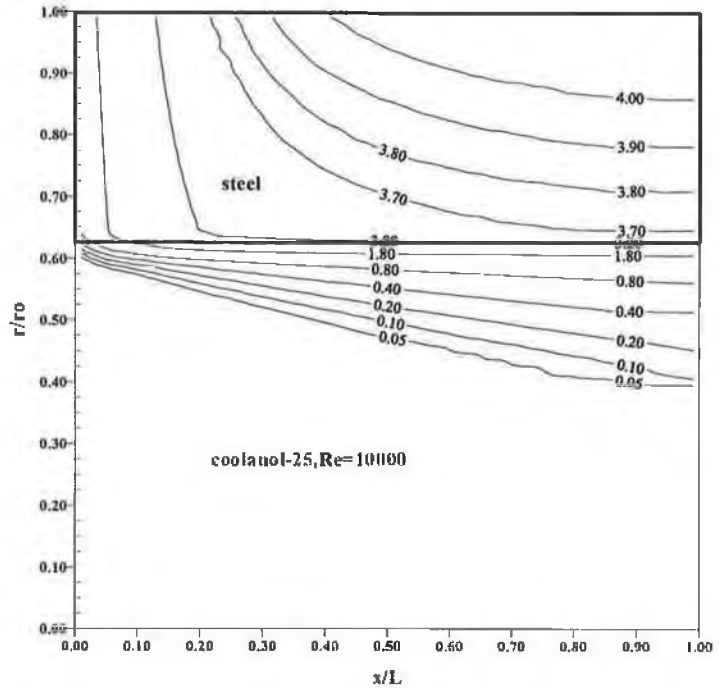


b. steel and coolanol-25.

Figure 4.3.3 Dimensionless temperature ($T^*$) contours for the case of steel pipe with water and coolanol-25 at Re = 10000.

Figures (4.3.4a) and (4.3.4b) show the dimensionless temperature contours in solid and fluid sides for water and coolanol-25 and copper pipe at Re=30,000. The temperature gradient reduces gradually in the solid along the radial direction. The temperature gradient attains large values as the axial distance along the pipe length increases. Similar to the observation made for figures (4.3.2a) and (4.3.2b), the temperature gradient changes rapidly in the solid close to the solid-fluid interface. The location of rapid temperature gradient change moves relatively close to the solid-fluid interface as compared to those that occur in figures (4.3.2a) and (4.3.2b). This is because of the convection cooling of the pipe, which is enhanced with increasing Reynolds number. The temperature contours extend inside the fluid towards the end of the pipe. This is more pronounced for water than coolanol-25, which is again due to the properties of the fluid used. The same observations are available in figures (4.3.5a) and (4.3.5b) that show the dimensionless temperature contours for water and coolanol-25 and copper pipe at Re=50,000.

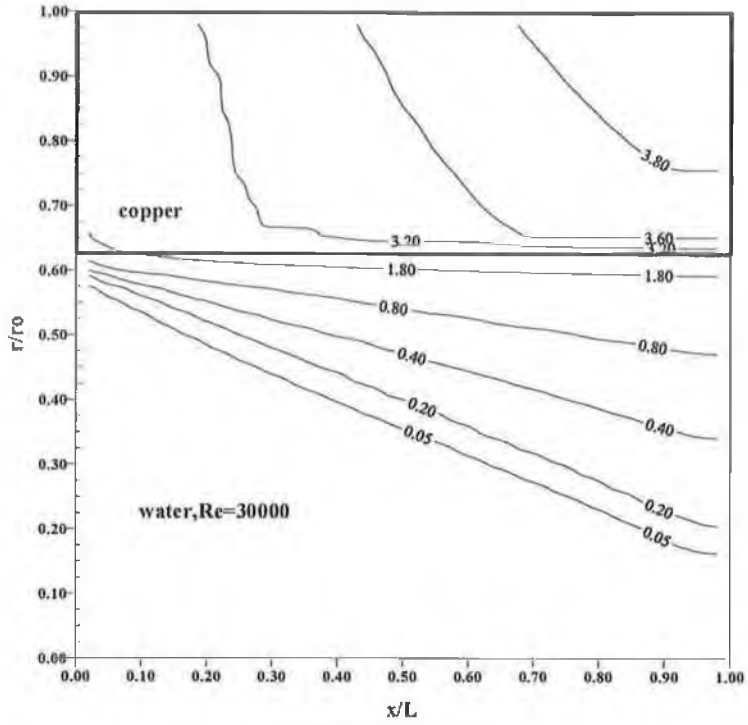


a. copper and water

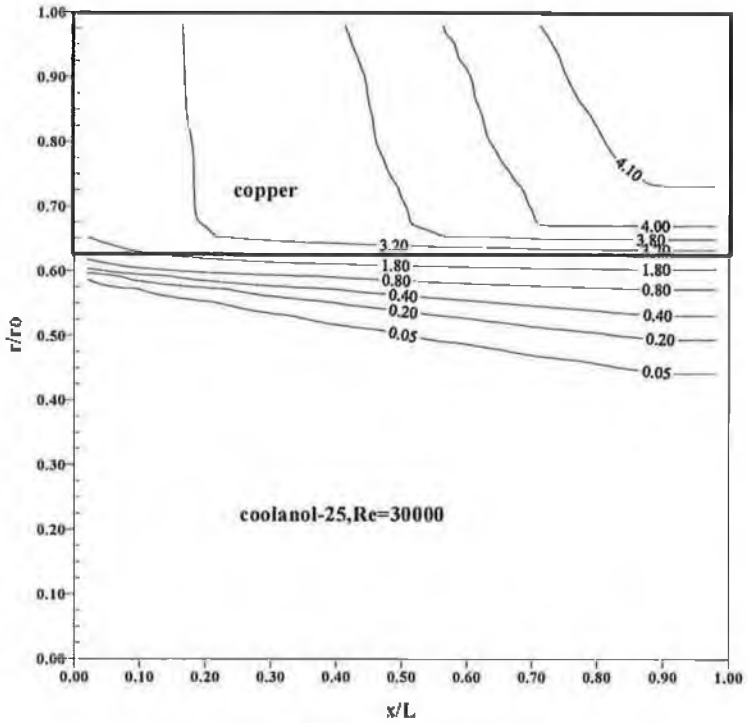


b. copper and coolanol-25

Figure 4.3.4 Dimensionless temperature ($T^*$) contours for the case of copper pipe with water and coolanol-25 at Re = 30000.

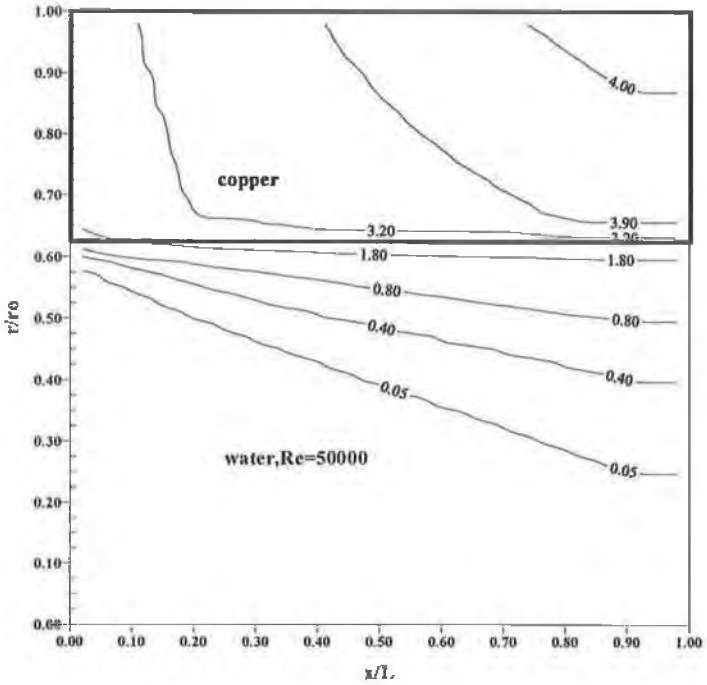


a. copper and water.

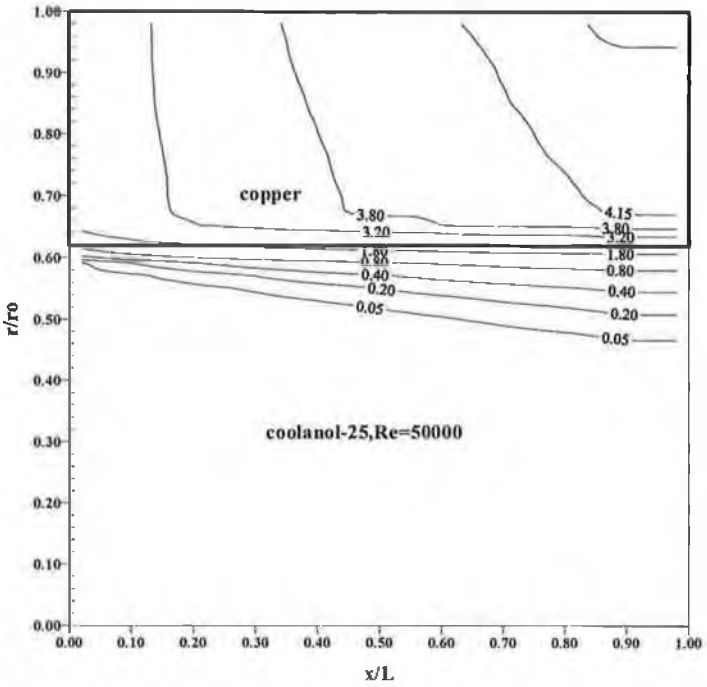


b. copper and coolanol-25.

Figure 4.3.5 Dimensionless temperature ($T^*$) contours for the case of copper pipe with water and coolanol-25 at Re = 50000

Figures (4.3.6a) and (4.3.6b) show the dimensionless temperature contours in the solid and fluid for water and coolanol-25 and steel pipe at Re=30,000. The temperature gradient in steel pipe reduces gradually along the pipe length except in the region close to the pipe inlet. In this case, the sharp decay of temperature gradients are observed at the pipe inlet, which is more pronounced for coolanol-25. When comparing the temperature profiles in steel and copper pipes, the temperature gradients decay more smoothly in the steel pipe as compared to that corresponding to copper pipe. This occurs because the high thermal conductivity of the copper, in which case rapid change of temperature gradient in the solid occurs, since the fluid acts as a heat sink for the solid due to convective cooling. When comparing figures (4.3.6a) and (4.3.6a), the effect of the Reynolds number on temperature gradient is evident in the solid side. In this case, the temperature gradient rapidly changes close to the solid-fluid interface along the pipe length at low Reynolds number. As the Reynolds number increases the rapid change of temperature gradients is observed close to the pipe inlet only., which is shown clearly in figures (4.3.7a) and (4.3.7b) that show the dimensionless temperature contours for water and coolanol-25 and steel pipe at Re=50000. This is because of the heat transfer rate along the pipe length, which is higher at the pipe inlet due to low fluid temperature. As the pipe length increases, the fluid temperature increases and heat transfer rate reduces so does the temperature gradient in the solid side.

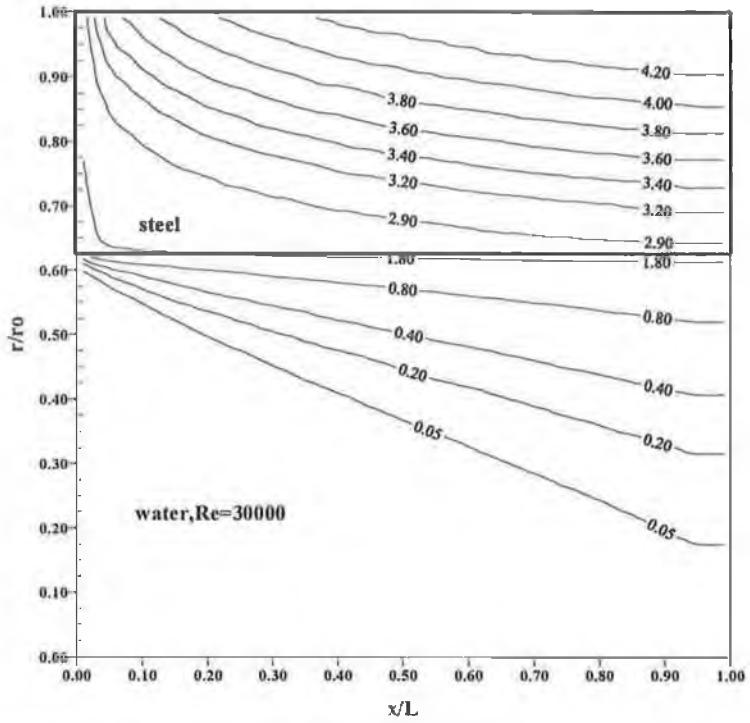


a. steel and water

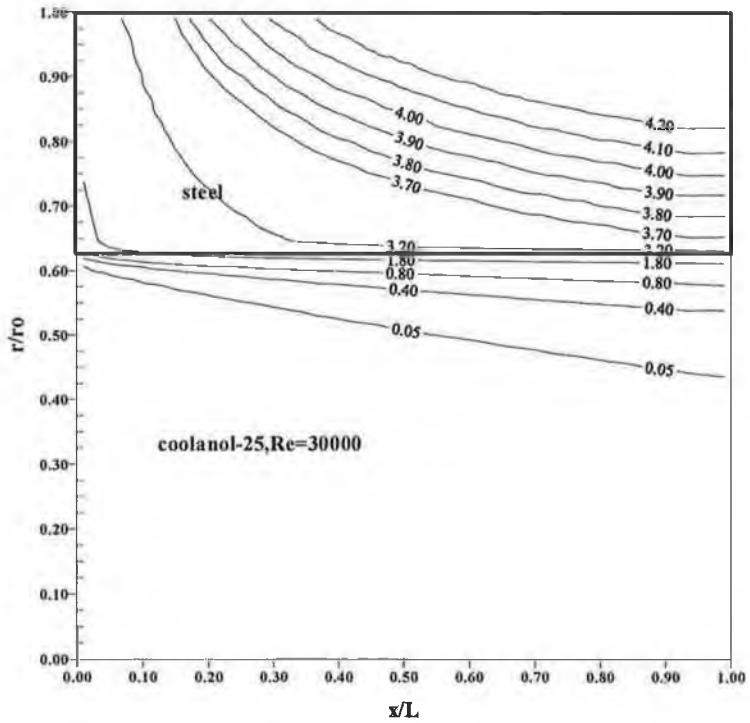


b. steel and coolanol-25

Figure 4.3.6 Dimensionless temperature ($T^*$) contours for the case of steel pipe with water and coolanol-25 at Re = 30000.

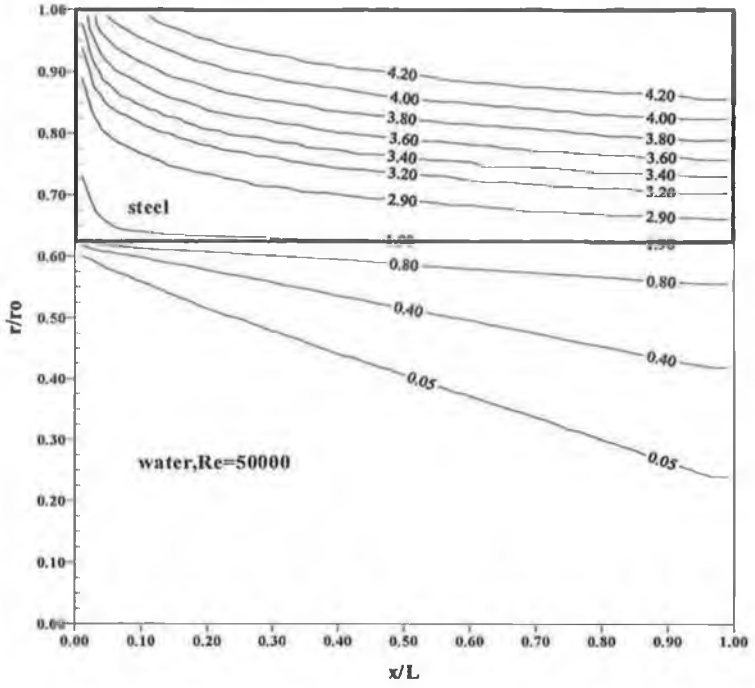


a. steel and water

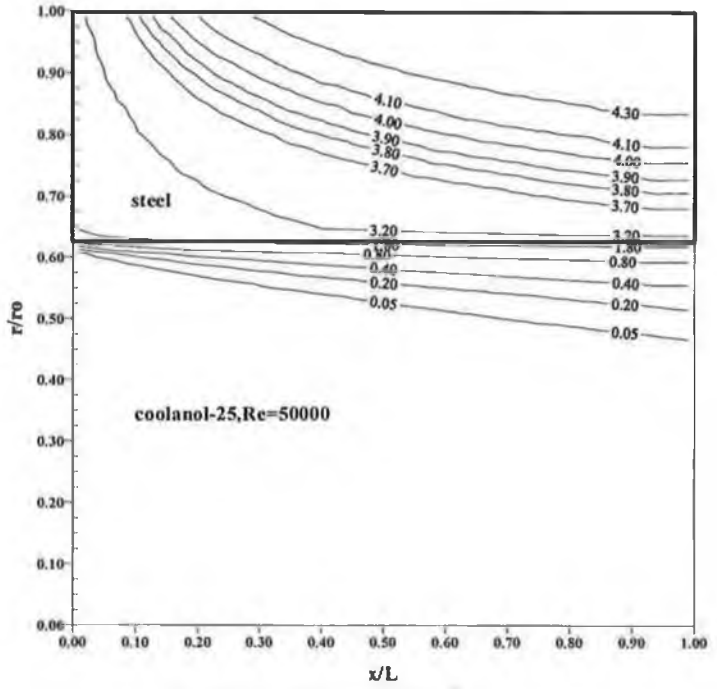


b. steel and coolanol-25

Figure 4.3.7 Dimensionless temperature ($T^*$) contours for the case of steel pipe with water and coolanol-25 at Re = 50000.

Figure (4.3.8) shows the effective stress with dimensionless radius ($r^*$) at mid-plane of the pipe for different combination of solid and fluid properties. In general, the effective stress reduces to minimum as the radial distance from the inner surface increases to almost 0.5. It then, increases as $r^*$ increases to reach 1. In the case of copper pipe, the effective stress does not alter to dimensionless radius $r^*$ to the point where $r^* < 0.5$. It increases to attain a steady value where $r^*$ further increases to 1. This occurs because the temperature gradient in the solid, which remains almost the same across the pipe cross-section due to high thermal conductivity of the substance (copper). In the case of steel pipe, effective stress is maximum at the pipe inlet and reduces to minimum at almost $r^* = 0.5$. It increases further as $r^*$ increases to 1. The effective stress attains higher values in the case of water as compared to the case corresponding to coolanol-25. This is because the temperature distribution in the solid, in which case it is water, results in higher temperature gradients in the solid. The effect of Reynolds number can be observed, when comparing figures (4.3.8a), (8.3.8b) and (4.3.8c). The effect of fluid properties on the effective stress becomes negligible as Reynolds number increases. In this case, the effective stresses due to water and coolanol-25 become identical along the dimensionless radius $r^*$. Moreover, the effect of solid material on the effective stress is negligible with increasing Reynolds number. This is because the heat transfer coefficient at solid-fluid interface attains steady value with increasing Reynolds number (figure (4.3.1)). Consequently, the temperature distribution in the fluid remains the same at high Reynolds number. However, the temperature distribution in the solid becomes the same for all Reynolds numbers.

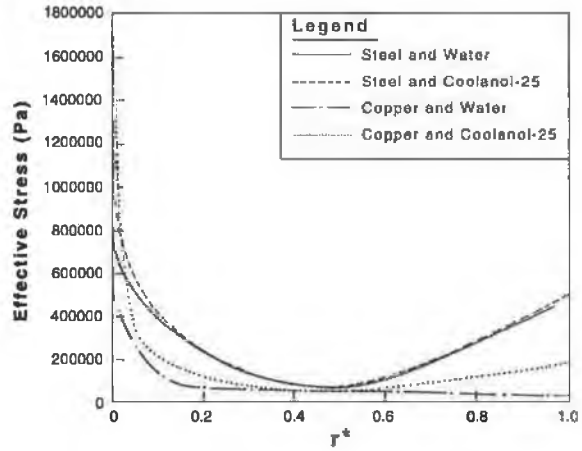


a. Re=10000

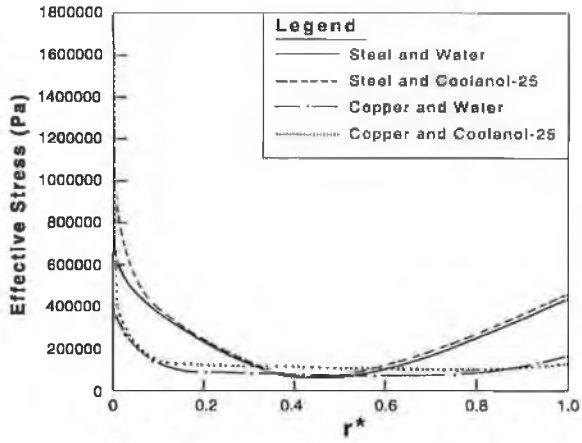


b. Re=30000

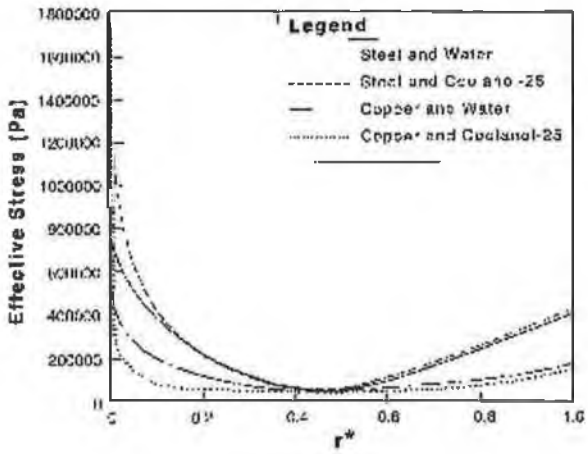


c. Re=50000

Figure 4.3.8 Mid-plane effective stresses for combinations of two solids and two fluids at three different Reynolds numbers.

## 4.4 Pulsating Flow

This section presents the results of a parametric study about thermal stresses in pipes due to pulsating flow. The parameters investigated in this study are the pipe diameter, the pipe thickness to diameter ratio, the length to diameter ratio, the Reynolds number, the fluid properties (Prandtl number), the pressure difference oscillating frequency and the amount of heat flux.

### 4.4.1 The Effects of Diameter Size and Thickness to Diameter Ratio on Thermal Stresses:

To investigate the effect of the pipe diameter and thickness on thermal stresses in pipes due to pulsating flow, two pipe diameters and two thickness to diameter ratios for each pipe diameter are simulated. The length to diameter ratio is kept constant. Table 4.4.1 provides the values of the parameters and the grid sizes used in this part. The heat flux is taken as 20,000 $W/m^2$ and the pressure difference oscillating frequency is equal to 0.1 Hz. Steel and water are considered as the solid and fluid respectively in this study.

| Pipe Inner Diameter, D (m) | Pipe Thickness, t (m) | Pipe Length, (m) | Mesh Size (no. cells) | | |
|---|---|---|---|---|---|
| | | | Radial (Fluid) | Radial (Solid) | Axial |
| 0.04 | 0.125 D = 0.005 | 7.5 D = 0.3 | 120 | 30 | 24 |
| | 0.5 D = 0.02 | 7.5 D = 0.3 | 120 | 120 | 24 |
| 0.08 | 0.125 D = 0.01 | 7.5 D = 0.6 | 120 | 30 | 24 |
| | 0.5 D = 0.04 | 7.5 D = 0.6 | 120 | 120 | 24 |

Table 4.4.1 The pipe diameters and thicknesses (Reynolds number = 500).

Figure (4.4.1) shows the temporal variation of temperature in the inner and outer walls at inlet and outlet planes of the pipe for two diameters and for a thickness to diameter ratio equal to 0.125. The temperature rise is almost steady with some oscillation at the outer wall of the outlet plane; however, oscillation in temperature occurs elsewhere. This is more pronounced at the inner wall of the inlet plane. In this case, oscillation in the temperature field in the fluid side results in similar behavior at the interface between the solid wall and the fluid. Consequently, the amplitude of oscillation becomes larger in this region. Moreover, the rise of temperature profile is higher at the outer wall than that corresponding to the inner wall. This is because of the heat input from the outer surface of the pipe. The effect of the pipe diameter on the temperature field results in less oscillation in the temperature profile at the outer wall and it becomes smoother and more steady for 0.08 m diameter pipe than that corresponding to 0.04 m diameter. This indicates that as the diameter of the pipe increases, the temperature oscillation in the pipe is damped out.

Figures (4.4.2) and (4.4.3) show the temporal variation of the effective stresses at the outer, mid- radial plane and inner walls at the inlet and outlet planes of the pipe for the 0.04 m and 0.08 m diameters and a thickness to diameter ratio equal to 0.125, respectively. The stresses at the mid-radial plane and outer walls of the pipe are not considerable. Moreover, the level of the stress increases at the inner wall of the pipe. In this case, a peak stress level of the order of about 12 MPa is observed. A larger amplitude of oscillation is observed in the inlet plane compared to that of the outlet plane. This is because of the temperature field in this region, i.e. the rise of temperature as well as its amplitude of oscillation are high in this region. In addition, thermally induced stress loading from the inner and outer surfaces of the pipe is also high in this region. In the case of the outlet plane, the oscillation in stress level is low due to the relative lower temperature rise in this region as compared to that corresponding to inlet plane. The effect of pipe diameter on the effective stress is only significant at the outlet plane of the pipe. In this case, as the pipe diameter becomes larger, the stress level at the outlet plane oscillates with lower amplitude.

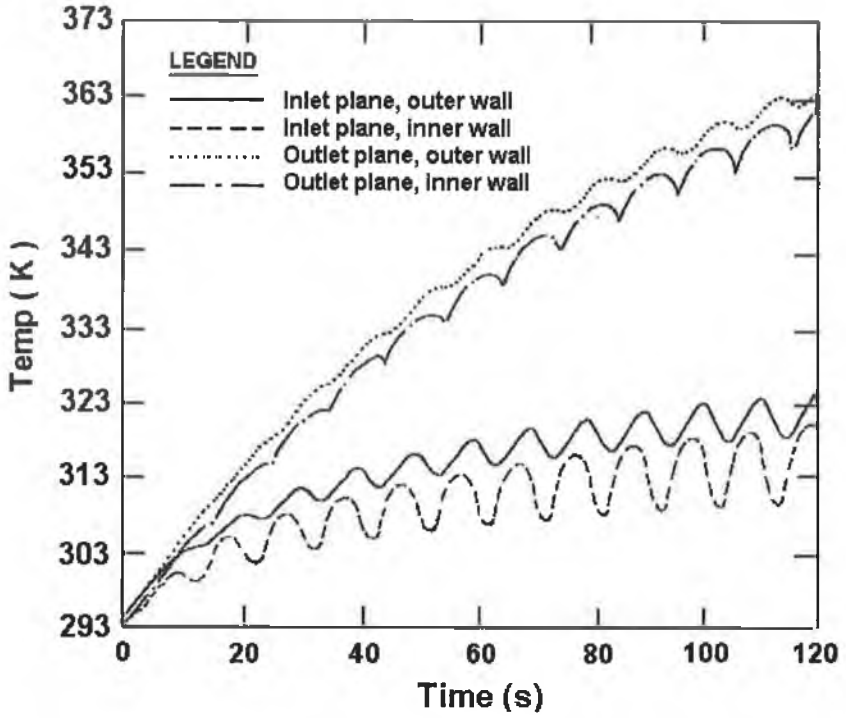


4.4.1a D = 0.04 m, t = 0.005 m

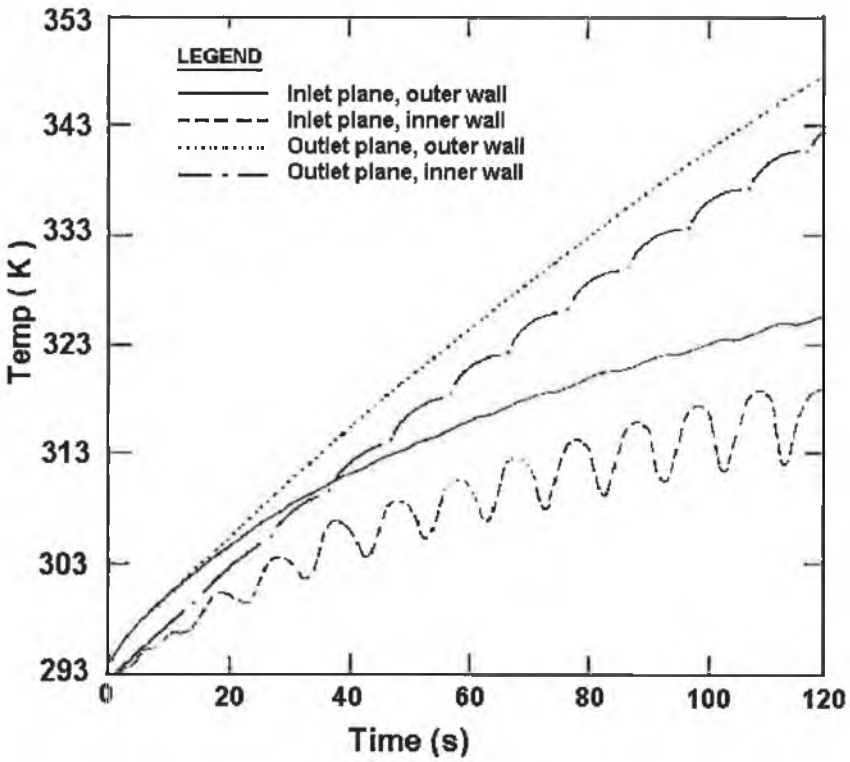


4.4.1b D = 0.08 m, t = 0.01 m

Figure 4.4.1 Inner and outer wall temperatures at the inlet and outlet planes for the cases of D = 0.04 m and D = 0.08 m and t = 0.125×D.

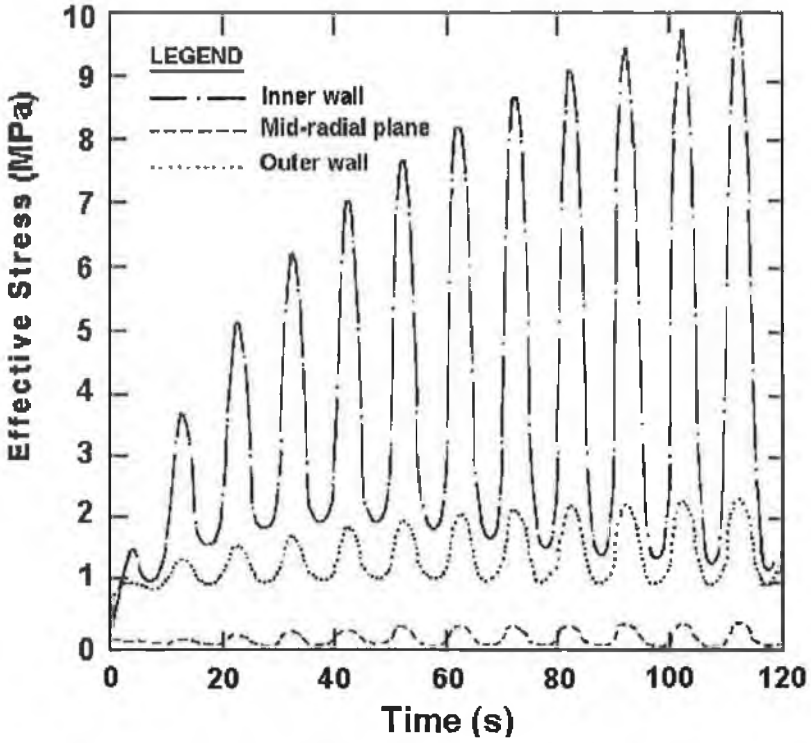


4.4.2a Inlet plane

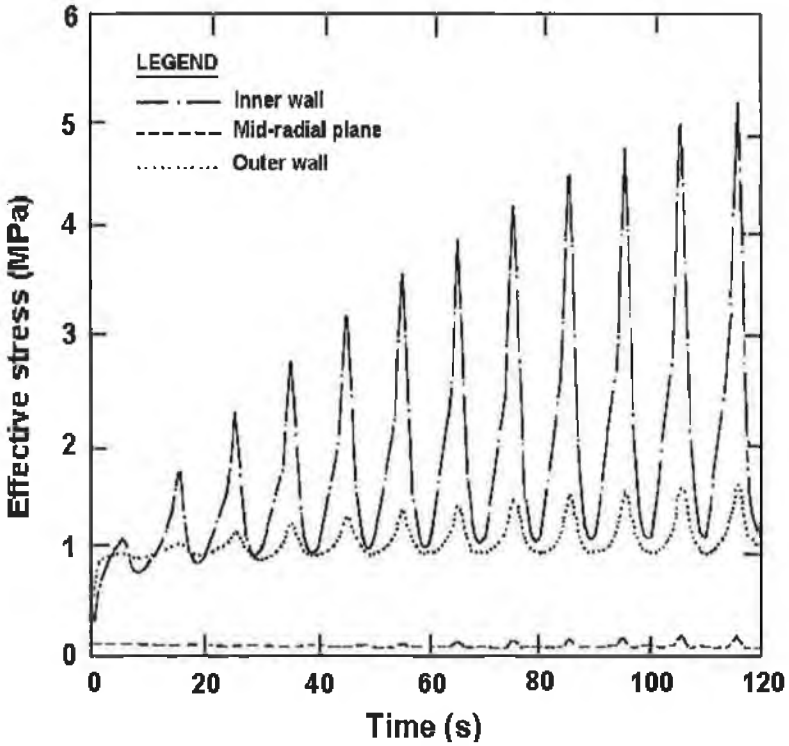


4.4.2b Outlet plane

Figure 4.4.2 Thermal stresses at inlet and outlet planes for the case of D = 0.04 m, t = 0.125×D = 0.005 m

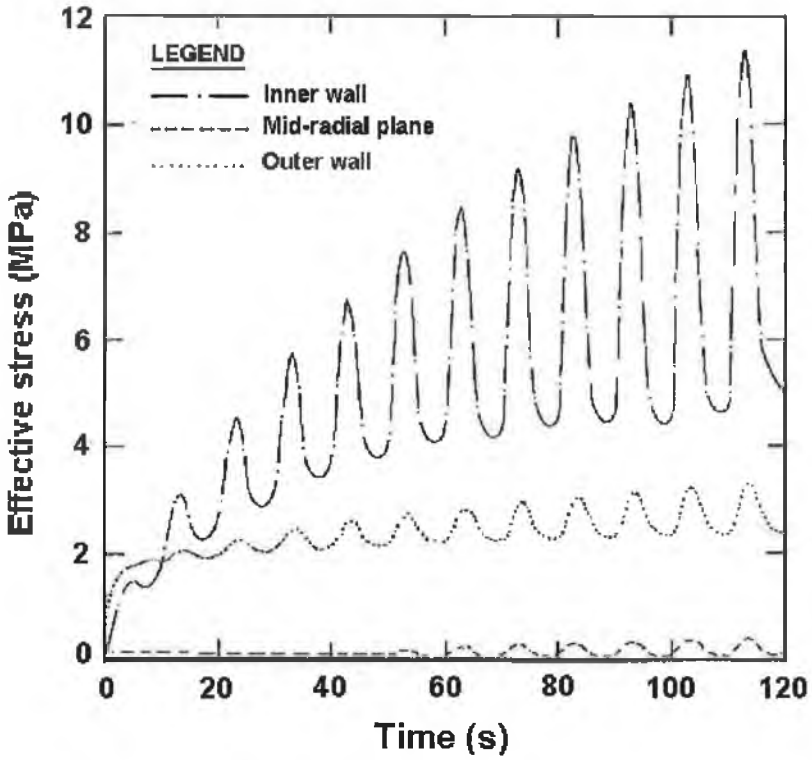


4.4.3a Inlet plane

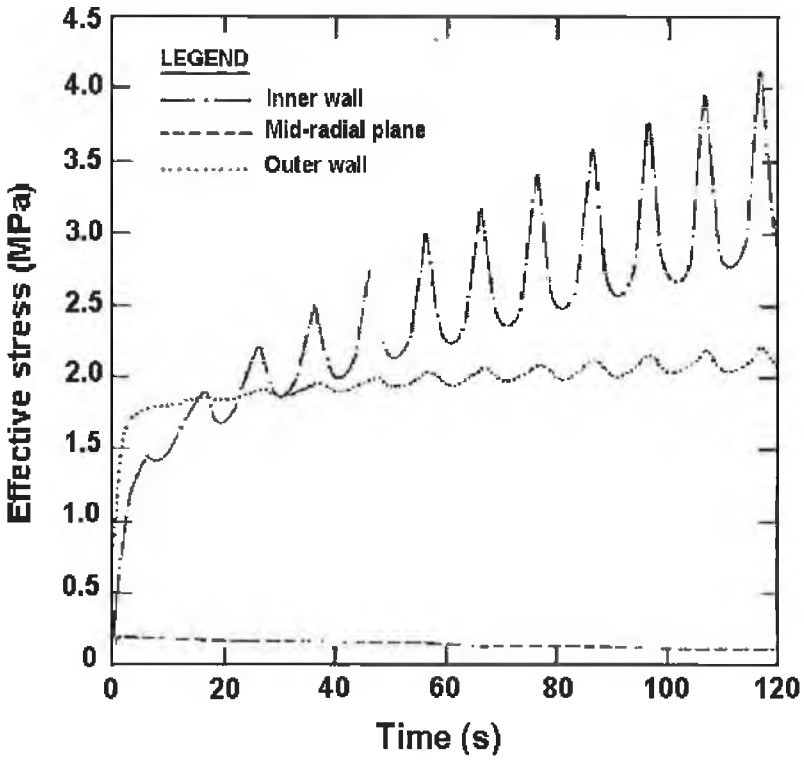


4.4.3b Outlet plane

Figure 4.4.3 Thermal stresses at inlet and outlet planes for the case of D=0.08 m, t=0.125×D = 0.01 m

Figure (4.4.4) shows the temperature profiles with time at the inner and outer walls of inlet and outlet planes two diameters and for a thickness to diameter ratio equal to 0.5. Oscillation in temperature profiles at inner walls of the pipe is evident. At the outer wall, the increase in temperature becomes mores steady (almost no oscillation). Moreover, oscillation in temperature profile at the inner wall of the inlet plane is higher than that corresponding to the inner wall at outlet plane. This is because of the oscillation of the velocity at the pipe inlet, i.e. velocity oscillation decays towards the end of the pipe, which in turn reduces the temperature oscillation. As the pipe diameter increases with the same thickness to diameter ratio, the magnitude of the oscillation in the inner and outer wall temperatures reduces. This is evident from figure (4.4.4b) in which the temperature profiles at the inner and outer wall locations are shown for a 0.04 m thick and 0.08 m diameter pipe. This occurs because of the thermal capacitance of the pipe wall. In this case, the energy stored by the pipe material increases as the transient heating progresses, i.e. the pipe wall acts as a heat source enhancing the fluid heating in the pipe. Consequently, the fluid convective cooling of the inner wall is suppressed and the temperature oscillation reduces. This also results in almost no oscillation at the outer wall of the pipe.

Figures (4.4.5) and (4.4.6) show the effective stresses in the region of the inner and outer wall of the pipe at the inlet and exit planes. The oscillation in the effective stress is low in the early heating period. This is because of the low temperature oscillations in this region. As the heating progresses, the amplitude of oscillation increases provided that this is more visible at the inner wall of the pipe. In this case, the temperature oscillation at the inner wall results in excessive stress oscillation in this region. This change in stress level is more pronounced at the inlet plane of the pipe, which is due to relatively larger amplitude in temperature at the inlet plane as compared to that corresponding to outlet plane. The rate of stress increase is high in the early heating period while the rise of stress is almost steady with time as the heating progresses. This is more pronounced at the mid and outlet planes. This is because of the temperature profiles in these planes, i.e. the high rate of temperature rise results in a similar rise in the stress levels.

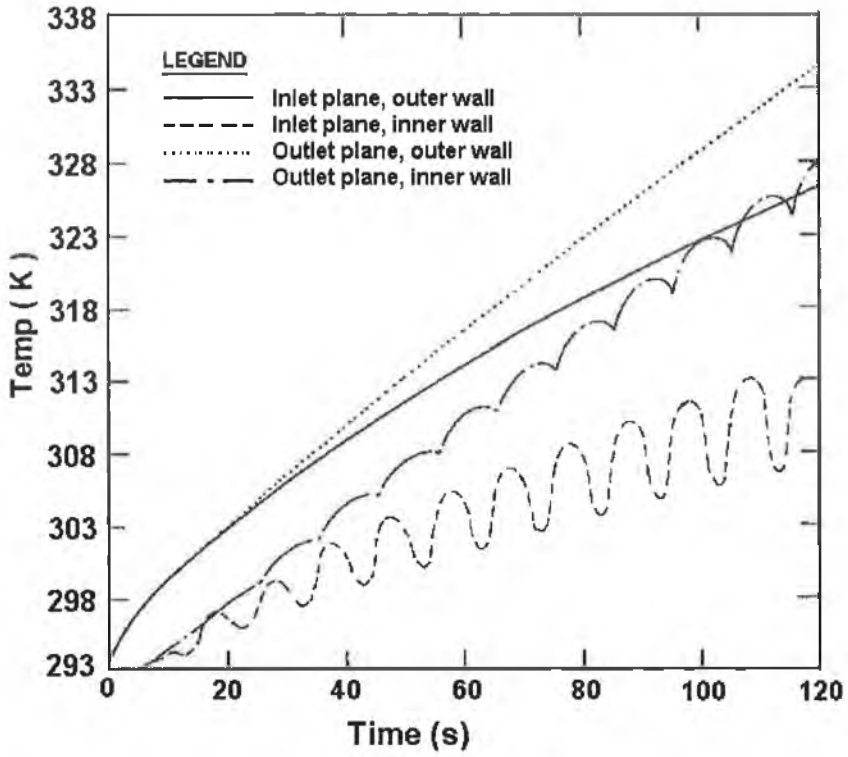


4.4.4a D = 0.04 m, t 0.02 m

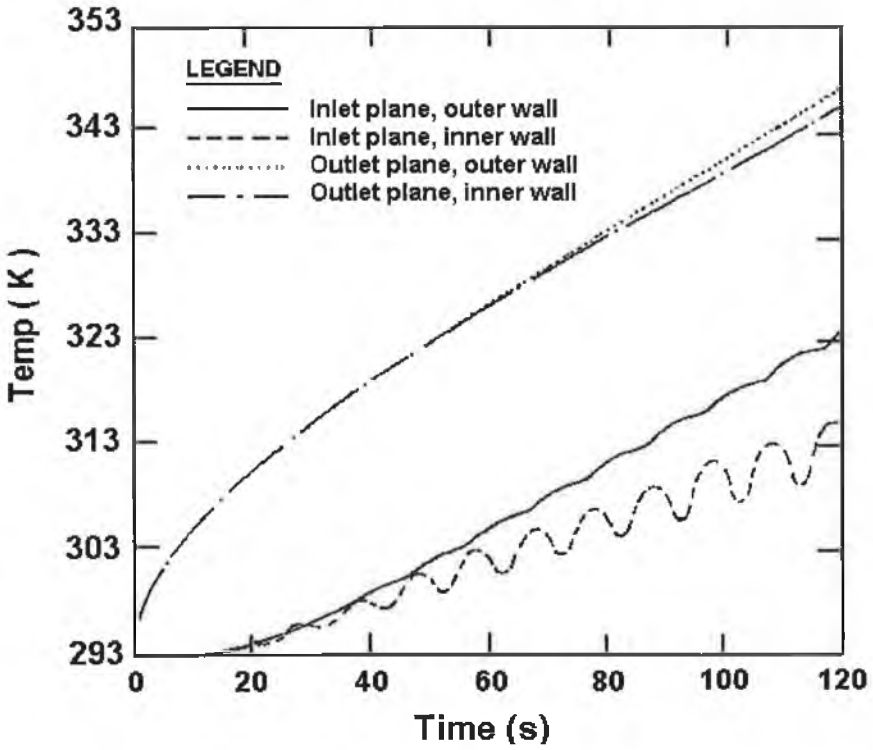


4.4.4b D = 0.08 m, t = 0.04 m

Figure 4.4.4 Inner and outer wall temperatures for the cases of D = 0.04 m and D = 0.08 m and t = 0.5×D.

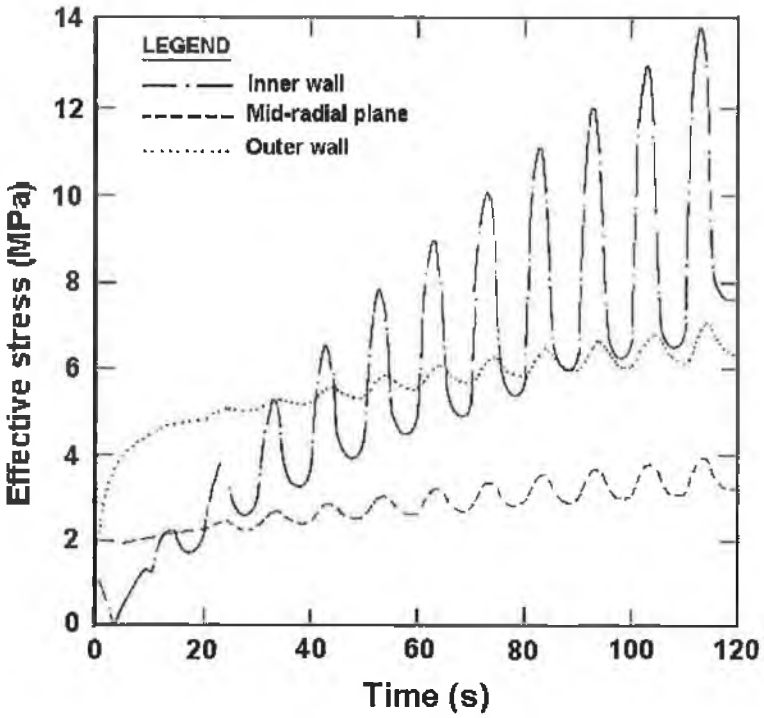


4.4.5a Inlet plane

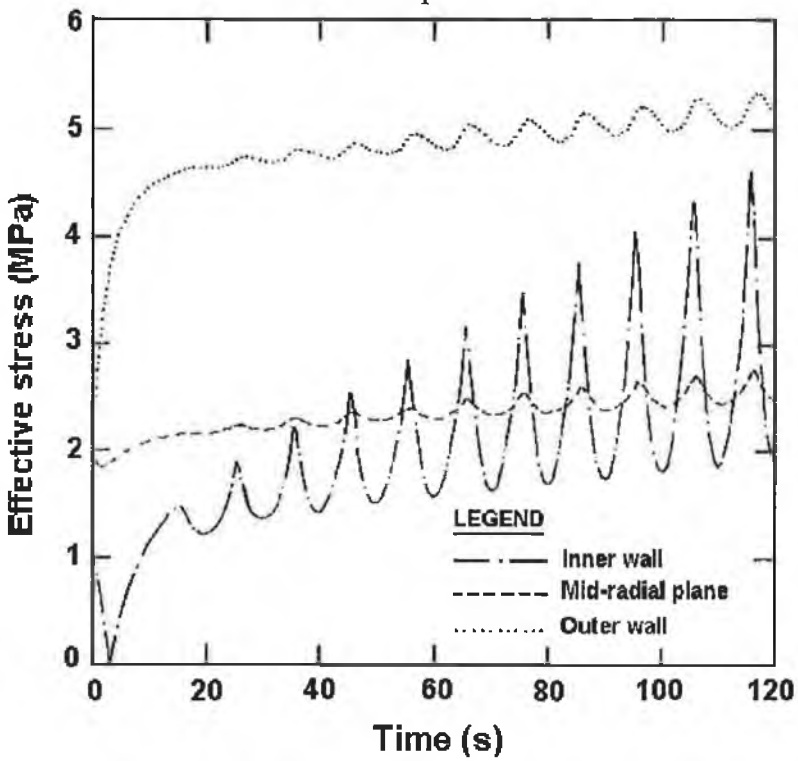


4.4.5b Outlet plane

Figure 4.4.5 Thermal stresses at inlet and outlet planes for the case of D = 0.04 m, t = 0.5×D = 0.02 m

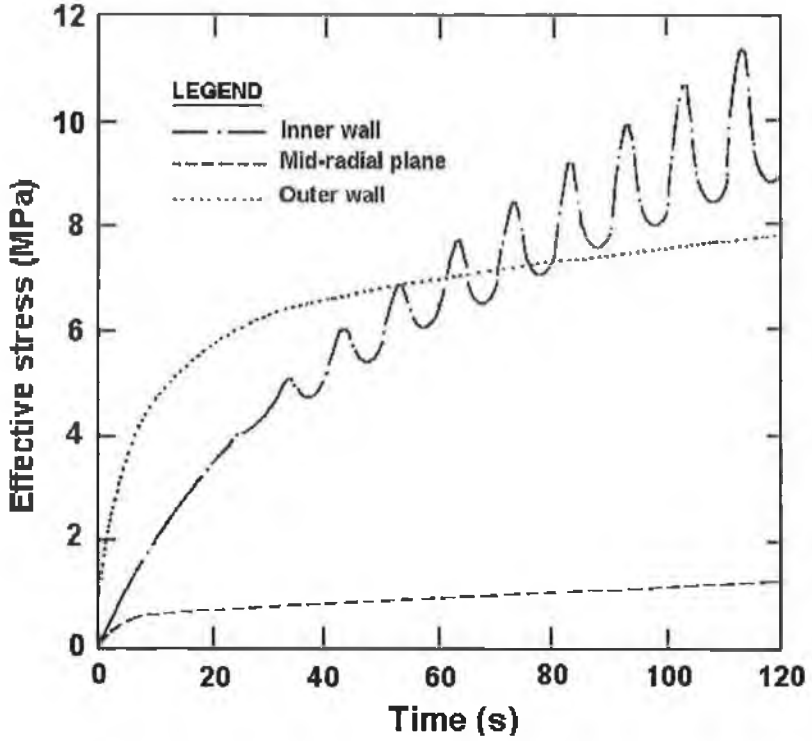


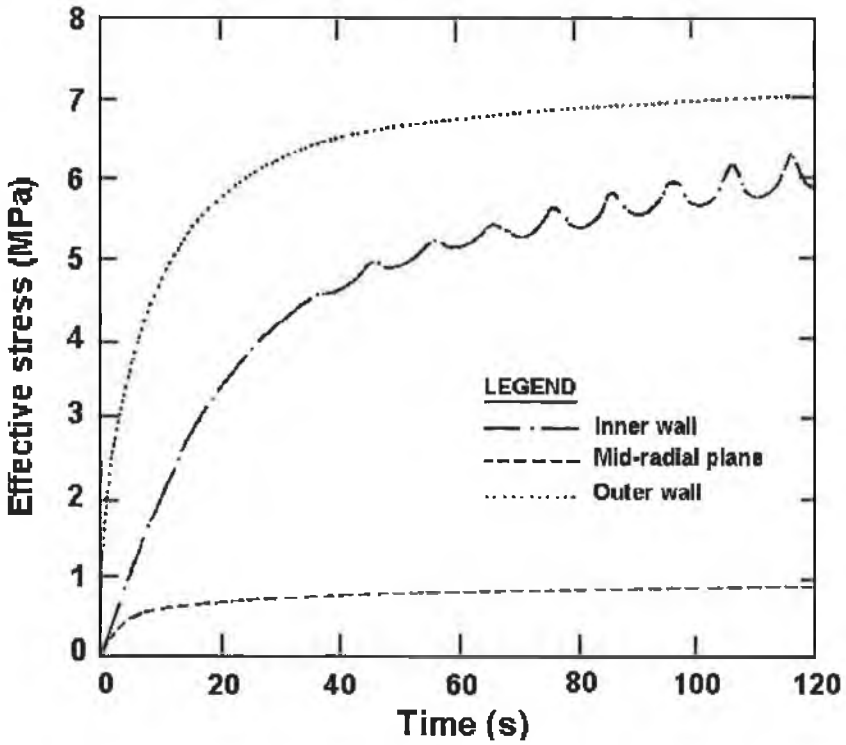


4.4.6a Inlet plane

4.4.6b Outlet plane

Figure 4.4.6 Thermal stresses at inlet and outlet planes for the case of D = 0.08 m, t = 0.5×D = 0.04 m

### 4.4.2 The Effects of Pipe Length Size on Thermal Stresses:

The second part of this section covers the effects of pipe length on the thermal stresses. The pipe inner diameter is taken as 0.08 m and the thickness to diameter ratio is kept constant. Three different lengths are used. The values of the parameters used in this part are provided in Table 4.4.2. The heat flux is taken as 20,000 $W/m^2$ and the pressure difference oscillating frequency is equal to 0.1 Hz. Steel and water are considered as the solid and fluid respectively in this study.

| Pipe Length, (m) | Mesh Size (no. cells) | | |
|---|---|---|---|
| | Radial (Fluid) | Radial (Solid) | Axial |
| 7.5 D = 0.6 | 120 | 30 | 24 |
| 12.5 D =1.0 | 120 | 30 | 40 |
| 17.5 D =1.4 | 120 | 30 | 56 |

Table 4.4.2 Pipe Lengths (Reynolds number = 500, t/D = 0.125).

Figure (4.4.7) shows the effect of pipe length on the temporal variation of temperatures at inner and outer walls at the pipe inlet, mid and exit planes. The effect of pipe length on the temperature field at different locations in the pipe is insignificant. This may be because of the relatively short period of heating, which is 120 seconds, i.e. the fluid inside the pipe is not heated to elevated temperatures due to the relatively short heating duration.

Figures (4.4.8) and (4.4.9) show the effective stress with time at the inlet and outlet planes for two pipe lengths. The effective stress oscillates at high amplitude at the inner wall and the amplitude of this oscillation reduces at the mid-radial plane and outer wall of the pipe. The effect of pipe length on the effective stress is more pronounced at the outlet plane of the pipe. In this case, increasing pipe length results in high stress levels in the inner wall of the pipe. This is because of the high temperature gradient attained at the solid-liquid interface in the pipe.

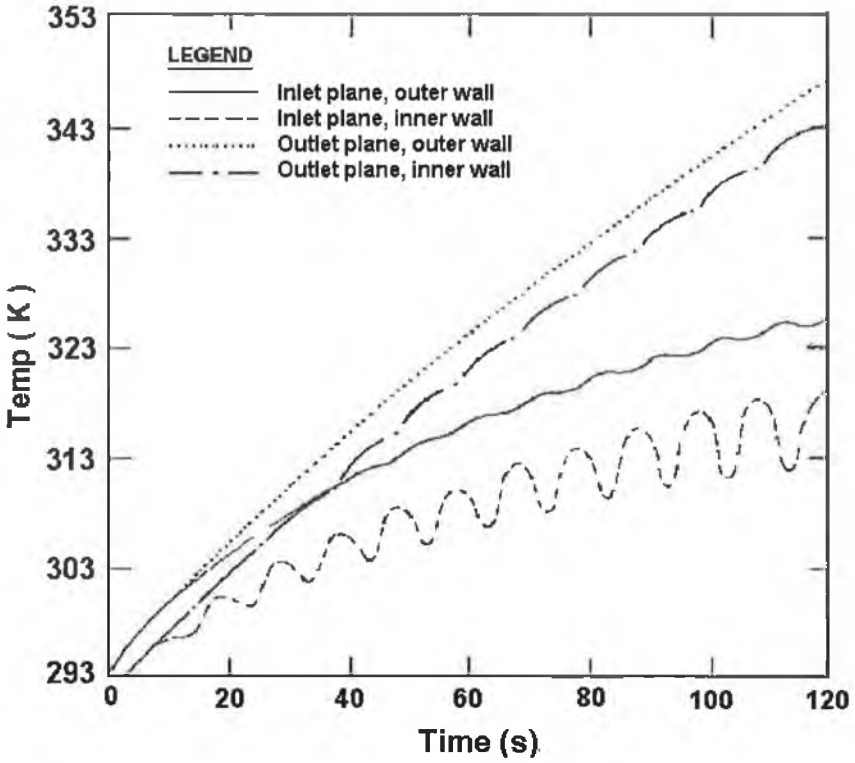


4.4.7a L = 12.5 × D

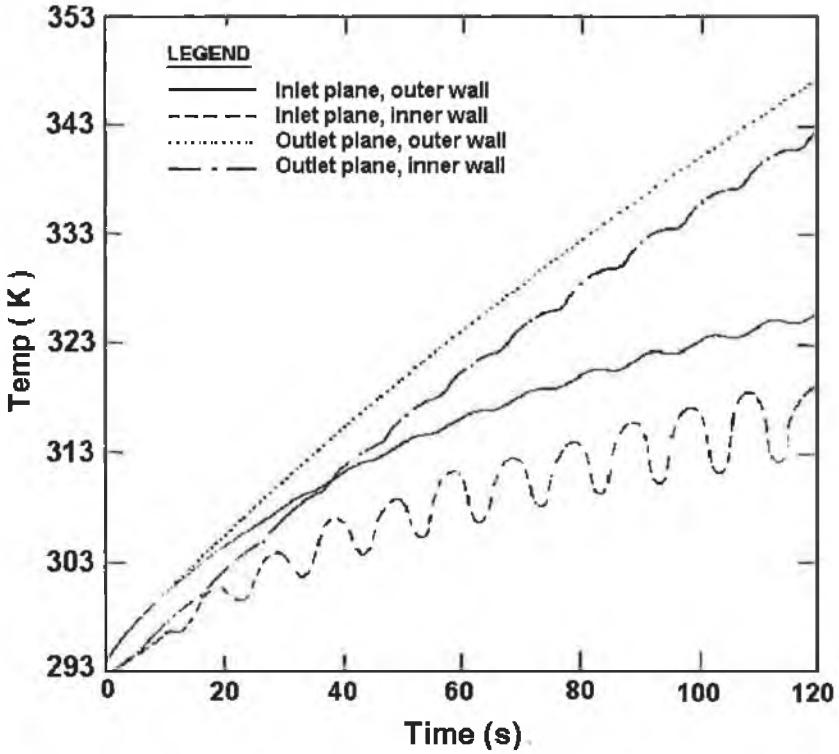


4.4.7b L = 17.5 × D

Figure 4.4.7 Inner and outer wall temperatures at inlet and outlet planes for the cases of (L = 12.5 × D) and (L = 17.5 × D)

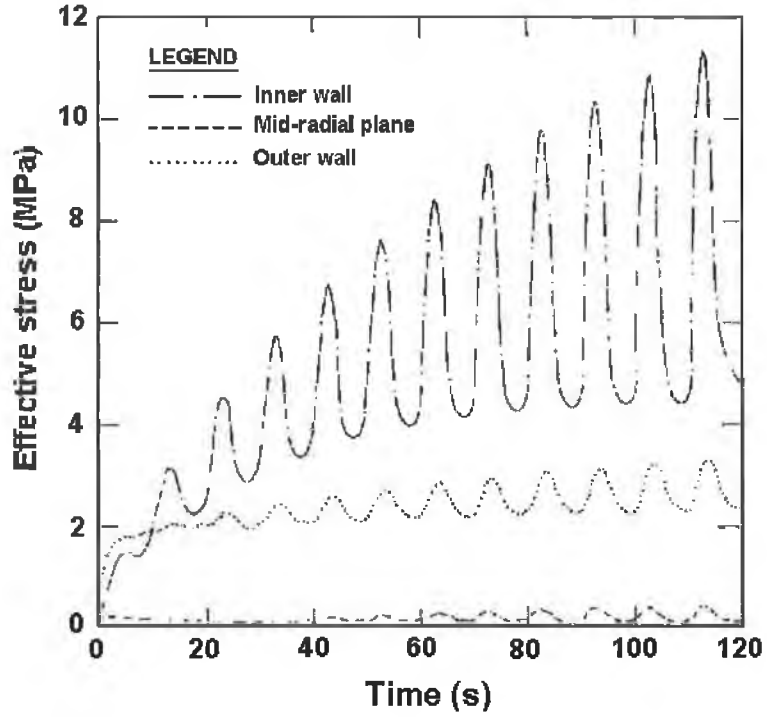


4.4.8a Inlet plane

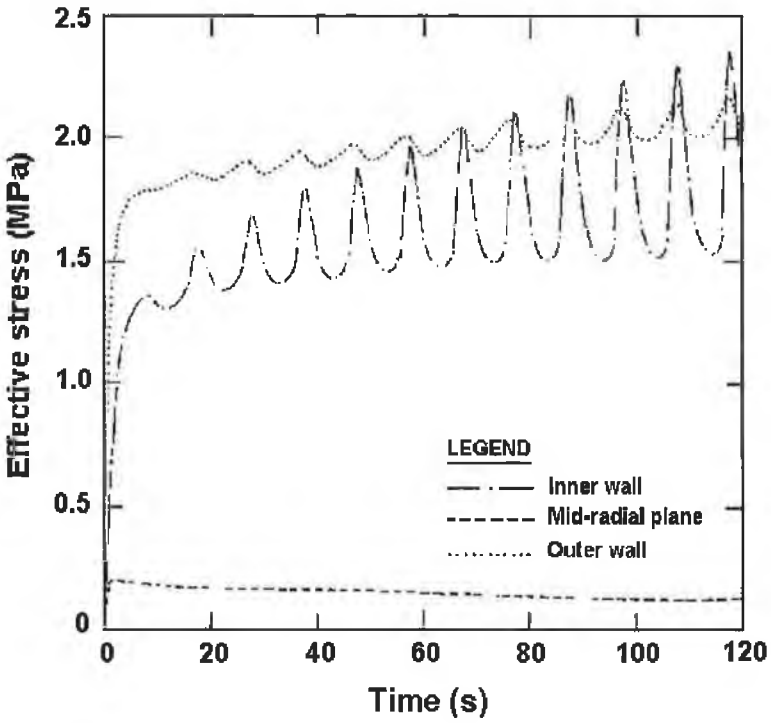


4.4.8b Outlet plane

Figure 4.4.8 Thermal stresses at inlet and outlet planes for the case of (L = 12.5 × D)

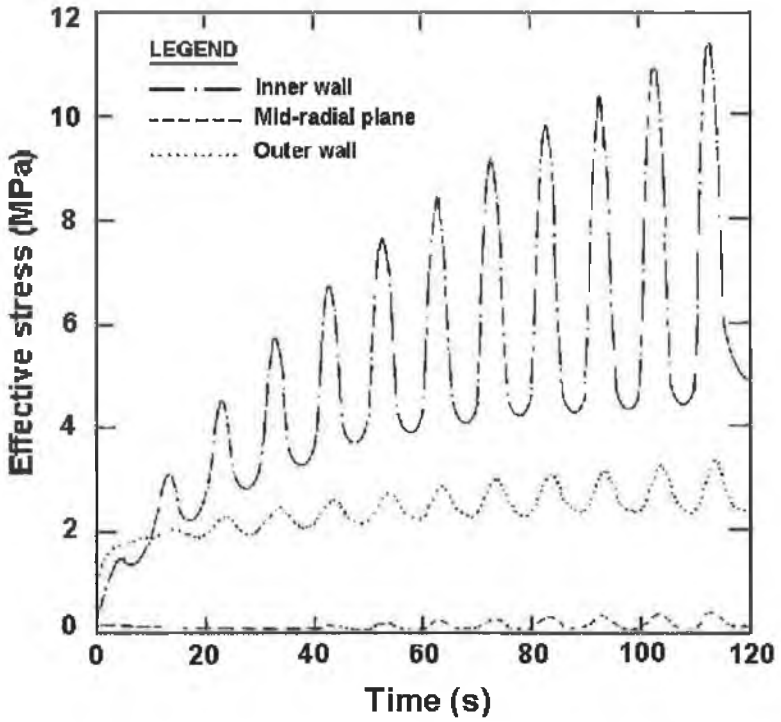


4.4.9a Inlet plane

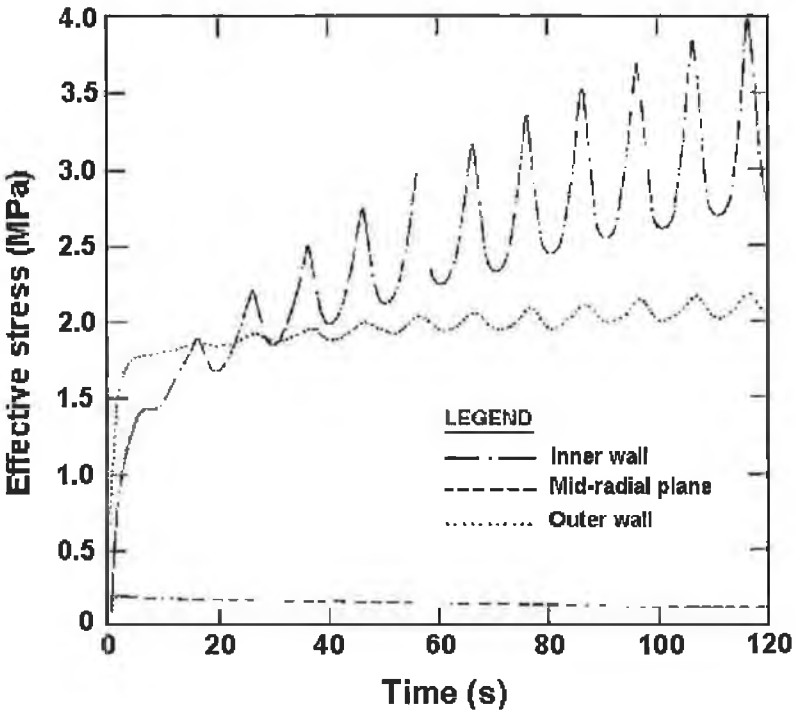


4.4.9b Outlet plane

Figure 4.4.9 Thermal stresses at inlet and outlet planes for the case of (L = 17.5 × D)

### 4.4.3 The Effects of Reynolds Number on Thermal Stresses:

A third part of this study is used to find the effects of the Reynolds number on thermal stresses. The pipe diameter is also taken as 0.08 m and the length of the pipe is taken as 7.5 times the pipe diameter. The pipe thickness is considered as 0.125 times the pipe diameter. Reynolds numbers of 500, 1000 and 1500 are used in the study. The heat flux is taken as 20,000 $W/m^2$ and the pressure difference oscillating frequency is equal to 0.1 Hz. Steel and water are considered as the solid and fluid respectively in this study. The grid size giving independent results is 120 radial cells in fluid, 30 radial cells in solid and 24 axial cells.

Figure (4.4.10) shows the effect of Reynolds number on temporal variation of temperatures at inner and outer walls of inlet, mid and outlet planes of the pipe. The magnitude of temperature reduces at all locations in the pipe as the Reynolds number increases. This is more pronounced as the heating progresses. Moreover, the amplitude of the temperature oscillation at the inner wall of inlet plane increases with increasing the Reynolds number. This occurs because of the amplitude of the inlet velocity, which increases with increasing the Reynolds number. In this case, a large amplitude temperature oscillation occurs at pipe inlet; however, the amplitude enhancement due to high Reynolds number reduces at mid and outlet planes of the pipe

Figures (4.4.11) and (4.4.12) show the effect of the Reynolds number on temporal variation of effective stresses at the inner and outer walls at the inlet, mid and outer planes of the pipe. The magnitude of the effective stress increases with increasing Reynolds number. In this case, thermal boundary layer becomes thin due to enhanced convective effect, which in turn results in high temperature gradient at the solid-liquid interface. Therefore, high temperature gradient increases the stress levels in this region. The enhancement in the magnitude of stress oscillation is more pronounced at the mid and exit planes of the pipe. The amplitude of oscillation in effective stress also increases as the heating period and Reynolds number increase. This is due to the temperature behavior across the pipe wall, i.e. temperature oscillation at the inner wall of the pipe results in a similar behavior of effective stresses in the pipe wall.

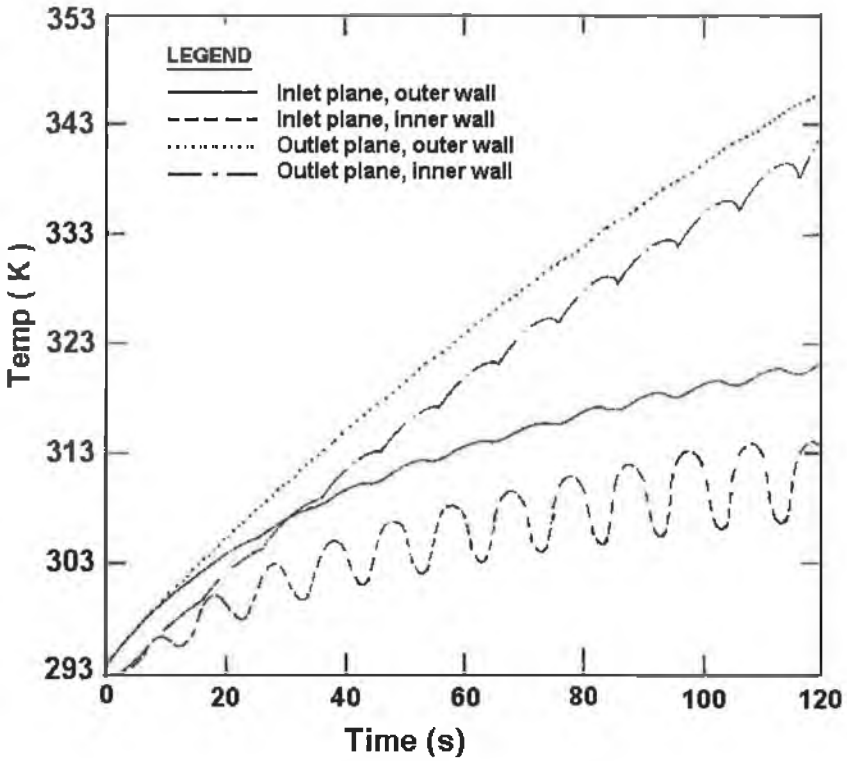


4.4.10a Re = 1000

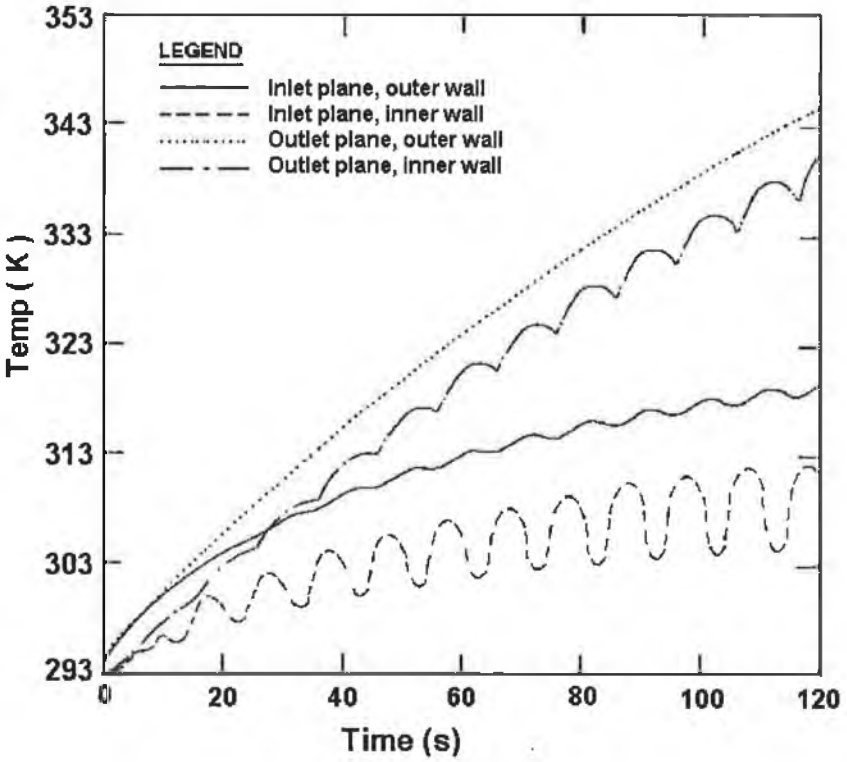


4.4.10b Re = 1500

Figure 4.4.10 Inner and outer wall temperatures at the inlet and outlet planes for the Cases of (Re = 1000) and (Re = 1500)

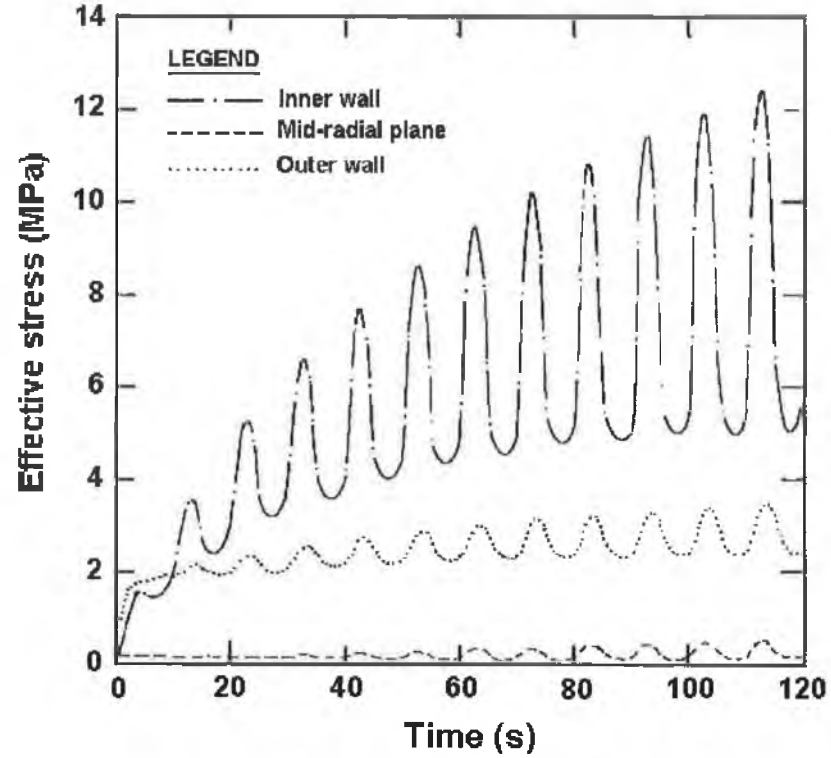


4.4.11a Inlet plane

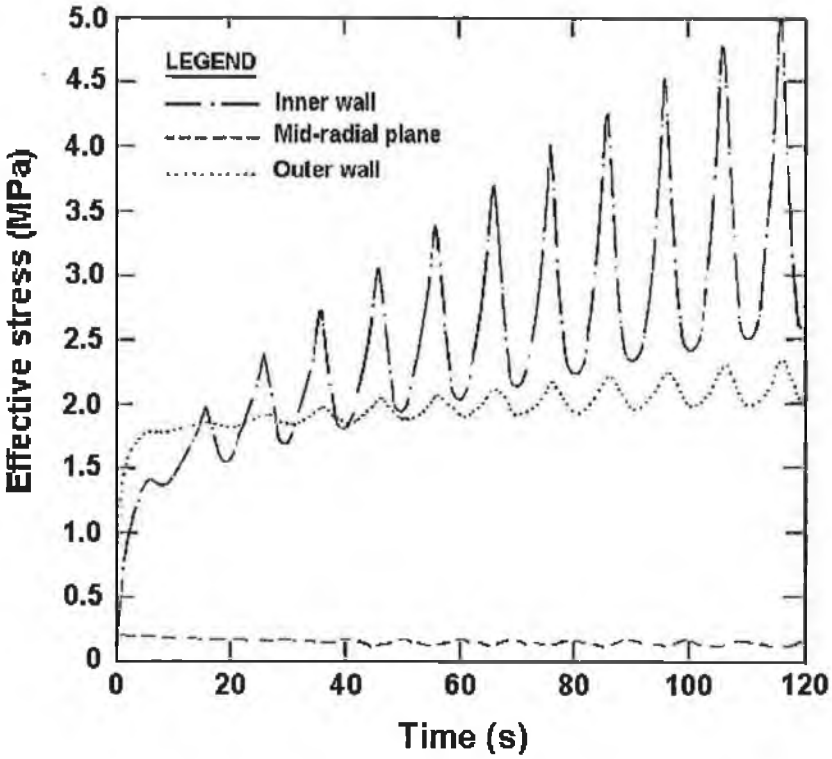


4.4.11b Outlet plane

Figure 4.4.11 Thermal stresses at the inlet and outlet planes for the case of (Re = 1000)

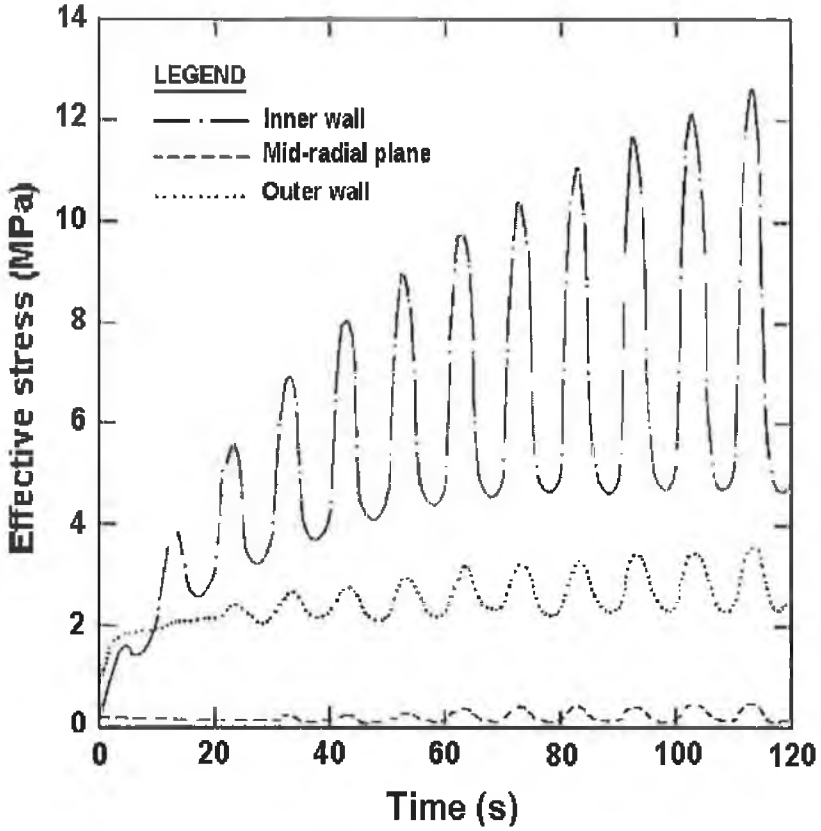


4.4.12a Inlet plane

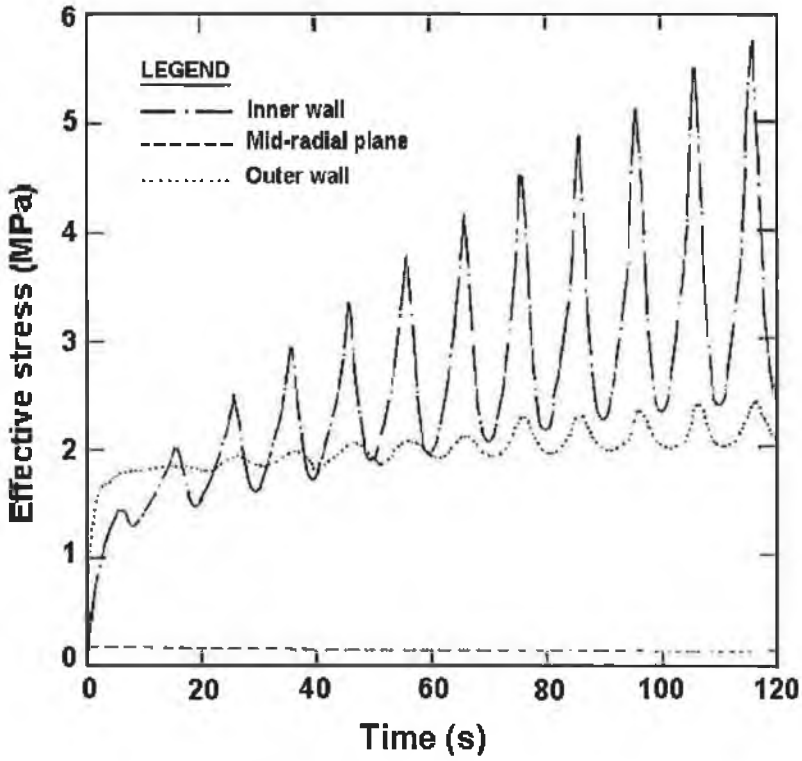


4.4.12b Outlet plane

Figure 4.4.12 Thermal stresses at inlet and outlet planes for the case of (Re = 1500)

### 4.4.4 The Effects of Fluid Properties (Prandtl Number) on Thermal Stresses:

To investigate the effect of the fluid properties (Prandtl number) on thermal stresses in pipes due to pulsating flow, three different fluids (water, coolanol-25 and mercury) are used. Steel is taken as the solid. The heat flux is taken as 20,000 $W/m^2$ and the pressure difference oscillating frequency is equal to 0.1 Hz. The pipe diameter is also taken as 0.08 m and the length of the pipe is taken as 7.5 times the pipe diameter. The pipe thickness considered is 0.125 times the pipe diameter. The heat flux is taken as 20,000 $W/m^2$. The grid size independent results for all cases are 120 radial cells in fluid, 30 radial cells in solid and 24 axial cells.

Figure 4.4.1b shows the temporal variation of temperature at different locations in inlet and outlet planes of the pipe wall for water. Figures 4.4.13a and 4.4.13b show the behavior in the case of coolanol-25 and mercury respectively. It can be observed that the outer wall temperature in the outer wall does not oscillate in all cases. In the case of water and coolanol-25, it can be observed that at the inner wall temperatures oscillates at inlet and outlet planes at a frequency of 0.1 Hz, which is the same frequency as the frequency of the oscillating fluid pressure difference. Temperature oscillation in the solid clearly reduces as the specific heat of the fluid reduces; thus there is no temperature oscillation at the outer wall at the inlet plane in the case of coolanol-25 and almost disappears at all locations in the case of mercury. However, the amplitude of temperature profile increases at inner wall at the inlet plane in the case of coolanol-25 as compared to the same location in the case of water. This is due to the lower thermal conductivity of coolanol-25 as compared to water.

Figure 4.4.3 shows the temporal distribution of effective stress at different locations in the pipe wall at inlet and outlet planes of the pipe for the case of water. Figures 4.4.14 and 4.4.15 show the effective stresses for the cases of coolanol-25 and mercury. Stress levels obtained at inner wall at inlet and outlet planes of the pipe are higher than those obtained for water and mercury. This is because of the higher temperature difference between the inner wall of the pipe and the other layers inside the pipe in the case of coolanol-25 as compared to water and mercury (figures 4.4.1b, 4.4.13a and 4.4.13b). Also, higher stress amplitudes are obtained at the inner wall in the case of coolanol-25. This is due to the higher temperature oscillation amplitude as was discussed before. In the case of mercury, stress oscillation almost disappears and stress amplitudes become smaller due to the temperature behavior in the solid. Oscillation in stress almost disappears at the outer wall in all cases due to the non-presence of temperature oscillation.

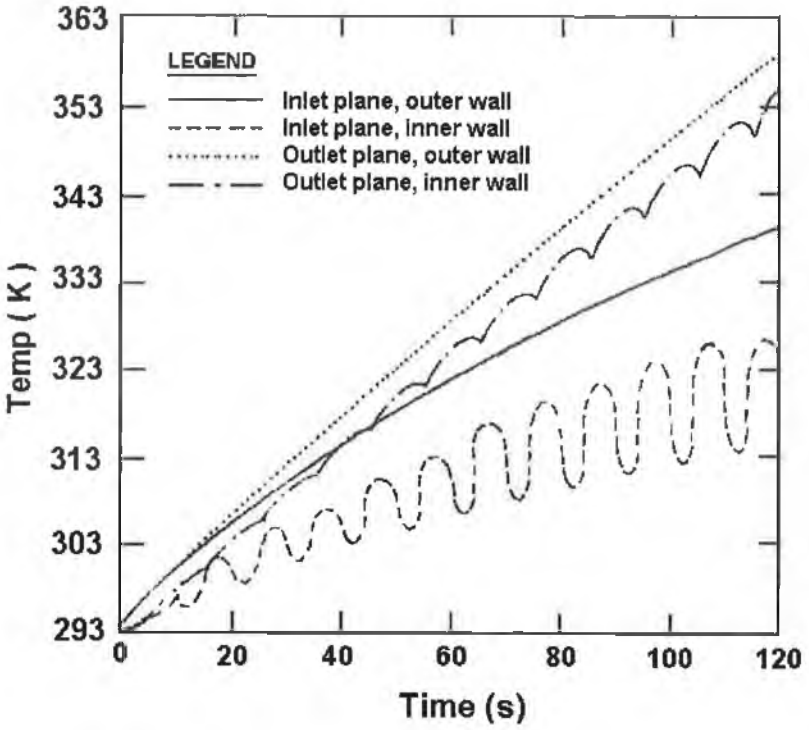


4.4.13a Coolanol-25

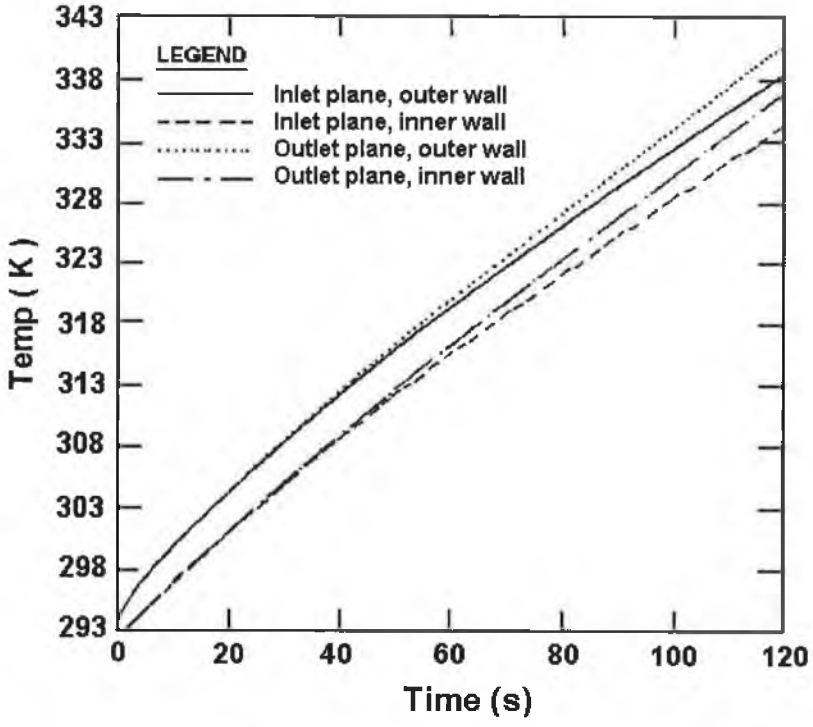


4.4.13b Mercury

Figure 4.4.13 Inner and outer wall temperatures at the inlet and outlet planes for the cases of coolanol-25 and mercury.

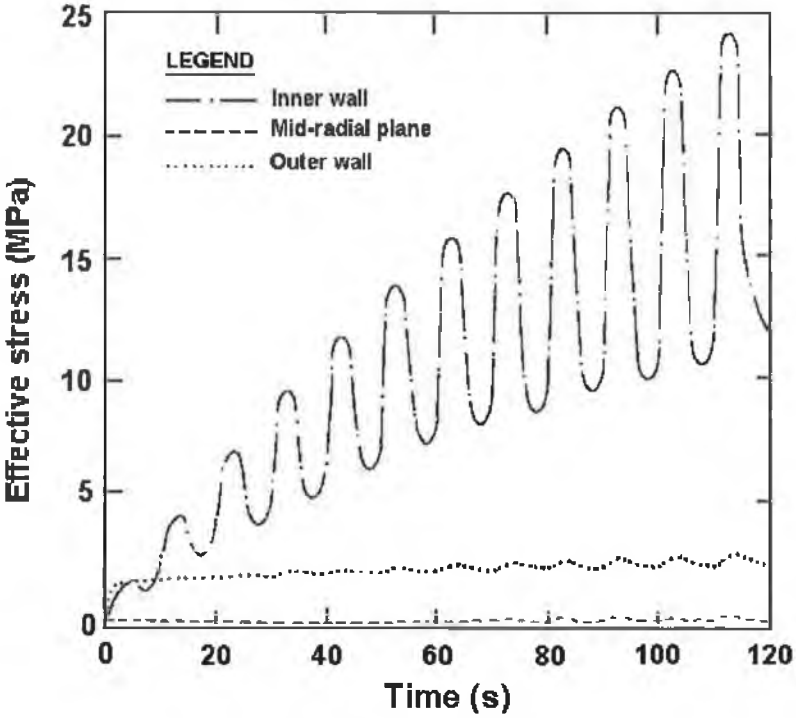


4.4.14a Inlet plane

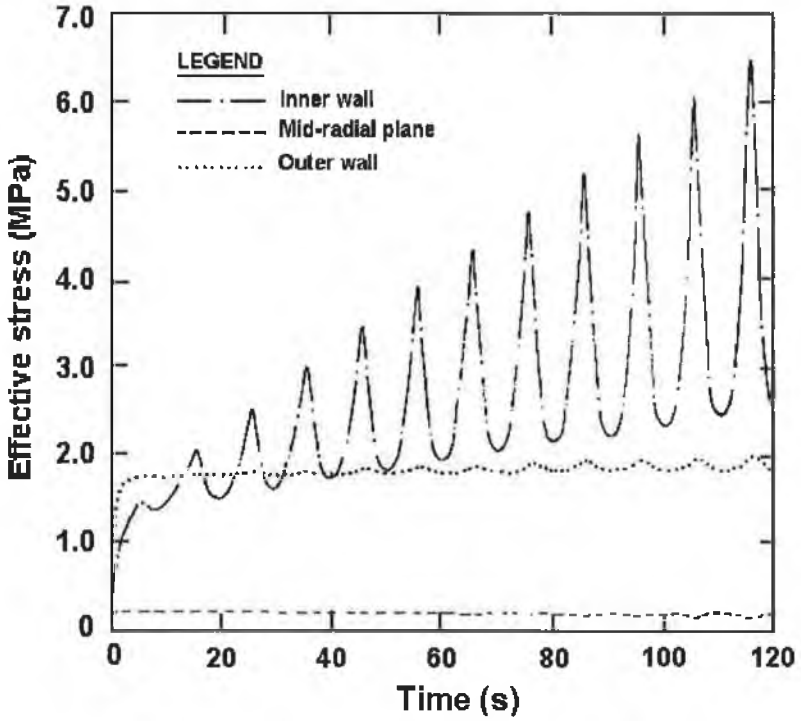


4.4.14b Outlet plane

Figure 4.4.14 Thermal stresses at inlet and outlet planes for the case of coolanol-25.

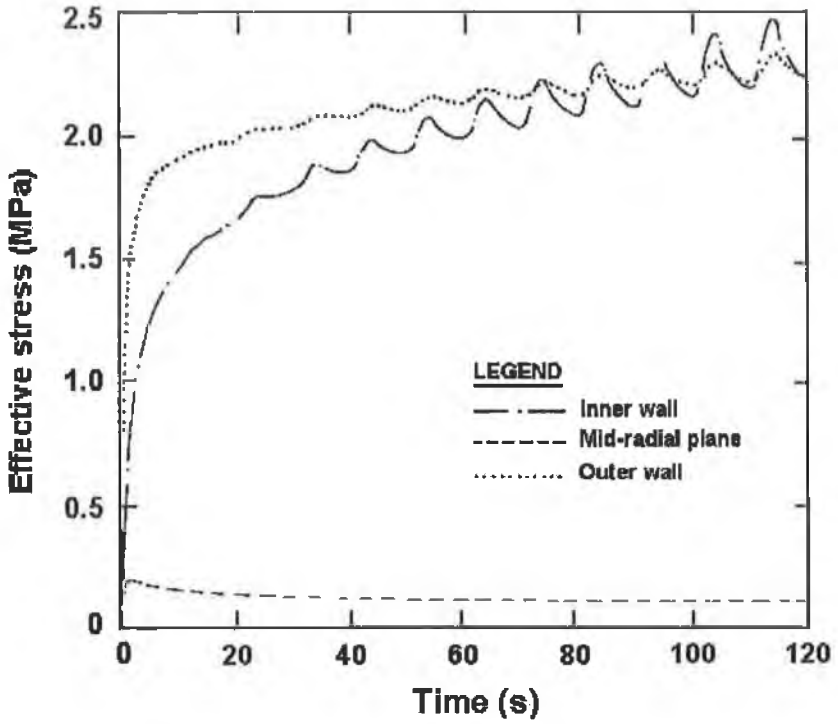


4.4.15a Inlet plane

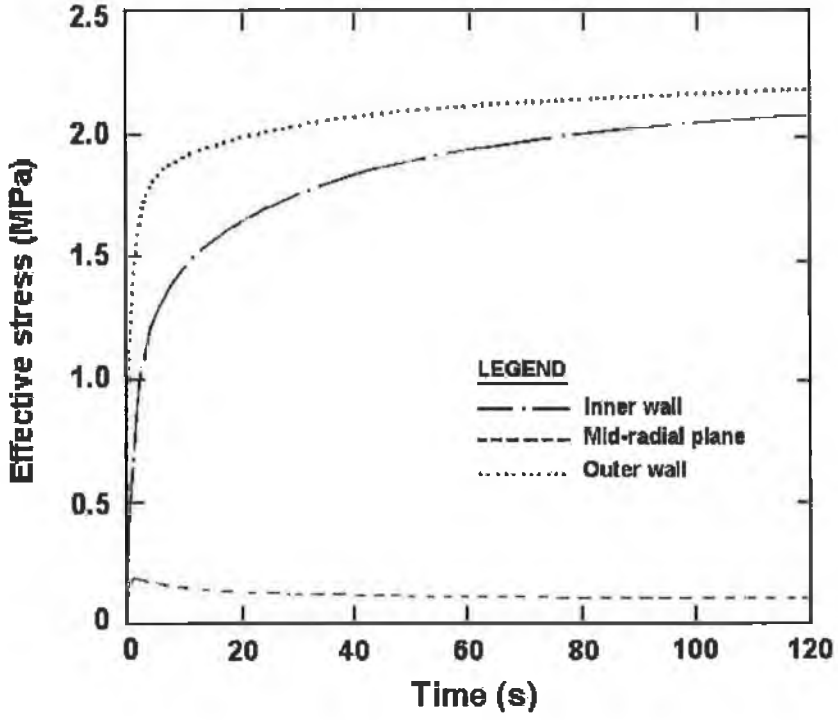


4.4.15b Outlet plane

4.4.15 Thermal stresses at inlet and outlet planes for the case of Mercury.

### 4.4.5 The Effect of Pressure Difference Oscillating Frequency on Thermal Stresses:

In this part of this study, the effect of oscillation frequency of pressure difference on thermal stresses is investigated. The pipe diameter is also taken as 0.08 m and the length of the pipe is taken as 7.5 times the pipe diameter. The pipe thickness is considered as 0.125 times the pipe diameter. The heat flux is taken as 20,000 $W/m^2$. Steel and water are considered as the solid and fluid respectively in this study. Three different pressure difference oscillating frequencies are used; 0.1 Hz (1 cycle per 10 second), 0.2 Hz (1 cycle per 5 second) and 1.0 Hz (1 cycle per 1 second). The grid size independent results for all cases are 120 radial cells in fluid, 30 radial cells in solid and 24 axial cells.

Figure 4.4.1b shows the temporal temperature variation for the case of 0.1 Hz frequency of oscillating pressure difference, while Figures 4.4.16a and 4.4.16b show the variation of temperatures for the cases of 0.2 Hz and 1 Hz respectively. By comparing the three cases, it can be observed that the temperature profiles at outer wall of the outlet plane show similar trend. Moreover, temperature profiles at other locations in the pipe differ considerably. This is especially true at the inner wall of the inlet and outlet planes. It is clear that as the frequency of oscillating pressure difference reduces, the temperature oscillation frequency reduces and the amplitude of oscillation increases. The increase in amplitude suggests that heat transfer rates to the fluid reduce significantly, which in turn results in high interface temperature between the solid and the fluid. This is more pronounced as the heating period progresses.

Figure 4.4.3 shows the effective stresses at inlet and outlet planes of the pipe in the case of an oscillating pressure difference equal to 0.1 Hz. Figures 4.4.17 and 4.4.18 show the effective thermal stresses the inlet and outlet planes in the cases of 0.2 Hz and 1.0 Hz respectively. It can be seen that effective stresses at inner wall at inlet plane oscillate in a frequency equal to the pressure difference oscillating frequency. The amplitude of oscillation of effective stresses at this location reduces as the frequency of oscillation of pressure difference reduces, i.e. the temperature oscillation altitude reduces as the oscillating pressure difference reduces. Also, the values of stress reduce as the frequency of oscillation reduces, because as was shown the difference in temperature between the inner wall of the pipe and the other pipe layers becomes smaller as the pressure difference oscillating frequency reduces. Similar trend is observed at the outlet planes, but with less oscillation amplitude and stress values. This is because the effective stresses follow the temperature profiles at the outlet planes, which have smaller temperature oscillation amplitudes at these locations.

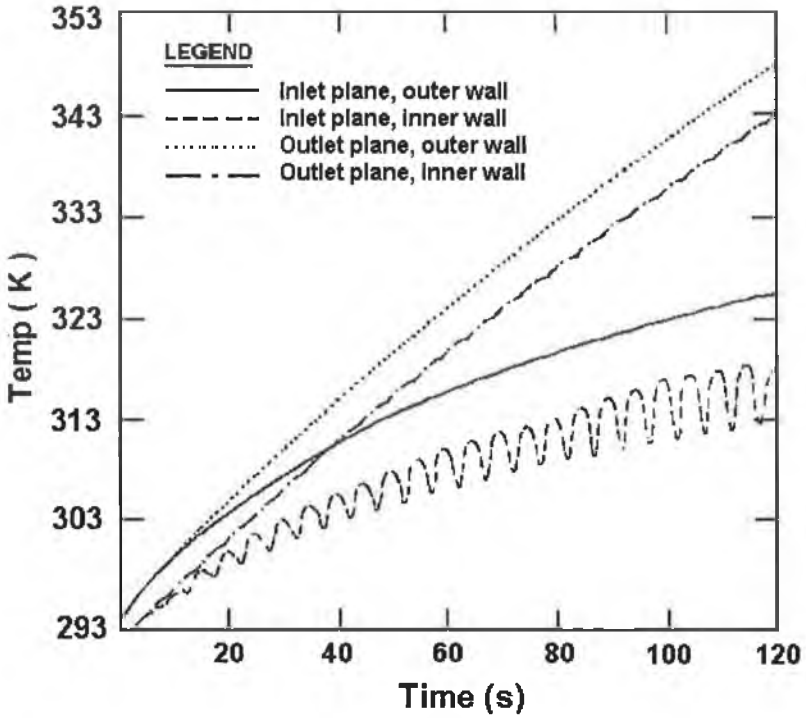


4.4.16a 0.2 Hz

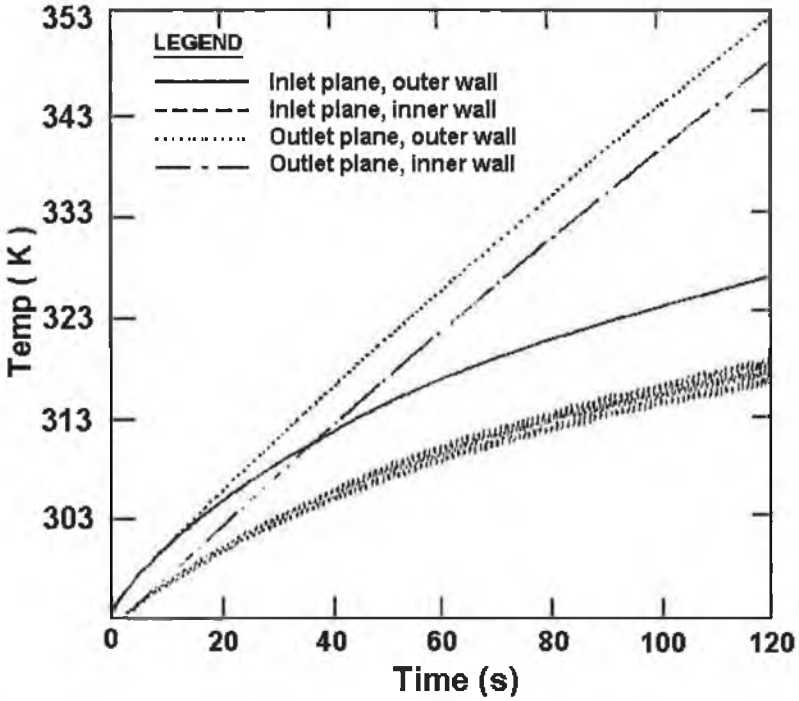


4.4.16b 1.0 Hz

4.4.16 Inner and outer wall temperatures at the inlet and outlet planes for the cases of 0.2Hz and 1 Hz.

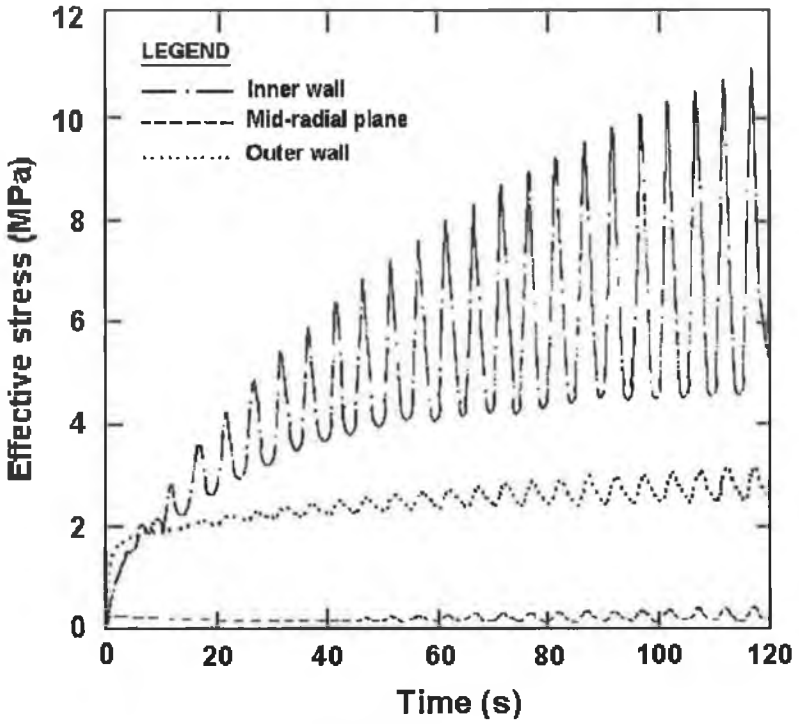


4.4.17a Inlet plane

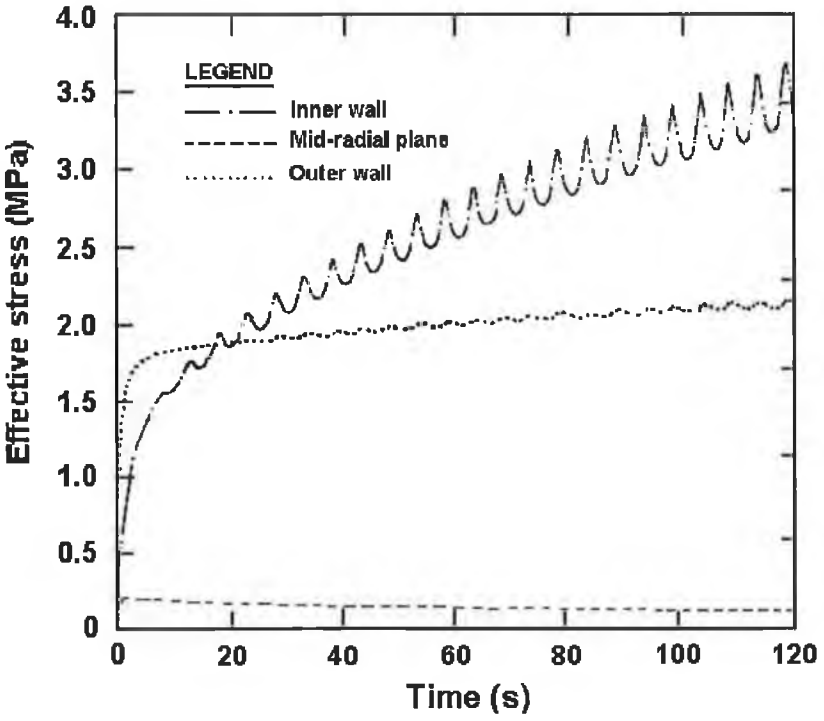


4.4.17b Outlet plane

4.4.17 Thermal stresses at inlet and outlet planes for the case of 0.2 Hz.

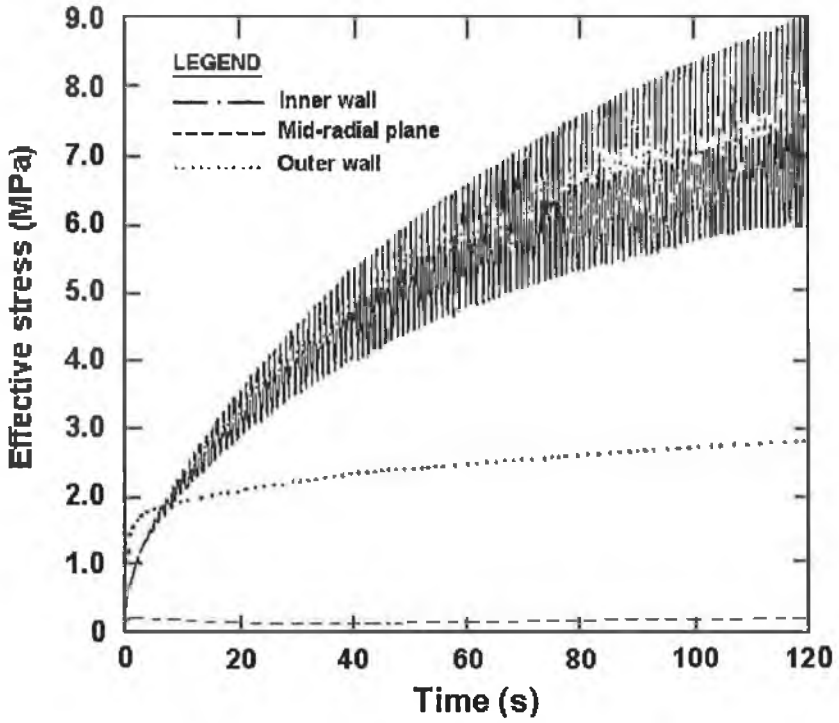


4.4.18a Inlet plane

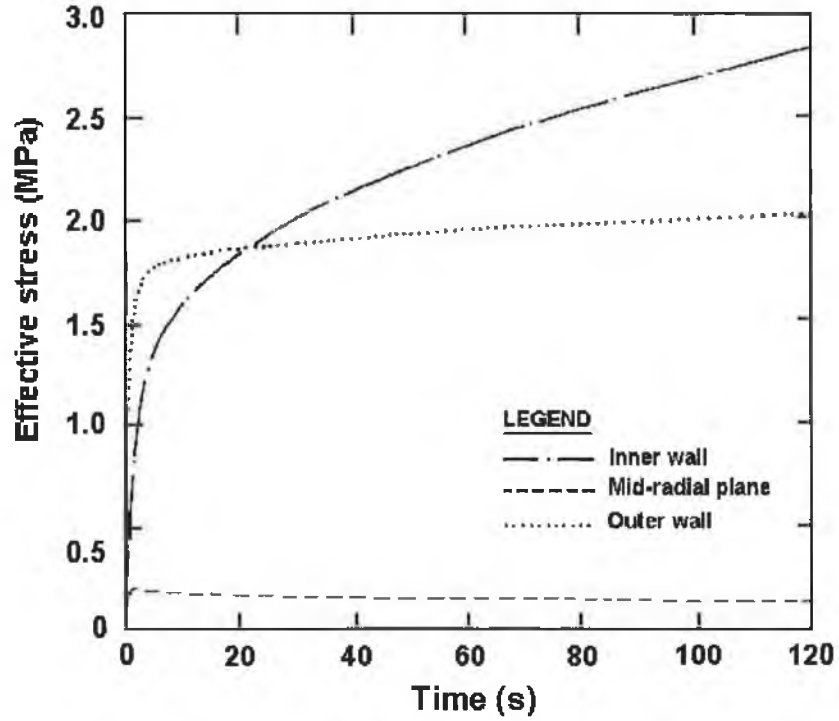


4.4.18b Outlet plane

4.4.18 Thermal stresses at inlet and outlet planes for the case of 1.0 Hz.

### 4.4.6 The Effect of Heating Load Magnitude on Thermal Stresses:

In this part of the section, the effect of oscillation frequency of pressure difference on thermal stresses is presented. The pipe diameter is taken as 0.08 m and the length of the pipe is taken as 7.5 times the pipe diameter. The pipe thickness is considered as 0.125 times the pipe diameter. Steel and water are considered as the solid and fluid respectively in this study. Three different heating load magnitudes are used; 2000 $W/m^2$, 10000 $W/m^2$ and 20000 $W/m^2$. The grid size independent results for all cases are 120 radial cells in fluid, 30 radial cells in solid and 24 axial cells.

Figure 4.4.19a and 4.4.19b show the variation of temporal temperatures for the cases of 2000 $W/m^2$ and 10000 $W/m^2$ of heating loads respectively. Figure 4.4.1b shows the temporal variation of temperatures for the case of 20000 $W/m^2$ of heating load. It can be seen that increasing heating load increases the levels of temperature, however, the frequency of temperature oscillation profiles does not change considerably.

By comparing the temporal stress variations at inlet and outlet planes of the pipe from figures 4.4.20, 4.4.21 and 4.4.3 for the cases of 2000 $W/m^2$, 10000 $W/m^2$ and 20000 $W/m^2$ respectively. It is clear that the stress levels show similar trend in oscillation for the three cases, but with an evident increase in stress levels accompanying the increase in heating loads.

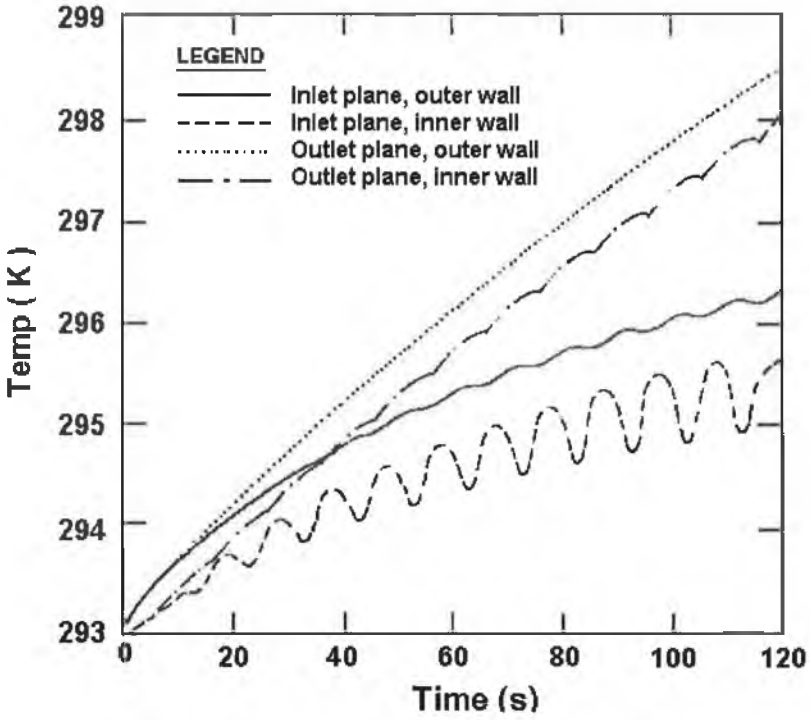


4.4.19a 2000 W/m$^2$

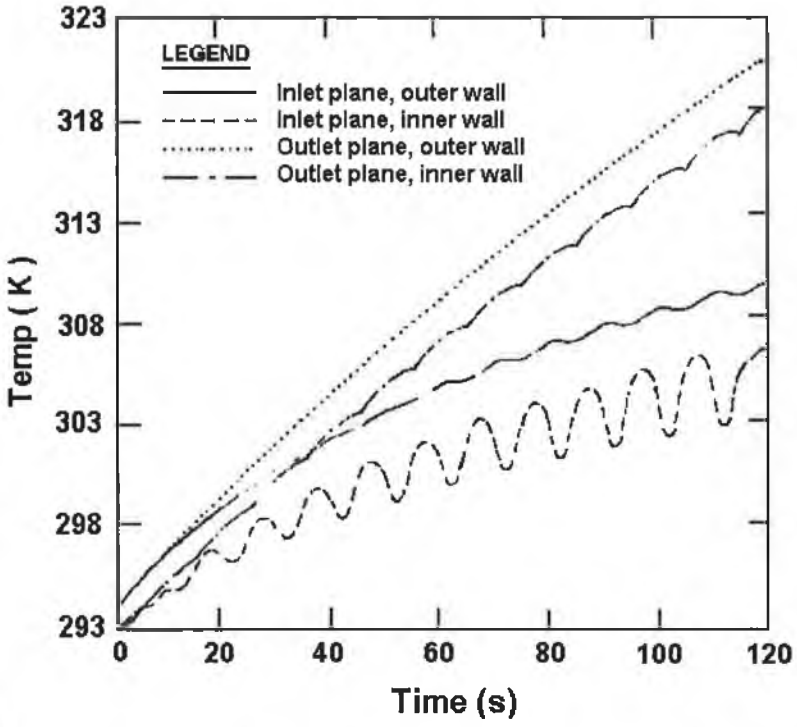


4.4.19b 10000 W/m$^2$

Figure 4.4.19 Inner and outer wall temperatures at the inlet and outlet planes for the cases of 2000 W/m$^2$ and 10000 W/m$^2$.

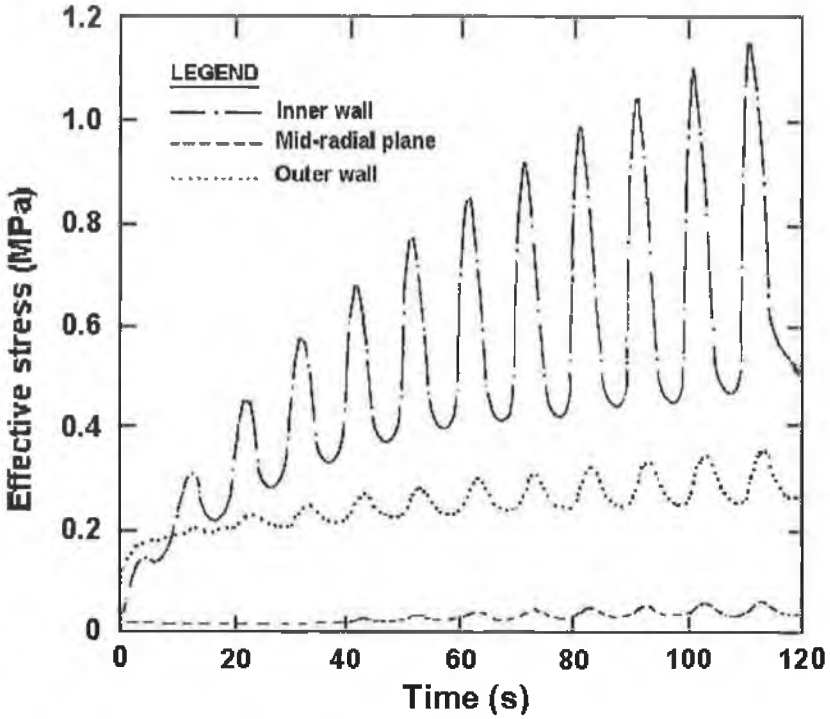


4.4.20a. Inlet plane

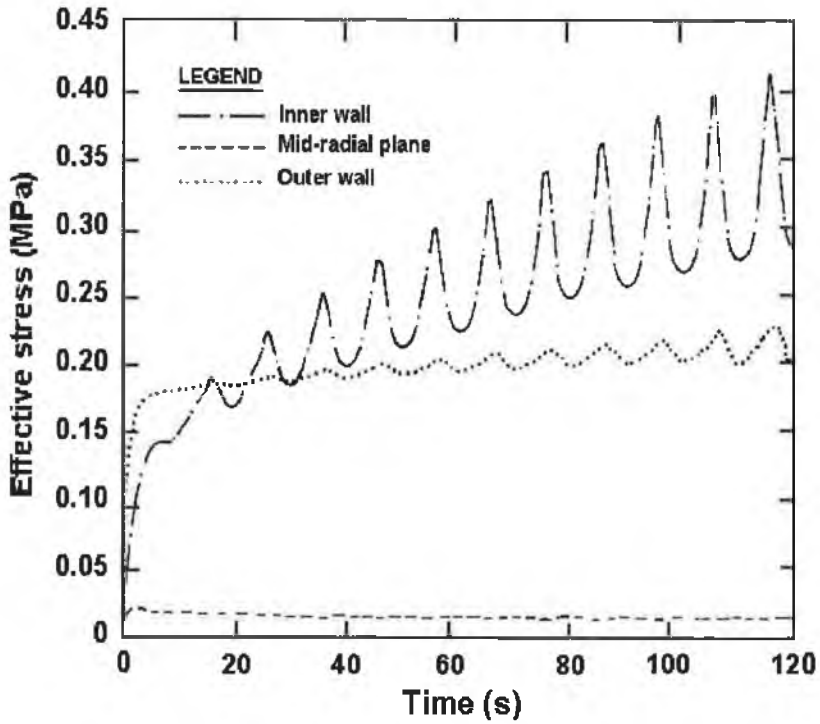


4.4.20b Outlet plane

4.4.20 Thermal stresses at inlet and outlet planes for the case of 2000 W/m$^2$.

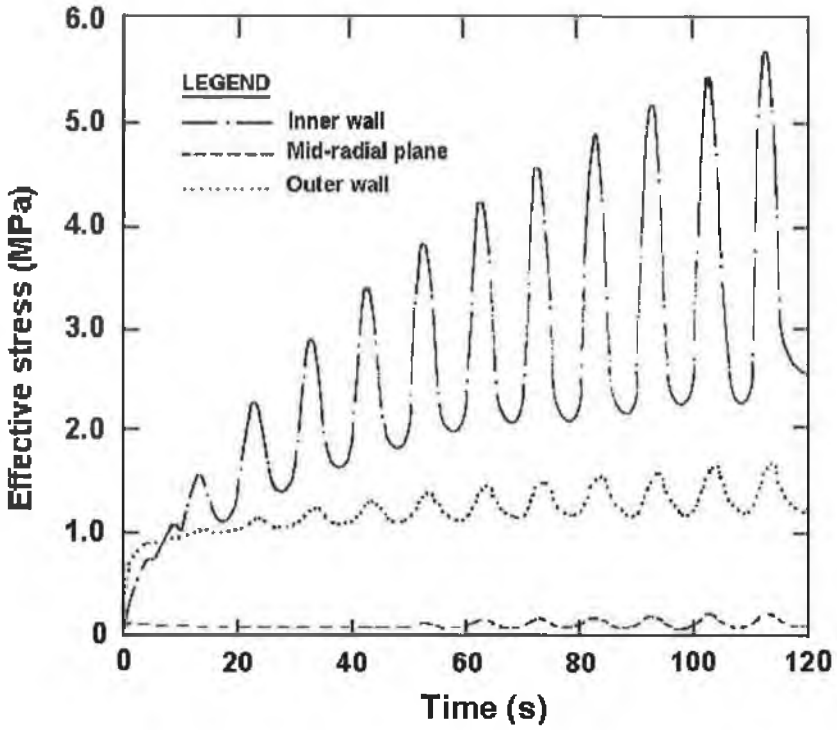


4.4.21a. Inlet plane

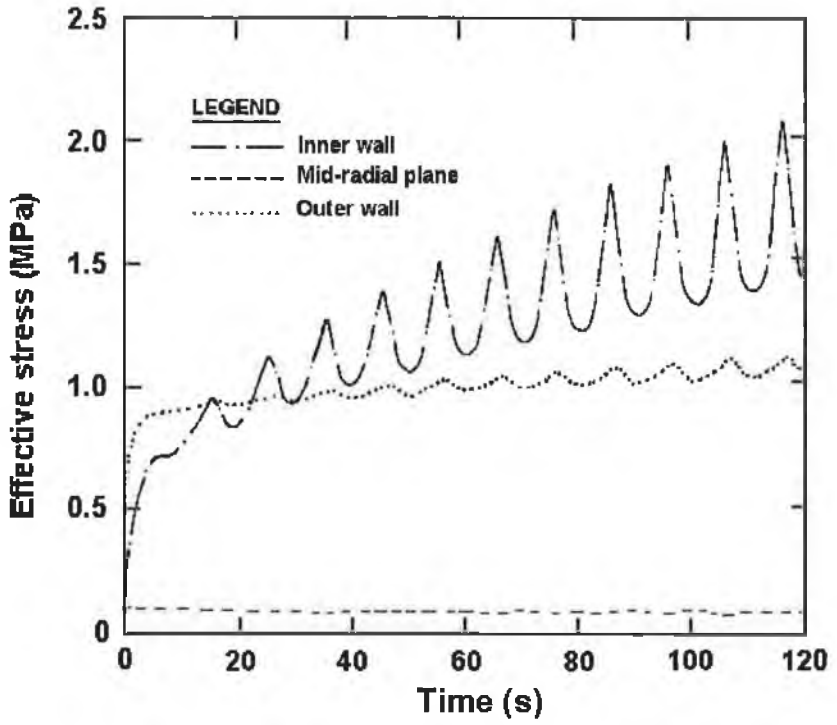


4.4.21b. Outlet plane

4.4.21 Thermal stresses at inlet and outlet planes for the case of 10000 W/m$^2$.

It is observed that the temperature profiles follow a certain trend in most of the cases simulated in this section; that is, the temperature in outlet plane rises sharply with time. This is true for inner and outer walls of the pipe. Moreover, interface temperature (inner wall temperature) at inlet plane oscillates with the frequency of pressure oscillation, especially at the inner wall of the pipe. The amplitude of oscillation increases as time increases. This occurs because of the flow oscillation at pipe inlet and as heating progresses, temperature oscillation increase due to externally heating load. However, the temperature oscillation at the interface of the outlet plane diminishes indicating the damping of fluid oscillation towards the pipe end. As time increases, due to convective heating of the fluid, temperature of the fluid towards the end of the pipe increases. This, in turn results in small temperature difference between the fluid and the pipe wall. Consequently, due to uniform heat input, wall temperature rises despite the cooling of the wall by the fluid at the interface.

The stress profiles are also observed to follow a certain trend. The stress levels are smaller at the outer plane of the pipe. The stress levels oscillate and increase with heating period at the interface between the fluid and the solid wall. This is more pronounced at the interface, i.e. it oscillates and its amplitude increase with increasing heating period. Consequently, the temporal behavior of temperature results in similar behavior of effective stress. A more steady and smaller rise of stress levels is observed at outlet planes of the pipe, which is due to the temperature filed in the pie wall, i.e. amplitude and frequency of temperature decay as the pipe length increases. It is also clear that the magnitude of stress level is higher at the inlet plane.

# CHAPTER 5

# CONCLUSIONS AND RECOMMENDATION FOR FUTURE WORK

## 5.1 Conclusions

The conclusions obtained from the present study for thermal stresses in pipes due to laminar flow, turbulent flow, and pulsating flow situations are summarized in the followings:

### 5.1.1 Laminar flow:

Fully developed laminar flow through a pipe with uniform heating is considered. In general, the radial stress generated in the inlet plane of the pipe is higher as compared to that corresponding to other planes in the axial direction. The effect of heat transfer on the thermal stresses due to different Prandtl numbers and thermal conductivity ratios are examined. In addition, low Prandtl number and low thermal conductivity ratios result in low radial effective stresses. The specific conclusions derived from the present work may be listed as follows:

The specific conclusions made about thermal stresses in pipes subjected to fully developed laminar flow are:

1. The temperature increases in the solid wall vicinity as L/D ratio increases for thinner pipes. This results in considerably high temperature gradient in this region.

2. As L/D ratio changes, the location of maximum temperature gradient changes such that as L/D ratio increases, the location moves inside the solid pipe. In addition, as the wall thickness of the pipe increases, the maximum temperature gradient is attained at the fluid-solid interface.

3. In general, the stress ratio reduces to minimum at some location on the pipe wall. Moreover, this location moves forwards to the pipe end as the axial distance increases.

4. The stress ratio increases when the thickness of the wall pipe increases; it attains almost three times more than that occurs for thinner pipes. Consequently, the stress ratio distribution and the location of the minimum stress ratio depend on the thickness of the pipe wall. Moreover, the locations of the minimum stress ratio become independent of axial planes when the thickness of the pipe wall increases.

5. The effect of Prandtl number and the conductivity ratio on the temperature distribution in the solid and fluid is significant. Low Prandtl number and low thermal conductivity ratio result in almost uniform temperature distribution in the solid and fluid. In this case, the temperature variation along the pipe axis is considerable.

6. A considerably high temperature gradient occurs at solid-fluid interface. The point of high temperature gradient moves inside the solid as the conductivity ratio increases. This may be because of the development of high heat transfer coefficient at the interface.

7. The radial effective stress attains high values at pipe inlet and the effective stress reduces as the distance in the axial direction increases. This may be due to the axial temperature gradient variation.

8. The minimum effective stress occurs close to the center of the pipe where $r^* \cong 0.5$. This may be because of the temperature gradient in this region, which is minimum.

### 5.1.2 Turbulent flow:

The turbulent flow in the thick pipe with external heating is considered and flows, temperature and stress fields are predicted. The temperature field in the solid was influenced by the fluid and pipe properties. However, as the Reynolds number increases, this influence becomes negligible. The effective stress at mid-plane of the pipe is not affected by the Reynolds number. However, the specific conclusions derived from the present study can be listed as follows:

1. The temperature increases in the solid wall vicinity as L/D ratio increases for thinner pipes. This results in considerably high temperature gradient in this region.

2. The Nusselt number predicted for different Reynolds numbers agree well with the experimental results obtained from the previous study.

3. The local Nusselt number attains higher values at the pipe inlet because the cool fluid enters the pipe. As the fluid flows in the pipe, the temperature rises due to heat transfer, and the local Nusselt number reduces. The coolanol-25 results in higher local Nusselt number as compared to water and the pipe material properties have almost no effect on the local Nusselt number.

4. The temperature profiles in the fluid extends further in the radial direction in the down stream of the pipe. This extension reduces as the Reynolds number increases, in which case, the fluid close to the solid wall is heated. In the case of coolanol-25, the fluid temperature distribution in the radial direction is limited to the region close to the solid wall.

5. The temperature profiles in the solid varies in the radial direction and this variation is not affected substantially by the Reynolds number. The temperature gradient in the solid changes rapidly in the vicinity of the solid-fluid interface. The changes in temperature gradient vary along the pipe axis.

6. The effective stress in the pipe does not vary considerably in the radial direction for copper pipe. In the case of steel pipe, the maximum effective stress occurs at the pipe inlet while it becomes minimum at $r^* \cong 0.5$. As $r^*$ increases, beyond 0.5, the effective stress increases. The location of the minimum stress is not affected by the Reynolds number and fluid properties.

### 5.1.3 Pulsating flow:

The simulation of the temperature and flow field in a pipe due to the oscillation conditions of inlet flow is carried out. It is found that the temperature oscillation during the heating period occurs The specific conclusions derived from the present work can be listed as follows:

1. The amplitude of temperature oscillation is high at the pipe inlet plane and it decays at the outlet plane of the pipe and it is more pronounced at low heating loads. This is because of the oscillation in the velocity, which has high amplitude at the inlet plane, and the convective heating of the fluid at relatively low temperature at the pipe inlet due to the uniform heat source. The temperature oscillation at outer planes is visible for relatively thin wall pipes (thickness $\leq$ 0.02m), while the temperature oscillation diminishes as the thickness increases. In this case, the pipe material acts as a heat source heating the fluid almost uniformly and damping the temperature fluctuations in the pipe wall. Oscillation in effective stress is observed. The magnitude of the oscillation is more pronounced at the pipe inlet plane. Moreover, the oscillation is amplified as the heating progresses.

2. Effective stress levels have frequencies of oscillation similar to those corresponding to tempaerature.

3. The interface (inner wall) temperature oscillation is more pronounced. This, in turn, causes effective stresses to oscillate more at the inner wall of the pipe and higher stress oscillation amplitudes are observed. This is because of the high magnitude of temperature gradient across the interface. This is more pronounced at the inlet plane of the pipe.

4. The effective stress rises rapidly in the early heating period and as the heating progresses the rate of rise in the stress level becomes almost steady. This is because of the wall temperature, which increases rapidly in the early heating period. As the pipe diameter reduces, the magnitude of effective stress reduces. This occurs because of the temperature gradient across the pipe wall, which reduces with reducing pipe diameter. The increase in pipe thickness enhances the stress levels, i.e. equivalent stress increases with increasing pipe thickness.

5. The effect of Reynolds number on the temperature profiles at different locations inside the pipe wall is more pronounced at outer planes. The effect of Reynolds number on the effective stress is similar to that on the temperature field. In this case, the amplitude of stress oscillation increases at the outlet plane.

6. The effect of the pipe length on the temperature profiles is almost insignificant and this is also true for the stress field at different locations in the pipe.

7. Increasing the heating load enhances (increases) the stress levels in the pipe wall, but it does not have an effect on the oscillation frequency and trend.

8. It is observed that temperature oscillation at the interface and inside the solid increases as the specific heat of the fluid increases. Due to this, more effective stress oscillation occurs in the solid due to the increase in the specific heat of the fluid. The levels of effective stress reduce as the thermal conductivity of the fluid reduces. This is because of the large difference in temperature between the interface and the inside layers of the solid.

9. As the frequency of pressure difference oscillation reduces, the temperature oscillation frequency reduces and the amplitude of oscillation increases. The increase in amplitude is due to the heat transfer rates reduction to the fluid. This results in an increase in the effective stress oscillation amplitudes. Also the levels of stress reduce as the frequency of oscillation reduces.

## 5.2 Recommendation for Future Work

In the present study, thermal stresses in pipes at different lengths, thickness and diameters are considered due to laminar, turbulent and pulsating flow situations. The experimental study validating the present predictions will be fruitful for further study. Moreover, the effect of swirling at pipe inlet is not taken into account in the analysis. In some of the pipe flow applications, inlet swirling occurs because of change in geometric configurations of the piping system. This situation can develop in the cases of flow inletting from the large diameter pipes (pipe joints), inletting from large sections (flat plate heat exchangers tubing), and reservoir exiting. Consequently, when modeling the flow and temperature fields, the inlet swirling needs to be introduced in the analysis. This, in turn, results in modification of flow and heat transfer equations employed in the simulations. This can be considered as first proposal for future work.

The second proposal for the future study can include the investigation into the stress developed at pipe joints, such as oblique joints, due to fluid flow and heat transfer. In this case, the boundary conditions for the governing equations of flow and heat transfer need to be modified accordingly.

# REFERENCES


1. E. Davis, and W. Gill, "The Effects of Axial Conduction in The Wall on Heat Transfer with Laminar Flow", Int. J. Heat Mass Transfer, Vol. 13, pp. 459-470, 1970.

2. M. Faghri and E.M. Sparrow, "Simultaneous Wall and Fluid Axial Conduction in Laminar Pipe-Flow Heat Transfer", Journal of Heat Transfer, Vol. 102, pp. 58-63, 1980.

3. B. Kraishan, "On Conjugated Heat Transfer in a Fully developed Flow", Int. J. Heat Mass Transfer", Vol. 25, No.2, pp. 288-289, 1982.

4. O.A. Arnas, and M.A. Ebadian, "Convective Heat Transfer in A Circular Annulus with Various Wall Heat Flux Distributions and Heat Generation", Journal of Heat Transfer, Vol. 107, pp. 334-337, 1985.

5. G.S. Barozzi, and G. Pagliarini, "A Method to Solve Conjugate Heat Transfer Problems: The Case of Fully Developed Laminar Flow in A Pipe", Journal of Heat Transfer, Vol. 107, pp. 77-83, 1985.

6. C. Parakash, and Ye. Liu, "Analysis of Laminar Flow and Heat Transfer in The Entrance Region of An Internally Finned Circular Duct", Journal of Heat transfer, Vol. 107, pp. 84-91, 1985.

7. J. Suces, "Analytical Solution for Unsteady Heat Transfer in a Pipe", J. Heat transfer, Vol. 110, pp. 850-854, 1988.

8. S. Olek, E. Elias, E. Wacholder, and S. Kaizwrman, "Unsteady Conjugated Heat Transfer in Laminar Pipe Flow", Int. J. Heat Mass Transfer. Vol. 34, No. 6, pp. 1443-1450, 1991.

9. R. Yen and W. Lee, "Conjugate Heat Transfer Analysis in the Entrance region of a Circular Pipe" Journal of the Chinese Society of Mechanical Engineers, Vol. 12, No.3, pp. 233-240, 1991.

10. Z. Huiren, and L. Songling, "Numerical Simulation of Traditional Flow and Heat Transfer in A Smooth Pipe", Int. J. Heat Mass Transfer, Vol.34, pp. 2475-2482, 1991.

11. R. Yang, R. and S.F. Chang, "A Numerical Study of Fully Developed Laminar Flow and Heat Transfer in A Curved Pipe with Arbitrary Curvature Ratio", Int. J. Heat and Fluid Flow, Vol. 14, No. 2, pp. 138-145, 1993.

12. M.A. Al-Nimr, and M.A. Al-Hader, "Transient Conjugated Heat Transfer in Developing Laminar Pipe Flow", J. Heat transfer, Vol. 116, pp. 234-236, 1994.

13. S. Bilir, "Laminar Heat Transfer in Pipes Including Two - Dimensional Wall and Fluid Axial Conduction" Int. J. Heat Mass Transfer", Vol. 38,No. 9, pp. 1619-1625, 1995.

14. D.J. Schutte, M.M. Rahman, and A. Faghri, "Transient Conjugate Heat Transfer in Thick-Walled Pipe with Developing Laminar Flow", Numerical Heat transfer, Vol. 21, pp. 163-186, 1992.

15. B. Shome, and M.K. Jensen, "Mixed Convection Laminar Flow and Heat Transfer of Liquids in Isothermal Horizontal Circular Ducts", Int. J. Heat Mass Transfer, Vol. 38, pp. 1945-1956, 1995.

16. T. Min, J. Y. Yoo, and H. Choi, "Laminar Convective Heat Transfer of a Bingham plastic in a circular pipe-Analytical Approach- thermally Fully Developed Flow and Thermally Developing Flow (the Graetz Problem Extended)", Int. J. Heat Mass Transfer, Vol. 40, No.13, pp. 3025-3037, 1997.

17. L. Lin, and A. Faghri, "Heat Transfer Analysis of Stratified Flow in Rotating Heat Pipes with Cylindrical and Stepped Walls", Int. J. Heat Mass Transfer, Vol. 40, No. 18, pp. 4393-4404, 1997.

18. K. Chien, "Predictions of Channel and Boundary-Layer Flows with a Low-Reynolds-Number Turbulence Model", AIAA Journal, Vol. 20, No. 1, pp.33-38, 1982.

19. M.A. Cotton, and J.D. Jackson, "Vertical Tube Air Flows in The Turbulent Mixed Convection Regime Calculated Using a Low – Reynolds - Number k~ε Model", Int. J. Heat Mass Transfer, Vol. 33, No. 2, pp. 275-286, 1990.

20. F. Trada, "Prediction of Rough - Wall Boundary Layers Using a Low Reynolds *k-ε* Model" Int. J. Heat and Fluid Flow, Vol. 11, No.4, pp. 331-345, 1990.

21. R. Mankbadi, A. and Mobark, "Quasi - Steady Turbulence Modeling of Unsteady Flows" Int. J. Heat and Fluid Flow, Vol. 12, No.2, pp.122-129, 1991.

22. K. Velusamy, V.K. Garg, and G. Vaidyanathan, "Fully Developed Flow and Heat Transfer in Semi - Elleptical Ducts", Int. J. Heat and Fluid Flow, Vol.16, No.2, pp. 145-152, 1995.

23. N. Ghariban, A. Haji-Sheikh, and S.M. You, "Pressure Drop and Heat Transfer in Turbulent Duct Flow: a Two - Parameter Variational Method", Journal of Heat Transfer, Vol. 117, pp. 289-295, 1995.

24. E. Choi,E. and Y.I. Cho, "Local Friction and Heat Transfer Behavior of Water in Turbulent Pipe Flow with Large Heat Flux at The Wall", Journal of heat transfer, Vol. 117, pp.283-288, 1995.

25. P.R. Bullen, D.J. Cheeseman, and L.A. Hussain, "A Study of Turbulent Flow in Pipe Contractions", Journal of Process Mechanical Engineering, Vol. 210, pp.170-180, 1996.

26. M. Wosnik, L. castillo and W. George, "A Theory for Turbulent Pipe and Channel Flows", J. Fluid Mechanicas, Vol. 421, pp. 115-145, 2000.

27. S. Thaker and J. Joshi, "CFD Modeling of Heat Transfer in Turbulent Pipe Flows", AIChE Journal, Vol. 46, No.9, pp. 1798-1812, 200.

28. S. Thaker and J. Joshi, "A Low reynolds Number k-ε modelling of Turbulent pipe Flow: Flow Pattern and energy Balance", The Canadian Journal of Chemical Engineering, Vol. 79, pp. 214-226, April 2001.

29. R. Siegel and M. Perlmutter, "Heat Transfer for Pulsating Laminar Duct Flow", Journal of Heat Transfer, pp. 111-122, May 1962.

30. J. Gerard and M. Hughes, "The Flow Due to an Oscillating Piston in a Cylindrical Tube: A Comparison between Experiment and a Simple Entrance Flow Theory", J. Fluid Mechanicas, Vol. 50, pp. 97-106, 1971.

31. M. Calmen, and P. Minton, "An Experimental Investigation of Flow in An Oscillating Pipe", J. Fluid Mech, Vol. 81, Part 3, pp. 421-431, 1977.

32. M. Faghri, K. Javandi, and A. Faghri, "Heat Transfer With Laminar Pulsating Flow in a Pipe", Letters in Heat and Mass Transfer, Vol. 6, pp. 259-270, 1979.

33. R. Creff, P. Andre, and J. Batina, " Dynamic and Convective Results for a Developing Laminar Unsteady Flow" International Journal for Numerical Methods in Fluids, Vol. 5, pp. 745-760, 1985.

34. U.H. Kurzweg, "Enhanced Heat Conduction in Fluids Subjected to Sinusoidal Oscillations" Journal of Heat Transfer, Vol. 107, pp. 459-462, 1985.

35. R.M. Cotta, and M.N. Ozisik, "Laminar Forced Convection Inside Ducts with Periodic Variation of Inlet Temperature", Int. J. Heat Mass Transfer, Vol. 29, No.10, pp. 1495-1501, 1986.

36. R. Siegel, "Influence of Oscillation-Induced Diffusion on Haet Transfer in a Uniformly Heated Channel", Journal of Heat Transfer, Vol. 109, pp. 244-247, 1987.

37. R.M. Cotta, D. Mikhailov and M.N. Ozisik "Transient Conjugated Forced Convection in Ducts with Periodically Varying Inlet Temperature", Int. J. Heat Mass Transfer, Vol. 30, No. 10, pp. 2073-2082, 1987.

38. R.A. Peattie, and R. Budwig, "Heat Transfer in Laminar, Oscillatory Flow in Cylindrical and Conical Tubes", Int. J. Heat Mass Transfer, Vol. 32, No.5, pp. 923-934, 1989.

39. H.W. Cho, and J.M. Hyun, "Numerical Solutions of Pulsating Flow Heat Transfer Characteristics in a Pipe", Int. J. Heat and Fluid Flow, Vol. 11, No. 4, pp. 321-330, 1990.

40. W. Li and S. Kakac, "Unsteady Thermal Entrance Heat Transfer in Laminar Flow with a Periodic variation of Inlet Temperature" Int. J. Heat Mass Transfer, Vol.34, No.10, pp. 2581-2592, 1991.

41. K.H. Ahn, and M.B. Ibrahim, "Laminar/Turbulent Oscillating Flow in Circular Pipes", Int. J. Heat and Fluid Flow, Vo.13, No. 4, pp.340-346, 1992.

42. S. Kim, B. Kang, and J. Hyun, "Heat Transfer in The Thermally Developing Region of a Pulsating Channel Flow", Int. J. Heat Mass Transfer, Vol.36, Np.17, pp. 4257-4266, 1993.

43. E.P. Valueva, V.N. Popov, and S.Y. Romanova, "Heat Transfer Under Laminar Pulsating Flow in a Round Tube", Thermal Engineering, Vol. 40, No.8, pp. 624-631, 1993.

44. M. Brunet and J. Lise, "A Moving Mesh Model for the Prediction of Hydrodynamic Viscous Force Acting on Oscillating Bodies", International Phoenics Journal, Vol.6, No.4, pp. 385-407.

45. D.M. Brown, W. Li, and S. Kakak, "Numerical and Experimental Analysis of Unsteady Heat Transfer with Periodic Variation of Inlet Temperature in Circular Ducts", Int. Comm. Heat Mass Transfer, Vol. 20, pp. 883-899, 1993.

46. T. Inaba, "Longitudinal Heat Transfer in Oscillatory Flows in Pipes with Thermally Permeable Wall", Journal of Heat Transfer, Vol. 177, pp. 884-888, November 1995.

47. L. Bauwens, "Oscillating Flow of a Heat-Conducting Fluid in a Narrow Tube", J. Fluid Mech., Vol. 324, pp. 135-161, 1996.

48. J. Zhang and C. Dalton, "Interaction of a Steady Approach Flow and a Circular Cyl;inder Undergoing Forced Oscillation", Journal of Fluids Engineering, Vol. 119, pp. 808-813, 1997.

49. Z. Guo and H. Sung, "Analysis of the Nusselt Number in Pulsating Pipe Flow", Int. J. Heat Mass Transfer, Vol. 40, No. 10, pp. 2086-2489, 1997.

50. Z, Guo, S. Kim, and H. Sung, "Pulsating Flow and Heat Transfer in a Pipe Partially Filled With a Porous Medium", Int. J. Heat Mass Transfer, Vol.40, No. 17, pp. 4209-4218, 1997.

51. T. Moschandreou, and M. Zamir, "Heat Transfer in a Tube with Pulsating Flow and Constant Heat Flux", Int. J. Heat Mass Transfer, Vol. 40, No. 10, pp. 2461-2466, 1997.

52. A. Yakhot, M. Arad and G. Ben-Dor, "Richardson's Annualr Effect in Oscillating Laminar Duct Flows", Journal of Fluids Engineering, Vol. 120, pp. 209-211, March 1998.

53. M. Habib, S. Said, A. Al-Farayedhi, S. Al-Dini, A. Asghar and S. Gbadebo, "Heat Transfer Characteristics of Pulsated Turbulent Pipe Flow", Heat and Mass Transfer, Vol. 34, pp. 413-421, 1999.

54. C. Chang, and W. Chu, "Stresses in a Metal Tube Under Both High Radial Temperature Variation and Internal Pressure", Journal of Applied Mechanics, pp. 101-108, 1954.

55. R. Sinha, "Thermal Stress Analysis of A Hollow Thick Cylinder by The Finite Element Method", J. Inst. Eng. (India) Mech. Eng., Division. 59, pp. 131-133, 1978.

56. M.A. Kalam, and T.R. Tauchert, "Stresses in an Orthotropic Elastic Cylinder Due to A Plane Temperature Distribution $T(r,\theta)$", Journal of Thermal Stresses, Vol. 1, pp. 13-24, 1978.

57. S. Stasyuk, V. Gromovyk and A. Bihuya, "Thermal-Stress Analysis of Hollow Cylinder with Temperature-Dependent Thermal Conductivity", Institute of Applied Problems of Mechanics and Mathematics, Academy of Sciences of The Ukrainian SSR, Lvov. Translated from Priblemy Prochnosti, No.1, pp. 41-43, 1979.

58. J.R. Shadley, N. Merah, and E. Rybicki, "The Effect of Induction Heating Stress Remedies on Existing Flaws in Pipes", J. Pressure Vessel Technology, Vol. 104, 193-197, 1982.

59. S. Naga, "Optimum Working Conditions in Thick Walled Cylinders" Journal of Engineering Materials and Technology, Vol. 108, pp. 374-376, 1986.

60. K. K. Tamma, and B. Railkar, "Nonlinear/Linear Unified Thermal Stress Formulations: Transfinite Element Approach", Computer Methods in Applied Mechanics and Engineering, Vol. 64, pp. 415-428, 1987.

61. S. Kardeniz, A. Ponter and K. Carter, "The Plastic Ratcheting of Thin Cylindrical Shells Subjected to Axisymmetric Thermal and Mechanical Loading", Journal of Pressure Vessel Technology, Vol. 109, pp. 387-393, November 1987.

62. G.A. Kardomateas, "Transient Thermal Stresses in Cylindrically Orthotropic Composite Tubes", Journal of Applied Mechanics, Vol. 56, pp. 411-417, 1989.

63. N. Sumi, and Y. Ito, "Dynamic Thermal Stresses in Composite Hollow Cylinders and Spherers Caused by Sudden Heating", JSME International Journal, Series I, Vol.35, No.3, pp. 259-264, 1992.

64. M. Kurashige, "Thermal Stresses of a Fluid-Saturated Poroelastic Hollow Cylinder", JSME International Journal, Series I, Vol. 35, No.4, 1992.

65. Y. Obata, and N. Noda, "Steady Thermal Stresses in A Hollow Circular Cylinder and A Hollow Sphere of A Functionally Gradient Material", Journal of Thermal Stresses, Vol. 17, pp. 471-487, 1994.

66. E. Russo, W. Cyr and P. Herrington, "Thermal Stresses in a Partially Filled Horizontal Vessel", Journal of Pressure Vessel Technology, Vol.116, pp. 302-305, August 1994.

67. K. Kaizu, T. Aoto, and S. Tanimura, "Two-dimensional Dynamic Thermal Stresses in A Semi - Infinite Circular Cylinder", J. Applied Mechanics, Vol. 62, pp. 257-259, 1995.

68. E.P. Russo, W.W. Cyr., and C. Davis, "Transient Thermal Stresses in Hollow Cylinders", ASME/JSME Thermal Engineering Conference, Vol. 1, pp. 59-62, 1995.

69. A. Zhdanov, L. Nikolaeva and S. Rossolenko, "Thermoelastic Stresses in Ribbons and Tubes Grown from the Melt by the Stepanov Method", Journal of Material Science, Vol. 30, pp. 75-84, 1995.

70. A. Kandil, A. El-Kady and A. El-Kafrawy, "Transient Thermal Stress Analysis of Thick - Walled Cylinders", Int. J. Mech. Sci., Vol. 37, No.7, pp. 721-732, 1995.

71. A.K. Naghdi, "Thermal Stresses in A Cylinder with Longitudinal Circular Cylindrical Cutouts", Journal of Thermal Stresses, Vol. 19, pp. 341-357, 1996.

72. A. Kandil, "Analysis of Thick - Walled Cylindrical Pressure Vessels Under The Effect of Cyclic Internal Pressure and Cyclic Temperature", Int. J. Mech. Sci., Vol. 38, No.12, pp. 1319-1332, 1996.

73. K. Tanaka, H. Watanabe, Y. Sugano, and Poterasu, V.F., " A Multicriterial Material Tailoring of A Hollow Cylinder in Fuctionally Gradient Materials: Scheme to Global Reduction of Thermoelastic Stresses", Compt. Methods Appl. Mech. Eng., Vol. 135, pp. 369-380, 1996.

74. J. Taler, B. Weglowski, W. Zima, S. Gradziel and M. Zborowski, "Monitoring of Transient Temperature and Thermal Stresses in Pressure Components of Steam Boilers", International Journal of Pressure Vessels and Piping, Vol. 72, pp. 231-241, 1997.

75. I. Klevtsov and R. Crane, "Evaluation of Accumulated Fatigue in Metals Due to Random Oscillating Thermal Stresses", Journal of pressure Vessel Piping, Vol. 120, pp. 43-50, 1998.

76. G. Praveen, C. Chin and J. Reddy, "Thermoelastic Analysis of Functionally Graded Ceramic-Metal Cylinder", Journal of Engineering Mechanics, Vol. pp. 1260-1267, November 1999.

77. J. Taler, B. Weglowski, W. Zima, S. Gradziel and M. Zborowski, "Analysis of thermal stresses in a Boiler Drum During Start-Up", Journal of Pressure Vessel Technology, Vol. 121, pp. 84-93, February 1999.

78. J. Beraun, J. Chen and D. Tzou, "Thermomechanical Fracture on a Pressurized Cylindrical Vessel Induced by Localized Energy Source", Journal of Pressure Vessel Technology, Vol. 121, pp. 160-169, May 1999.

79. L. Yu, and C. Chen, "Application of the Hyprid Method to the Transient Thermal Stresses Response in Isotropic Annular Fins", Journal of Applied Mechanics, Vol. 66, pp. 340-346, June 1999.

80. W. Reinhart, R. Kizhatil and G. McClellan, "Analysis of a Tubesheet Undergoing Rapid Transient thermal Loading", Journal of Pressure Vessel Technology, Vol. 122, pp. 476-481, November 2000.

81. C. Becht IV and Y. Chen, "Span Limits for Elevated Temperature Piping", Journal of Pressure Vessel Technology", Vol. 122, pp. 121-124, May 2000.

82. T. Igari, H. Wada and M. Ueta, "Mechanism-Based Evaluation of Thermal Ratcheting Due to Travelling Temperature Distribution", Journal of pressure Vessel Technology, Vol. 122, pp. 130- 138, May 2000.

83. J.H. Fauple, and F.E. Fisher, Engineering Design - A Synthesis of Stress Analysis and Material Engineering, John Wiley and Sons, New York, 1981.

84. B.A. Boley, and J.H. Weiner, Theory of Thermal Stresses, Section 9.10, 2nd Ed. Dover, 1997.

85. A.D. Gosman, E.E. Khalil, and H.J. Whitelaw, "The Calculation of Two - Dimensional Turbulent Recirculating Flows" Published in Turbulent shear flows (Selected papers from the First International Symposium on Turbulent Shear Flows, the Pennsylvania State University, University Park, Pennsylvania, USA, April 18-20, 1977), Springer-Verlag Berlin Heidelberg, New York, 1997.

86. W.M. Kays, and M.E. Crawford, Convective heat and mass transfer, Mcgraw-Hill, Inc., 1993.

87. S. Patankar, Numerical Heat Transfer and Fluid Flow, Hemisphere Publishing Corporation, 1980.

88. H. Schlichting, Boundary - Layer Theory, McGraw-Hill Publishing Company, 1979.

# Papers in Conferences and Journals

1. I.T. Al-Zaharnah, M.S. Hashmi and B. Yilbas, "Thermal Stresses in Thick Walled Pipes Subjected to Fully Developed Laminar Flow", Proceedings of the International Conference on Advances in Materials and Processing Technology, AMPT'99 and 16th Annual Conference of the Irish Manufacturing Committee, IMC 16, pp. 1073-1085.

2. I.T. Al-Zaharnah, B.S Yilbas and M.S. Hashmi, "Conjugate Heat transfer in Fully Developed Laminar Pipe Flow and Thermally Induced Stresses" Comput. Methods Appl. Mech. Engg., Vol. 190, pp. 1091-1104, 2000.

3. I.T. Al-Zaharnah, M.S. Hashmi and B. Yilbas, "Thermal Stresses in Thick Walled Pipes Subjected to Fully Developed Laminar Flow", Journal of Materials Processimg Technology, Vol. 118, pp. 50-57, 2001.

4. I.T. Al-Zaharnah, B.S Yilbas and M.S.J. Hashmi, "Pulsating Flow in Circular Pipes-The Analysis of Thermal Stresses" International Journal of Pressure Vessels and Piping, Vol. 78, pp. 567-579, 2001.